



Nanosecond-Pumped Resonance Raman Random lasing from
Micro-/Nano-granular Materials toward Chemical
Detection from Distance

Panuwat Srisamran

A Thesis Submitted in Partial Fulfillment of the Requirements for the
Degree of Master of Science in Physics
Prince of Songkla University
2019
Copyright of Prince of Songkla University



Nanosecond-Pumped Resonance Raman Random lasing from
Micro-/Nano-granular Materials toward Chemical
Detection from Distance

Panuwat Srisamran

A Thesis Submitted in Partial Fulfillment of the Requirements for the
Degree of Master of Science in Physics
Prince of Songkla University
2019
Copyright of Prince of Songkla University

Thesis Title Nanosecond-Pumped Resonance Raman Random lasing
from Micro-/Nano-granular Materials toward Chemical Detection
from Distance

Author Mr. Panuwat Srisamran

Major Program Physics

Major Advisor

.....
(Asst. Prof. Dr. Chalongrat Daengngam)

Examining Committee :

.....Chairperson
(Dr. Atcha Kopwitthaya)

.....Committee
(Asst. Prof. Dr. Paphavee van Dommelen)

.....Committee
(Asst. Prof. Dr. Chittanon Buranachai)

.....Committee
(Asst. Prof. Dr. Chalongrat Daengngam)

The Graduated School, Prince of Songkla University, has approved this thesis
as partial fulfillment of the requirements for the Master of Science Degree in Physics

.....
(Prof. Dr. Damrongsak Faroongsarng)
Dean of Graduate School

This is to certify that the work here submitted is the result of the candidate's own investigations. Due acknowledgement has been made of any assistance received.

.....Signature
(Asst. Prof.Dr.Chalongrat Daengngam)
Major Advisor

.....Signature
(Mr.Panuwat Srisamran)
Candidate

I hereby certify that this works has not been accepted in substance for any degree, and is not being currently submitted in candidature for any degree.

.....Signature

(Mr.Panuwat Srisamran)

Candidate

ชื่อวิทยานิพนธ์	การกระตุ้นสัญญาณเรโซแนนซ์รามานเลเซอร์แบบสุ่มจากสารขนาด ไมโคร- /นาโน-เมตรด้วยเลเซอร์ห้วงสั้นระดับนาโนวินาที เพื่อการตรวจวัดสารเคมี จากระยะไกล
ผู้เขียน	นายภาณุวัฒน์ ศรีสำราญ
สาขาวิชา	ฟิสิกส์
ปีการศึกษา	2561

บทคัดย่อ

เทคนิคการตรวจวัดและระบุชนิดของสารประกอบระเบิดหรือสารเคมีอันตรายที่มีปริมาณน้อยจากระยะไกลเป็นที่ต้องการเพื่อเหตุผลด้านความปลอดภัย วิธีการตรวจวัดสัญญาณรามานจากระยะไกลโดยการกระตุ้นด้วยเลเซอร์เป็นหนึ่งในเทคนิคทางสเปกโตรสโกปีที่มีประสิทธิภาพสูงสำหรับการระบุชนิดของโมเลกุลของเป้าหมายได้อย่างรวดเร็วและมีความแม่นยำ อย่างไรก็ตามการตรวจวัดสัญญาณรามานส่วนใหญ่ขึ้นอยู่กับกลไกการเปล่งแสงแบบเกิดขึ้นเอง (spontaneous emission) ซึ่งมีความเข้มของสัญญาณที่น้อยจึงยากต่อการตรวจวัดจากระยะไกล ในการวิจัยครั้งนี้จึงศึกษาการเปล่งสัญญาณรามานเลเซอร์แบบสุ่ม (random Raman lasing) ซึ่งสามารถใช้เป็นวิธีการขยายสัญญาณรามานได้ การเปล่งสัญญาณรามานเลเซอร์แบบสุ่มจำเป็นต้องอาศัยการขยายสัญญาณด้วยการกระเจิงสัญญาณรามานแบบกระตุ้น (stimulated Raman scattering) เพื่อใช้เป็นกลไกการเพิ่มพลังงานแสง และอาศัยการสะท้อนหลายครั้ง (multiple scattering) ของสัญญาณรามานจากในสารตัวอย่างที่มีลักษณะเป็นผง เพื่อป้อนกลับแสงรามานในสารตัวอย่างโดยหลักการแล้วนั้น กระบวนการรามานเลเซอร์มีความแตกต่างกับเลเซอร์แบบทั่วไป โดยกระบวนการรามานเลเซอร์ต้องการกระตุ้นด้วยเลเซอร์ห้วงสั้นเพื่อให้เกิดจำนวนอิเล็กตรอนแบบผกผัน (population inversion) ในระดับชั้นพลังงานสมมติ ดังนั้นในงานวิจัยครั้งนี้จึงเลือกศึกษากระบวนการดังกล่าวโดยการกระตุ้นด้วยเลเซอร์ห้วงสั้นที่มีช่วงเวลาในระดับ 10 นาโนวินาทีและความยาวคลื่น 355 นาโนเมตร และเลือกใช้แบเรียมไนเตรต (barium nitrate) ในรูปผงเพื่อเป็นสารตัวอย่าง เนื่องจากมีค่าสัมประสิทธิ์การขยายสัญญาณรามานสูงและมีโครงสร้างที่ไม่เป็นระเบียบ อีกทั้งสัญญาณรามานของสารดังกล่าวยังมีความคล้ายคลึงกับสารประกอบระเบิดหลายชนิด กระบวนการเปล่งแสงรามานเลเซอร์แบบสุ่มได้ถูกกระตุ้นในย่านเรโซแนนซ์ เพื่อเพิ่มความเข้มของสัญญาณรามานแบบ Stokes สำหรับเพิ่มประสิทธิภาพการเกิดรามานเลเซอร์แบบสุ่ม พฤติกรรมของสัญญาณเรโซแนนซ์รามานที่กระเจิงภายใต้การกระตุ้นด้วยเลเซอร์ที่ความเข้มต่าง ๆ จาก 0.12 ถึง 21.30 เมกะวัตต์ต่อตารางเซนติเมตร แสดงให้เห็นถึงความสัมพันธ์แบบไม่เป็นเชิงเส้นเนื่องจากการแข่งขันระหว่างกระบวนการสูญเสียสัญญาณจากการดูดกลืนและการขยายสัญญาณจากการกระเจิงสัญญาณรามานแบบกระตุ้น ค่าขีดเริ่มของสัญญาณรามานเลเซอร์แบบสุ่มสามารถพบได้ในตัวอย่างสารที่มีโครงสร้างแบบหลวมที่

ความเข้มของเลเซอร์กระตุ้น 18 เมกกะวัตต์ต่อตารางเซนติเมตร ซึ่งเป็นความเข้มที่ทำให้กระบวนการขยายสัญญาณมีค่ามากกว่ากระบวนการดูดกลืนสัญญาณ ประสิทธิภาพของการแปลงสัญญาณรามานเลเซอร์แบบสุ่มจากแสงกระตุ้นที่ความเข้ม 21.30 เมกกะวัตต์ต่อตารางเซนติเมตรมีค่าเท่ากับ 4.25×10^{-4} ซึ่งมากกว่าการแปลงสัญญาณรามานแบบปกติที่อยู่ในระดับ 10^{-8} ความเข้มของการแปลงสัญญาณรามานเลเซอร์แบบสุ่มมีค่าเพิ่มขึ้นตามรัศมีของการขยายสัญญาณซึ่งสามารถประมาณได้จากขนาดของเลเซอร์กระตุ้น (ประมาณ 2 มิลลิเมตรในการศึกษาครั้งนี้) สัญญาณรามานเลเซอร์แบบสุ่มที่แพร่ออกนอกรัศมีของการขยายสัญญาณจะสูญเสียพลังงานเนื่องจากการดูดกลืน นอกจากนี้โครงสร้างภายในของตัวอย่างมีผลอย่างมีนัยสำคัญต่อกระบวนการแปลงสัญญาณรามานเลเซอร์แบบสุ่ม ผลของการวัดการกระเจิงกลับแบบอาพันธ์ (coherent backscattering) ที่สอดคล้องกันแสดงให้เห็นว่าเลเซอร์กระตุ้นเดินทางในโครงสร้างตัวอย่างแบบหลวมได้ไกลกว่าและมีการดูดกลืนสัญญาณน้อยกว่าเมื่อเทียบกับโครงสร้างตัวอย่างแบบอัดแน่น การจำลองโดยอาศัยโปรแกรม COMSOL Multiphysics แสดงให้เห็นถึงการเดินทางและการกักเก็บพลังงานแสงในสารตัวอย่างที่มีโครงสร้างแบบสุ่ม ผลการจำลองแสดงให้เห็นว่าเลเซอร์กระตุ้นสามารถเดินทางเข้าไปในโครงสร้างตัวอย่างที่หลวมได้มากกว่า แต่โครงสร้างตัวอย่างที่แน่นกว่าสามารถกักเก็บพลังงานแสงได้ดีกว่า ดังนั้นโครงสร้างของตัวอย่างที่สามารถสนับสนุนการเกิดสัญญาณรามานเลเซอร์แบบสุ่มได้ดีที่สุดต้องมีความสมดุลระหว่างปริมาณของแสงที่เดินทางเข้าไปในโครงสร้างและความสามารถในการกักพลังงานแสงไว้ในระดับที่นานเพียงพอ ในส่วนสุดท้ายงานวิจัยชิ้นนี้ได้สาธิตการตรวจวัดสัญญาณรามานเลเซอร์แบบสุ่มจากโครงสร้างตัวอย่างแบบหลวมด้วยกล้อง CCD จากระยะไกล

Thesis Title	Nanosecond-Pumped Resonance Raman Random lasing from Micro-/Nano-granular Materials toward Chemical Detection from Distance
Author	Mr. Panuwat Srisamran
Major Program	Physics
Academic Year	2018

Abstract

For security purpose, there is an increasing demand of techniques capable of detecting and identifying trace amount of explosive or dangerous chemicals from a safe distance. A laser-based standoff Raman detection is one of the promising spectroscopic techniques that affords quick detection of targeted molecules with high specificity. However, conventional Raman detection is primarily based on weak spontaneous emission, which undermines the vitality of such technique to perform at remote distance. Therefore, this research studied a new type of much stronger Raman generation process, called Raman random lasing (RRL), in which the optical amplification of Raman signal can be achieved. The RRL process requires stimulated Raman scattering (SRS) as a gain mechanism, and relies on multiple scattering in powder medium to supply optical feedback inside the gain medium. In principle, Raman lasing differs from conventional laser as it requires ultrashort excitation to create population inversion on a virtual state rather than a real electronic state. Thus, a nanosecond UV laser at wavelength 355 nm, and pulse duration 10 ns was used as a pump to excite RRL. Barium nitrate powder with high gain coefficient was chosen as a disordered Raman-active medium with Raman peaks similar to those of many explosive compounds. The RRL was excited near electronic resonance condition to achieve higher Stokes signal for SRS process. The behavior of resonant Raman scattering signal at pump pulse intensity, ranging from 0.12 to 21.30 MW/cm², showed nonlinear response resulting from the competition between absorption loss and SRS gain mechanisms in the excited medium. The RRL threshold can be founded for a loosely-packed powder sample at pump intensity around 18 MW/cm², where the SRS gain surpasses loss. The efficiency of the RRL signal at the highest pump intensity of 21.30 MW/cm² is 4.25 x 10⁻⁴, which is much higher than conventional Raman efficiency of typically 10⁻⁸. It was found that the RRL power grows within the gain radius, comparable

to the laser pump spot size of 2 mm. The sample region outside gain radius absorbed RRL energy, causing high loss. Furthermore, sample packing structure played an important role for RRL generation. The coherent backscattering measurement results show that the pump beam energy can penetrate longer into a loosely-packed sample with lower absorption loss, when compared with a closely-packed sample. The finite different time domain run in COMSOL Multiphysics was also used to investigate energy penetration and storing inside a random medium. The simulation results also support that a low density sample allows higher pump pulse energy to propagate inward. On the contrary, a denser sample can provide greater multiple scattering to prolong light energy confinement inside the random medium. As such, it should exist an optimum particles density which gives a balance between pump energy penetration and degree of multiple scattering. Lastly, it was demonstrated that the RRL for a loosely-packed sample was efficient as the Raman spectrum can be detected at standoff distance using a CCD camera.

ACKNOWLEDGEMENTS

I would like to deeply thank to all personages who helped me to achieve the challenging goal of this thesis.

Deeply thanks to Asst. Prof. Dr.Chalongrat Daengngam for his advices and continuous support during the studying.

Thanks to Dr.Atcha Kopwittahaya from National Electronics and Computer Technology Center (NECTEC) for her participation as the chairperson.

Thanks to Asst. Prof. Dr.Chittanon Buranachai and Asst. Prof. Dr.Paphavee van Dommelen for attention as committees.

Thanks to team members of Nanophotonics research group at department of Physics, faculty of Science, Prince of Songkla University. Especially, Mr.Sukrit Thongrom for photographing of the Raman spectrum, Mr.Paphon Pewkhom and Mr.Sirawit Boonsit for simulation studying.

Thanks to Mr.Jamras Na Suwan for his insight of opto-mechanics components designing and creating.

Thanks to the Development and Promotion of Science and Technology Talents project (DPST scholarship) for the financial support.

Thanks to Graduated school at Prince of Songkla University and Thailand Center of Excellence in Physics (Thep center) for partially supports of research budget.

Panuwat Srisamran

CONTENTS

CONTENT	PAGE
ABSTRACT (IN THAI)	v
ABSTRACT (IN ENGLISH)	vii
ACKNOWLEDGEMENTS	ix
CONTENTS	x
LIST OF TABLES	xii
LIST OF FIGURES	xiii
CHAPTER 1 INTRODUCTION	1
1.1 Motivation of the research	1
1.2 Literature review	5
1.3 Objectives	9
1.4 Studying scope	10
CHAPTER 2 THEORY	11
2.1 Conventional Stimulated Emission	11
2.2 Spontaneous Raman Scattering	13
2.3 Stimulated Raman Scattering	18
2.4 Absorption and effective gain efficiency	22
2.5 Behavior of light in a disordered medium	23
CHAPTER 3 METHODOLOGY	26
3.1 Sample preparation and standard characterization methods	26
3.2 Study of Raman random lasing	29
3.2.1 Experiment I: control of the pump pulse intensity	31
3.2.2 Experiment II: Investigation of resonant Raman random lasing	32
3.2.3 Experiment III: Effect of sample packing structures	33
3.2.4 Experiment IV: Coherent backscattering	34

3.3	Simulation studying via COMSOL Multiphysics	36
3.3.1	The geometries	37
3.3.2	Transient electromagnetic wave	37
3.3.3	Boundary conditions	38
3.3.4	Scattering boundary condition	39
3.3.5	Evaluated values	39
3.4	Detection of Raman Random Lasing using a CCD camera	40
CHAPTER 4 RESULTS AND DISCUSSIONS		42
4.1	Sample characterizations	42
4.2	Results of Raman random lasing	45
4.2.1	Result I: Control of the pump pulse intensity	45
4.2.2	Result II (1): Threshold of resonant Raman random lasing	45
4.2.3	Result II (2): Effect of sample layer thickness	48
4.2.4	Result III: Effect of sample packing structures	50
4.2.5	Result IV: Coherent backscattering result	51
4.3	COMSOL simulation result	54
4.4	Detection of Raman Random Lasing using a CCD camera	59
CHAPTER 5 CONCLUSION		62
5.1	Conclusion	62
5.2	Recommendations	63
REFERENCES		64
APPENDIX		71
VITAE		81

LIST OF TABLES

TABLES		PAGE
4.1	Transport mean free path (l_t) of loosely-packed sample and closely-packed sample.	59
4.2	Absorption length (l_a) of loosely-packed sample and closely-packed sample.	59

LIST OF FIGURES

FIGURE		PAGE
1.1	Graph shows the trend of terrorist incident events from 1970-2016 (START, 2018).	1
1.2	Statistical report of terrorist incident in Thailand (a) total in number of events (b) pie chart of tactic used for attacking.	2
1.3	Weapon used in terrorist incident events worldwide in 2017 (START, 2018).	2
1.4	The use of IED in terrorist attack in (a) Boston Marathon 2013, Boston, USA (Levs and Plott, 2013) (b) Bangkok shrine 2015, Bangkok, Thailand (C. and Olarn, 2015).	3
1.5	(a) Threshold characteristic indicates the occurrence of Raman random lasing. (b) Bright Raman emission is simply detected by a CCD camera.	8
2.1	Energy diagram of a four-level system and transition of electrons.	12
2.2	Energy diagram of scattering processes.	14
2.3	Example of Raman spectrum from Pentaerythritol Tetranitrate (PETN) (Nagli et al. 2008).	15
2.4	Behavior of Raman scattering cross section respects to the excitation wavelength (Faris and Copeland, 1997).	18
2.5	The schematic of the SRS process.	19
2.6	The schematic explains a molecular scale interaction of the SRS process.	19
2.7	The behavior of χ'_R and χ''_R respect to Stokes frequency.	21
2.8	Scattering processes in a Raman gain medium.	23
2.9	Conceptual schematic of pump and Stoke radiation intensity in a Raman gain medium.	25
3.1	Standard Raman spectroscopy characterization system.	27
3.2	Pellet preparation tool in the process of preparing closely-packed sample.	28
3.3	Scanning electron microscope machine.	29
3.4	A schematic of the setup to observe resonant Raman random lasing signal. The setup used a pump of OPO laser at 355 nm to pump the samples.	30
3.5	Optical component line for preparing the incident pulse.	31

LIST OF FIGURES (CONTINUED)

3.6	Setup for measurement of incident laser pulse.	32
3.7	The setup for experiment II (a) Schematic of the setup (b) the sample holder system (c) Scattered signal coupling part.	33
3.8	The setup for experiment IV (a) schematic of the setup (b) coherent backscattering setup.	35
3.9	Coherent backscattered peak which is the plot of scattered light intensity versus backscattered angle (Akkermans, Wolf and Maynard, 1986).	36
3.10	The created structure of (a) Fill factor = 0.25 (b) Fill factor = 0.5 (loosely-packed sample), and (c) Fill factor = 0.8 (closely-packed sample).	37
3.11	Example of boundary condition used for studying. The red line is scattering boundary with Gaussian incident field. The black line is scattering boundary with no field.	39
3.12	Schematic of the setup for capturing color photo of RRL from a loosely-packed sample.	40
3.13	Schematic of the setup for capturing monochrome photo of RRL from a loosely-packed sample.	41
4.1	Raman spectrum of $\text{Ba}(\text{NO}_3)_2$ from standard Raman microscope spectrometer.	43
4.2	Raman spectrum of $\text{Ba}(\text{NO}_3)_2$ measured by the optical setup at pump intensity $\sim 21.3 \text{ MW/cm}^2$.	43
4.3	SEM image of the sample with magnification 100x (left), 500x (middle), and 4000x (right).	44
4.4	Particle size distribution determined from SEM images.	44
4.5	Graph shows result of incident pulse intensity versus relative angle.	45
4.6	Raman spectrum of 2 mm-thickness sample with various pump pulse intensity ranging from 0.12 to 21.30 MW/cm^2 .	46
4.7	Plot of Raman scattering signal versus pump intensity for 2 mm-thickness sample.	47
4.8	Schematic of the experimental setup for determining the RRL power.	48

LIST OF FIGURES (CONTINUED)

4.9	Raman spectrum of loosely-packed sample from various thickness, ranging from 1 to 4 mm, using 21.30 MW/cm ² pump intensity.	49
4.10	Graph of forward Raman scattering signal at 1034 cm ⁻¹ versus pump intensity at sample thickness 1 to 4 mm.	49
4.11	Raman spectrum of loosely-packed sample and closely-packed sample using pump intensity 21.30 MW/cm ² .	50
4.12	Behavior of Raman scattered light at 1034 cm ⁻¹ evolution of loosely-packed sample and closely-packed sample.	51
4.13	Normalized scattered light intensity vs backscattered angle of loosely-packed sample.	52
4.14	Normalized scattered light intensity vs backscattered angle of closely-packed sample.	52
4.15	Fitting of CBS result with model described in equation 3.3.	53
4.16	Simulated E field of a laser pulse in random medium with fill factor = 0.25 at different time step.	55
4.17	Simulated E field of a laser pulse in random medium with fill factor = 0.50 (loosely-packed sample) at different time step.	56
4.18	Simulated E field of a laser pulse in random medium with fill factor = 0.80 (closely-packed sample) at different time step.	57
4.19	Graph of wave energy stored in the random medium when excited by a short laser pulse with pulse duration 10 fs.	58
4.20	Photo of light scattered from a loosely-packed sample. This photo was captured by a cell phone camera (i.e. iPhone SE), bundled with a grating.	59
4.21	Photo of light scattered from a loosely-packed sample taken by a monochrome CCD camera.	60
4.22	Extended Raman spectrum of Barium Nitrate, ranging for 0 to 8000 cm ⁻¹ , from loosely-packed sample using 21.30 MW/cm ² pump intensity.	61

CHAPTER 1 INTRODUCTION

1.1 Motivation of the research

Defense technology is the major concern for all countries worldwide. This technology can provide safety and stability of citizen's daily life in several ways e.g. drug suppression, security patrolling, and law enforcement. For example, explosion in resident area can cause lethal damage for surrounded innocents. It is important to screen and defuse the bomb before it exploded. To achieve screening application, chemical detection, especially for trace quantity of explosive residues, is required to support identification of suspected objects.

In the last few years, a number of terrorist attacks have been increasing. Statistical database, retrieved from the Global Terrorism Database (GTD) (The Department of Homeland Security Science and Technology Center of Excellence, University of Maryland), reports the numbers of terrorist incident events. The trend is rising as shown in Figure 1.1. The incident can cause injuries and lethal consequences to number of people, especially for innocents. In Thailand, there are numbers of terrorist incidents especially in the southern area. Statistical database of incidents from 2004 to 2016 shows constant trend (Figure 1.2 (a)). Bombing can be counted as ~ 26.6% of the tactic used to attack as shown in Figure 1.2 (b) (Jitpiromsri, 2017).

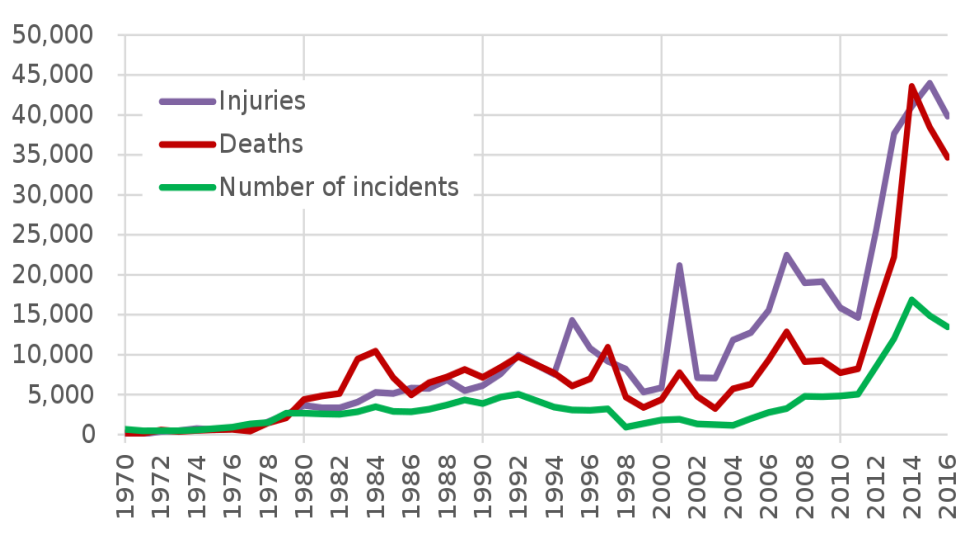


Figure 1.1 Graph shows the trend of terrorist incident events from 1970-2016 (START, 2018).

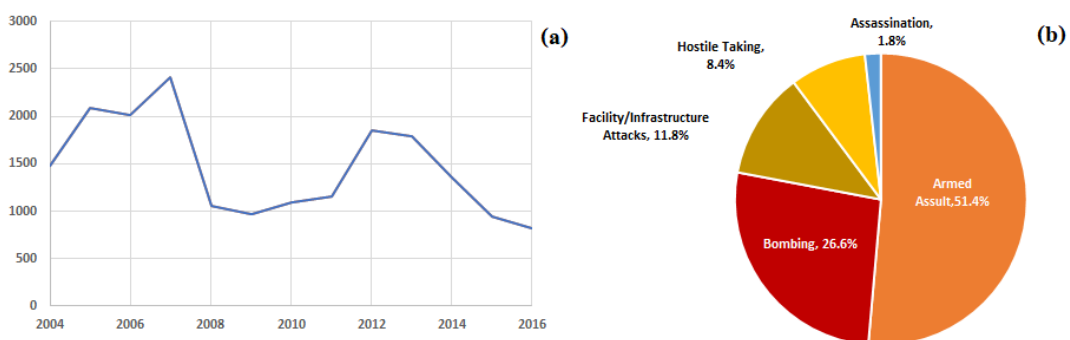


Figure 1.2 Statistical report of terrorist incident in Thailand (a) total in number of events (b) pie chart of tactic used for attacking.

For worldwide statistical database, bombing is the mostly used tactic since it can create largest area of incident when compared with other methods e.g. armed assault, and assassination. In 2017, bombing events is a half number of total incident events as shown in Figure 1.3. Improvised explosive devices (IEDs) are homemade explosive devices, commonly used in terrorist incident. An IED was produced and used in many incident events, example shown in Figure 1.4.

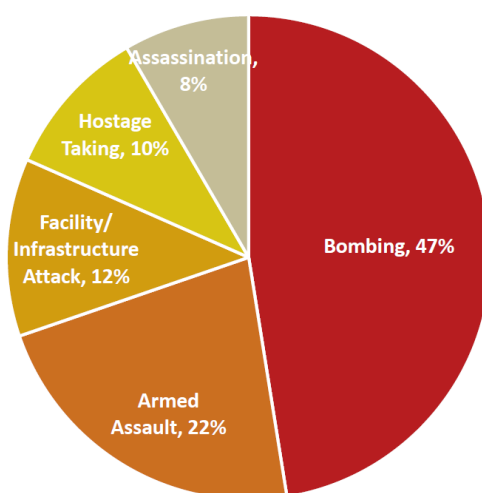


Figure 1.3 Weapon used in terrorist incident events worldwide in 2017 (START, 2018).



Figure 1.4 The use of IED in terrorist attack in (a) Boston Marathon 2013, Boston, USA (Levs and Plott, 2013) (b) Bangkok shrine 2015, Bangkok, Thailand (C. and Olam, 2015).

An IED can be made of several types of chemical ranging from military-graded chemicals, e.g. trinitrotoluene (TNT), cyclotrimethylenetrinitramine (RDX), to local-graded chemicals, e.g. agriculture-graded fertilizers (Sharma, Misra and Sharma, 2005; Sharma, 2007). This device can be contained in various forms of container. It can be set in a huge container e.g. a trunk of a van, or a small container like a can of soft drink (Chivers, 2015). The variation of container leads to the difficulty of IEDs visualization or preventing. In real situation, explosive compounds generally contaminate the surrounding at low concentration, either in vapor or powder mixture phase. For instance, vapor pressure of TNT is 4.2×10^{-4} Pa at 25 °C, equivalent to 8 ppb. RDX is one of the widely used explosive substance, which exhibits much lower vapor pressure of 7.2×10^{-4} Pa at ambient condition. This vapor pressure equivalent to concentration at 6 ppb (Brady et al., 2012).

Several identification techniques, for example neutron activation analysis (Bach et al., 1993), ion mobility spectroscopy (Ewing and Miller, 2001), and fluorescence-quenching sensors (Germain and Knapp, 2008), can be employed to detect a trace amount of explosive chemicals. Some of the aforementioned techniques can sense the chemical amount down to ppt (part per trillion) levels. However, these techniques require physical interaction of sample drawing process in a close proximity. It is the limitation for performing in real use with ensure safety. Any operations processes near to a suspicious target are very dangerous and can be lethal for the operating staffs or nearby innocents. From this reason, it is justified that standoff detection techniques are strongly needed (Ehlerding et al., 2012). These techniques

require the capability of identification for chemicals with non-invasion, high selectivity, and high sensitivity from a safe distance outside blast radius.

The most viable techniques for standoff explosive detection are laser-based spectroscopies. Standoff Raman spectroscopy (ST-Raman) is the promising laser-based optical technique that can be used for the security applications (Mogilevsky et al., 2012). The technique can be operated in various condition e.g. night time (Sharma et al., 2005), day time (Wu et al., 2000), ambient light (Carter et al., 2005), and snow (Pettersson et al., 2009). Raman spectroscopy technique is regarded as a reliable spectroscopic technique. It allows high-selectivity detection such that the “chemical fingerprint” information of targeted molecules can be extracted. However, the only disadvantage is that the weak signal of spontaneous Raman scattering process: approximately 10^8 excitation photons generate only 1 Raman photon. This weak interaction leads to low signal-to-noise ratio (SNR), unviable for real use. To make this technique capable for practical use, high-performance detection devices would be required. The SNR of spontaneous Raman detection can be enhanced by the used of an intensify couple charged device (ICCD) camera as a detector in synchronous with pulsed laser excitation in sub-nanosecond time scale (Pettersson et al., 2010). Another signal enhancing approach is to enhance backscattered Raman signal using ultrafast pump pulses e.g. picosecond pulses (Åkeson et al., 2011) or femtosecond pulses (Katz et al., 2008), where nonlinear growth of Raman signal can be achieved.

Recently, there is another novel approach to unravel this issue by inducing a “random Raman lasing” process which spontaneous Raman scattering signal is amplified by stimulated Raman scattering (SRS) in a random medium. Multiple scattering caused by a disordered medium provides optical feedback for lasing oscillation. This property increases the dwell time of pump and Raman components in the Raman active medium. This process results in bright emission of Raman signal in random direction. In fact, most of the explosive materials can support multiple scattering, since they are in powder form. Also, this random Raman lasing scheme, in principle, can occur in turbid media, e.g. as biological tissue (Freudiger et al., 2008) and colloidal suspension (Bingi, Warriar and Vijayan, 2013), which should enhance Raman detection for such media. Since SRS is a nonlinear optical phenomenon, its conversion efficiency linearly depends on the incident intensity.

Another Raman enhancement technique is to set the incident photon energy near to the excited state of molecules (in UV or deep UV region), such that Resonant Raman scattering can be produced. The possibility for the incident photon to produce Raman photon increases significantly.

This thesis focuses on the investigation of resonant Raman Random lasing activated by a UV nanosecond-pulsed laser. This process requires SRS to support optical gain mechanism and relies on multiple scattering in disordered material to produce optical feedback for generation of lasing type emission. This paradigm can lead to optically amplified Raman signal, which should allow better detection efficiency. Particularly, Barium nitrate ($\text{Ba}(\text{NO}_3)_2$) powder is selected as a Raman active and multiple scattering medium without the need of an additional optical cavity. The Raman random lasing properties were studied for several parameters such as pump intensity, sample layer thickness and packing structure. The multiple scattering parameters are also determined by coherence backscattering experiment. The nonlinear increasing and threshold characteristic of Raman signal with various pump energy is experimentally demonstrated for the evidence of Raman random laser (RRL).

1.2 Literature review

The process of stimulated Raman gain mechanism and light propagation in a multiple scattering medium are the two major requirements to generate RRL. The differences from conventional random laser (RL) are explained as followed.

Laser is a process of light emission which is amplified by stimulated emission process. It requires two major optical components to produce lasing emission, which are a gain medium and optical resonator. Light emits from gain medium oscillates in a resonator producing optical feedback for stimulated emission. That is, light is circularly amplified through the gain medium, which is optically or electrically pumped by an external source. If the pump energy is high enough such that the gain surpasses the loss in resonator, laser oscillation starts. For conventional lasing process, a gain mechanism is based on population inversion, where higher numbers of electrons occupy the excited states of the atoms compared to that of the ground state. These electrons are stimulated by feedback photons to release extra photons coherent with the stimulating photons (Powers and Haus, 2017).

In the context of RL, optical feedback is provided by multiple scattering in a disordered medium rather than mirrors in a typical resonator. The behavior of light propagation in the multiple scattering medium can be explained by random walk type motion, or through a diffusive nature of radiation energy via diffusion equation. The scattering medium also has loss from e.g. light absorption. Therefore, sufficient pump energy is required to produce sufficient gain that exceeds loss in order to radiate RL (Eichhorn, 2014).

For RRL, the optical gain is based on SRS mechanism instead of electronic population inversion. This RRL process also needs the Raman gain material to act as multiple scattering centers for optical feedback. Diffusion of light in a random medium promotes the interaction of pump and Raman photons. It leads to the conversion of pump power into Raman power. In RRL process, pump component suffers from several loss mechanisms e.g. SRS conversion process and absorption, while Raman component experiences both gain from SRS process and loss from absorption. When the gain of SRS supersedes loss, high amplified radiation of Raman wavelength is produced in random direction.

Resonant Raman scattering can be created using high energy photon (UV or deep UV wavelength) to pump a Raman active medium. In this process, the electrons in ground state are excited by incident photon energy near to the energy gap of the molecule. Raman cross section from this process is higher than off-resonant Raman case. The increase of Raman scattering cross section allows the medium to produce more Raman photons. This process can be used to enhance efficiency of RRL since SRS at near resonance condition directly produces more Raman photons to supply multiple scattering and optical feedback.

SRS is a third-order nonlinear optical process that allows pump photon and Raman photon interaction through nonlinear polarization of the Raman gain medium. Basically, electrons in ground state of the medium are pumped into a virtual state with incident pulse. They are immediately stimulated to release their energy by spontaneous Raman photons. This process leads to the amplification of the Raman signal. In the last few decades, SRS principle has been developing for many kinds of application, especially on light generation source and spectroscopy.

Initially, SRS application was mainly focus on laser source application. This method provides a new paradigm to generate light at various wavelength, provided by the Raman shift of the media, from a photonic crystal or Organic liquids, e.g. benzene, toluene, and pyridine, were set as a gain medium in laser cavity (Eckhardt et al., 1962). These organic materials radiated a strong signal at their Raman wavelength. The Raman signal was amplifying while the light was oscillating inside the laser cavity. This liquid medium is able to produce intense Raman signal with only a single-pass of pump pulse. $\text{Nd}^{+3}:\text{POCL}_3:\text{ZrCl}_4$, set in a laser cavity, can converse pump power to Raman power with efficiency of 10^{-2} which is much stronger than conventional Raman case (typically in efficiency of 10^{-8}) (Green et al., 1975). SRS theory was presented through a model of three-level system (Raymer, Mostowski and Carlsten, 1979). Raman gain of monochromatic pump was evaluated. Here, the comparison of pump pulse duration (T_p) and dephasing time of Raman scattering phenomenon (T_2) can categorize the SRS into two limits. Transient limit is applied for $T_p \ll T_2$ case. In contrast, steady-state limit is valid for $T_p \gg T_2$. In general, transient SRS shows higher Raman gain compared to steady-state limit. This property allows SRS process to be enhanced easier in the transient operation. Using short laser pulses, electrons in ground state can be sharply excited into virtual state and stimulated to release efficient Raman energy in ultrashort period (in sub-ps regime) (Chunaev and Karasik, 2006). This Raman gain approximation shows good agreement to experimental verifications (Bret and Weber, 1968; Gazengel, Xuan and Rivoire, 1979).

The SRS process plays a central role as a gain mechanism of RRL in a disordered Raman gain medium. As stated, the disordered Raman gain medium has the role of both gain material and scattering centers to provide optical feedback. Complex behavior of light penetration in a multiple scattering medium can be estimated by simulation studying. The recent studied result shows the possibility of sufficient energy confinement and laser radiation for both pump component (Andreasen et al., 2011) and Raman component (Hokr and Yakovlev, 2014). SRS radiation was experimentally confirmed in various types of sample. Liquid sample can produce very intense Raman radiation (de Oliveira et al., 2019; Yui et al., 2002; Li et al., 2019; Seifert, 2003). In liquid sample, concentration of Raman gain material in a solution can be adjusted. Varying solution concentration leads to the change of multiple scattering property of the medium since the numbers of particles are

changed. It leads to the variation the gap between particles which relates to light confinement property of the structure. RRL can be produced easily in material structure where light can be strongly confined. RRL does not require the specific wavelength for an incident pump and not specific to the energy gap of electronic structure. Thus, the incident wavelength can be chosen to avoid peak absorption of RRL material. Furthermore, RRL generation process can also be performed in granular material (Gummaluri, Krishnan and Vijayan, 2018; Bingi et al., 2013; Frank et al., 2019; Bachelard et al., 2014). Such granular materials contain higher amount of Raman scattering centers compared to a liquid sample. This leads to stronger light confinement with higher Raman conversion efficiency. In this case, it shows a clear characteristic laser threshold and bright emission of Raman wavelength as depicted in Figure 1.5. (a) and (b), respectively (Hokr et al., 2014). Moreover, the threshold characteristics of SRS signal can be observed from other types of sample, e.g. crystal structure (Savitski, Reilly and Kemp, 2013; Basiev et al., 1999), and nonlinear optical fiber (Yiou et al., 2005; Pan et al., 2018). The recent pioneer study has demonstrated that chemical characterization using SRS as gain mechanism can be measured from standoff distance (Hokr et al., 2014). Furthermore, this method requires just only a single shot of a 10 ps pump pulse to perform the identification of powder sample from a distance of ~ 400 m in laboratory.

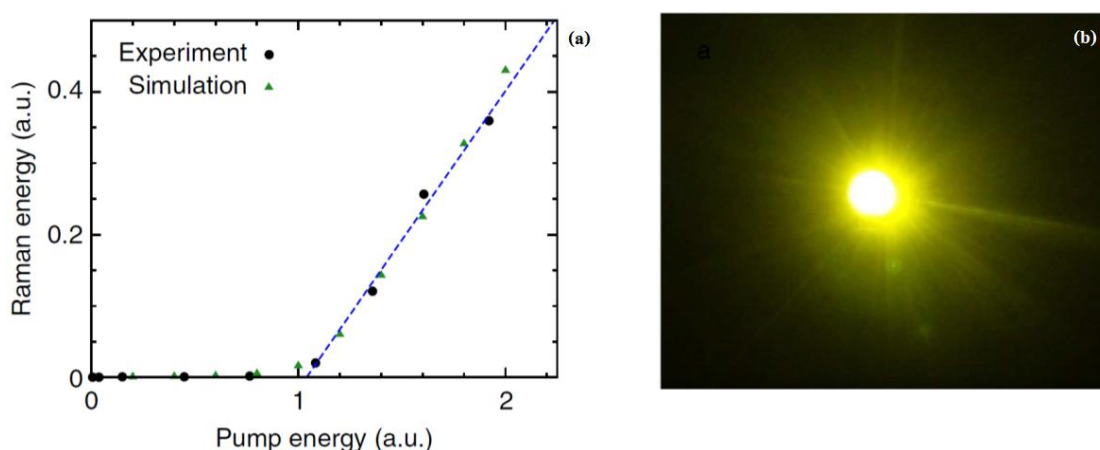


Figure 1.5 (a) Threshold characteristic indicates the occurrence of Raman random lasing. (b) Bright Raman emission is simply detected by a CCD camera.

For RRL, multiple scattering is a critical factor to provide optical feedback of pump and Raman components in order to generate the lasing signal. It allows light energy to be captured in a random or granule-disordered media. The studies of photon localization in disorder media are reported. (Segev, Silberberg and Christodoulides, 2013; Wiersma et al., 1997; Hokr et al., 2017; Wu et al., 2004) This property relates to the strength of optical feedback signal. The behavior of light penetrated in the disordered medium can be described through relevant length scales. Transport mean free path (l_t) is a parameter associated with the average light travelling distance in a disordered sample before the propagation direction turns randomized, caused by multiple scattering. The l_t of a random medium can be evaluated by coherent backscattering (CBS) experiment (Akkermans, Wolf and Maynard, 1986; Wolf and Maret, 1985; Zhu, Pine and Weitz, 1991). Furthermore, absorption length (l_a) and gain length (l_g) are other length parameters that can be estimated by from the CBS pattern of a sample. In general, l_g is the traveling distance in a gain medium, upon which the radiation intensity is amplified by factor of e . Whereas, l_a is the distance that radiation intensity is absorbed by factor of e .

Enhanced by multiple scattering property of the structure and near resonance excitation condition, nanosecond laser pulses could be used as a pump for RRL in a Raman random medium instead of picosecond or femtosecond pumps. The resonant Raman allows much stronger generation of Stokes wavelength residing in a multiple medium ready to be a sufficient optical feedback to induce the energy transfer from the pump power to Raman power via SRS gain mechanism. This research explores the feasibility and effectiveness of generating RRL using a nanosecond pulsed laser by focusing the Raman excitation near the electronic state resonance, i.e. using UV excitation pump. The nanosecond laser is quite a mature technology which is more practical for real implementation, compared to sophisticated ultrashort pulsed laser, i.e. picosecond or femtosecond pulsed laser system.

1.3 Objectives

- (1) To demonstrate the generation of Raman random lasing at near resonant condition, pumped by a nanosecond UV pulsed laser
- (2) To investigate the threshold characteristic of resonant Raman random lasing and the effect of medium structures.

1.4 Studying scope

The Raman sample in this study is Barium Nitrate ($\text{Ba}(\text{NO}_3)_2$). The sample is excited by a nanosecond-pulsed laser, with wavelength ~ 355 nm, pulsed duration ~ 10 ns, to create resonant Raman random lasing. Raman scattered signal strength and laser threshold phenomenon of a sample are detected in various pump pulse intensities, ranging from 0.12 to 21.30 MW/cm^2 . This behavior is also studying under the variation of sample packing structures, a loosely-packed sample and pressurized pellet form as a closely-packed sample.

In addition, a simulation of multiple scattering process is performed using finite element time domain method solved by COMSOL Multiphysics, electromagnetic wave (transient) module. The behavior of a Gaussian laser pulse, incident onto a random structure, is studied. Fill factor of the structure is ranging from 0, 0.25, 0.50, and 0.80. Refractive index of the random structure is set at 1.5756, respect to $\text{Ba}(\text{NO}_3)_2$, on the background of air (refractive index = 1). The comparative energy storing property of a structure was observed by surface integration of $|E|^2$.

CHAPTER 2

THEORY

In this chapter, the theories related to Raman random laser are reviewed. To demonstrate lasing phenomenon, two major parts consisting of gain mechanism and optical feedback, are required. Raman random laser is amplified by stimulated Raman emission process. This process can be created by coupling of pump and Raman wavelength in a Raman gain medium. The process requires fast and high-intense pump, typically picosecond or sub-picosecond pulsed laser. In this process, the Raman wavelength grows as laser gained rate. Optical feedback of Raman random laser can be provided by multiple scattering of a disordered medium. Light penetration behavior in the disordered medium leads to the increasing of dwell time for pump and Raman energy in the random structure. It permits signals to support Raman lasing phenomenon, even pumped by a nanosecond pulsed laser. Details of each theory can be found as followed.

2.1 Conventional Stimulated Emission

The stimulated emission can be explained by, for example, a four-level system diagram as shown in

Figure 2.1. The electrons in ground state (E_1) are optically pumped to excited state (E_4). These electrons undergo fast non-radiative transition to a metastable state (E_3), which supports relatively longer lifetime transition. At this state, the numbers of electrons, resulting in population inversion between the metastable state and a short lifetime state (E_2). These levels are called lasing levels. The electrons in E_3 are stimulated to release energy to E_2 , resulting in stimulated emission phenomenon. The electrons then restore to the ground state by a fast transition process.

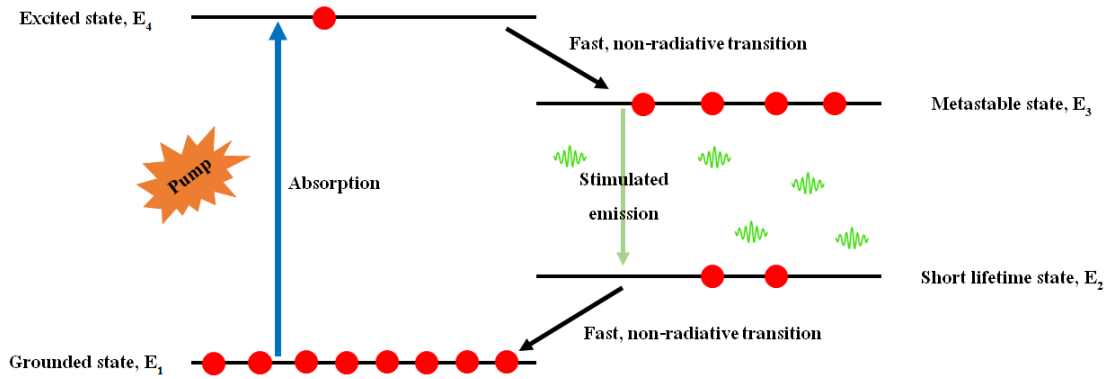


Figure 2.1 Energy diagram of a four-level system and transition of electrons.

Consider lasing levels in equilibrium, gain coefficient of the lasing signal through conventional stimulated emission in a laser medium can be expressed by (Eichhorn, 2014),

$$\alpha_L(\omega) = \sigma_{32}(\omega) \cdot \Delta N, \quad 2.1$$

where $\sigma_{32}(\omega)$ is the stimulated emission cross section with respect to frequency ω . ΔN is population inversion of electron in the atom in lasing level. The $\sigma_{32}(\omega)$ can be written by,

$$\sigma_{32}(\omega) = B_{32} \frac{\lambda^2}{8\pi n^2} g(\omega), \quad 2.2$$

where λ is the pump wavelength, n is the refractive index of the medium, $g(\omega)$ is the normalized broadening function of gain medium, and B_{32} is the Einstein's coefficient for stimulated emission process. In equilibrium, Einstein's coefficient for absorption process and for stimulated emission process are equivalent. The coefficient can be estimated by,

$$B_{32} = \frac{\Gamma_{32}}{N_3 \mu(\omega)}, \quad 2.3$$

where Γ_{32} is the stimulated emission rate, N_3 is the number of electrons in higher metastable state, and $\mu(\omega)$ is the radiation energy per unit volume which respects to pump intensity. The growing rate of laser intensity along the traveling distance z in the gain medium depends on the gain coefficient by,

$$\frac{dI_L}{dz} = \alpha_L(\omega) \cdot I_L(0), \quad 2.4$$

where I_L is the laser intensity, z is the position in a stimulated medium. $I_L(0)$ is the initial intensity generated by produced spontaneous emission. Therefore, the laser intensity is amplified exponentially along the propagation direction, such that,

$$I_L(z) = I_L(0)e^{\alpha_L \cdot z}. \quad 2.5$$

2.2 Spontaneous Raman Scattering

Scattering is an ultrafast interaction of light and matter. An incident photon transfers its energy to an electron in atom. The electron is excited into virtual state and immediately release energy back to the ground state. This process allows the atom to perform as a light source. Scattering process can be categorized into two groups based on the change of its released photon energy. Energy diagram of scattering processes are shown in Figure 2.2.

Elastic scattering occurs when scattered photon energy is the same to the incident photon energy. Rayleigh scattering is one of the elastic scattering processes which wavelength of the scattered light is not shifted from the incident wavelength.

Inelastic scattering defines for the scattering process that deals with gain or loss of scattered photon energy. Raman scattering was first experimentally observed in liquids by C.V. Raman and K.S. Krishnan (Raman and Krishnan, 1928). It can be categorized into two types: Stokes and anti-Stokes Raman scattering. Stokes Raman scattering is a process that electrons in ground state is pumped into a virtual state, rapidly release the energy, and fall to molecular vibrational mode in the ground state. The scattered wavelength shifts toward red spectrum compared to the incident wavelength. In the reverse case, anti-Stokes Raman scattering is the process of electrons transition from the vibrational modes to virtual state and fall back further to the ground

state. This anti-Stokes Raman scattering produces a higher photon energy compared to the incident light. The scattered wavelength is shifted toward blue spectrum with respect to the incident wavelength.

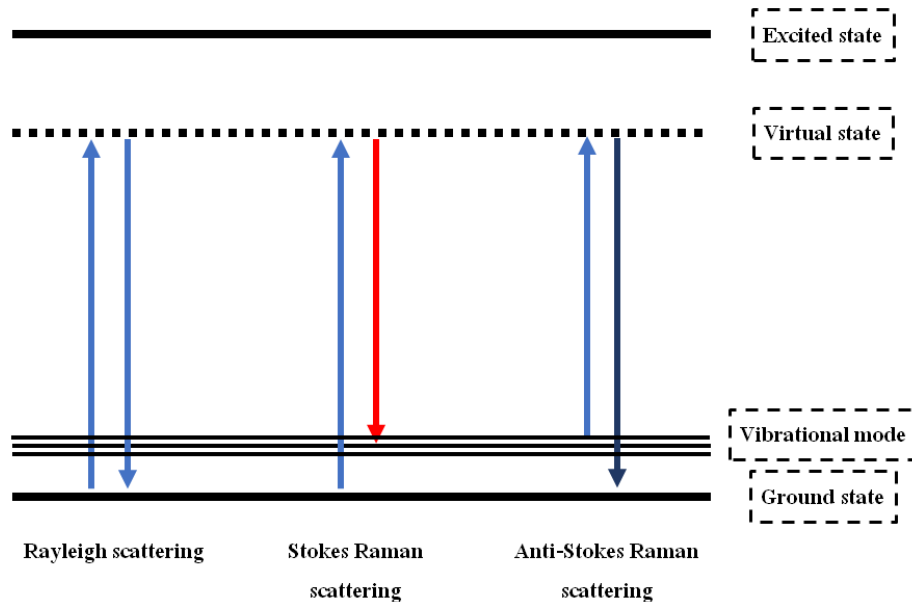


Figure 2.2 Energy diagram of scattering processes.

The value of the shifted wavelength relates to the chemical bonding type of the atom. Raman shift can be calculated by,

$$\Delta\omega = \left(\frac{1}{\lambda_p} - \frac{1}{\lambda_s} \right) \times 10^7, \quad 2.6$$

where $\Delta\omega$ is Raman shift in cm^{-1} , λ_p is the pump wavelength in nm, λ_s is the Stokes wavelength in nm. From definition of Stokes and anti-Stokes Raman scattering, value of $\Delta\omega$ is plus and minus, respectively. The collection of scattered light intensity at each wavelength constitutes Raman spectrum with specific peaks, referred to as “chemical fingerprint”. Example of Raman spectrum is shown in Figure 2.3.

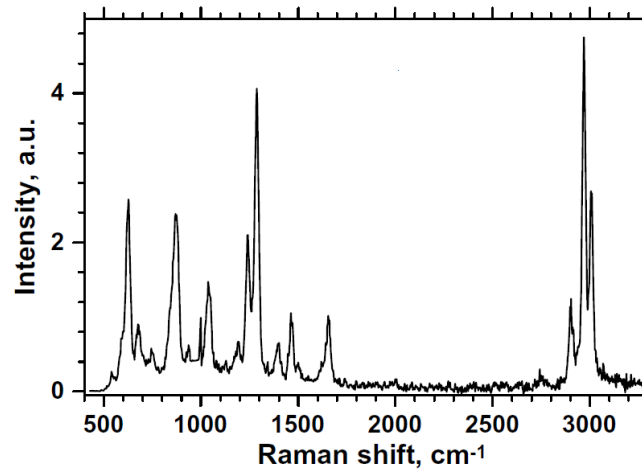


Figure 2.3 Example of Raman spectrum from Pentaerythritol Tetranitrate (PETN) (Nagli et al. 2008).

The theoretical prediction of Raman scattering can be considered through the polarizability of a molecule. The polarizability is the property determines the interact strength between a molecule and an external electric field through the induced dipole moment The induced dipole moment respective to the incident field is given by (Colthup, Daly and Wiberley, 1990),

$$\mathbf{p} = \alpha \mathbf{E}, \quad 2.7$$

where \mathbf{p} is the induced dipole moment, α is the polarizability, and \mathbf{E} is the incident electric field. The incident electric field can be written in the following form,

$$\mathbf{E} = \mathbf{E}_p \cos(2\pi\omega_p t), \quad 2.8$$

where \mathbf{E}_p is the amplitude of the incident electric field, and ω_p is the oscillating frequency of the pump electric field. The time-dependent induced dipole moment is,

$$\mathbf{p} = \alpha \mathbf{E}_p \cos(2\pi\omega_p t). \quad 2.9$$

Consider physical displacement, caused by vibrational of atoms in a molecule. It can be expressed by,

$$dq = q_0 \cos(2\pi\omega_v t), \quad 2.10$$

where q_0 is the maximum displacement from the equilibrium position, and ω_v is the vibrational frequency. For small displacement of the atom, the magnitude of polarizability of the molecule can be expanded using Taylor's series reads,

$$\alpha = \alpha_0 + \frac{\partial\alpha}{\partial q} dq, \quad 2.11$$

where α_0 is the polarizability of the molecular mode at equilibrium position. Substituting equation 2.10, the polarizability can be given by,

$$\alpha = \alpha_0 + \frac{\partial\alpha}{\partial q} q_0 \cos(2\pi\omega_v t). \quad 2.12$$

Substitute equation 2.12 into equation 2.9, we obtain the induced dipole moment by,

$$\mathbf{p} = \alpha_0 \mathbf{E}_p \cos(2\pi\omega_p t) + \frac{\partial\alpha}{\partial q} q_0 \mathbf{E}_p \cos(2\pi\omega_p t) \cos(2\pi\omega_v t). \quad 2.13$$

Using trigonometric identity, we achieve,

$$\begin{aligned} \mathbf{p} &= \alpha_0 \mathbf{E}_p \cos(2\pi\omega_p t) \\ &+ \left(\frac{\partial\alpha}{\partial q} \frac{Q_0 \mathbf{E}_p}{2} \right) \{ \cos[2\pi(\omega_p - \omega_v)t] + \cos[2\pi(\omega_p + \omega_v)t] \}. \end{aligned} \quad 2.14$$

It can be that the left-hand side of equation 2.14 is the induce dipole moment of the molecule. The polarization \mathbf{P} can be calculated by,

$$\mathbf{P} = N\mathbf{p} \quad 2.15$$

Where N is molecules density per unit volume. The polarization acts as a source term for electromagnetic wave radiation. On the right-hand side, radiation terms can be categorized in to three components with different frequencies. The first term relates to elastic scattering, for which the frequency of scattered light is unchanged. The second term is Stokes Raman scattering with down-shifted frequency ($\omega_p - \omega_v$). As explained above, this term gives a scattered light with longer wavelength than incident wavelength. The final term is anti-Stokes Raman scattering with up-shifted frequency ($\omega_p + \omega_v$). This case gives a shorter wavelength of scattered light compared to the incident light.

Resonance Raman scattering is a process that Raman efficiency is enhanced when using high energy photon excitation. It leads to the transition of electrons from ground state to virtual state, near to electronic state. It can increase the Raman scattering efficiency by two orders of magnitude. In general, Raman cross section depend on the frequency of excitation photon can be explained by,

$$\sigma_{Res} = K\omega_p(\omega_p - \Omega)^3 \left[\frac{\omega_i^2 + \omega_p^2}{(\omega_i^2 - \omega_p^2)^2} \right]^2, \quad 2.16$$

where σ_{Res} is the Raman cross section, K is a constant, ω_i is the frequency of the excitation state, ω_p is the frequency of the pump radiation, and $\Omega = \omega_p - \omega_i$ is the frequency associated with transition energy of vibrational energy state. Basically, light frequency relates to it wavelength. Behavior of Raman cross section respect to the wavelength is shown, in Figure 2.4. Raman cross section is significantly increase when the Raman active molecule was excited via ultraviolet wavelength.

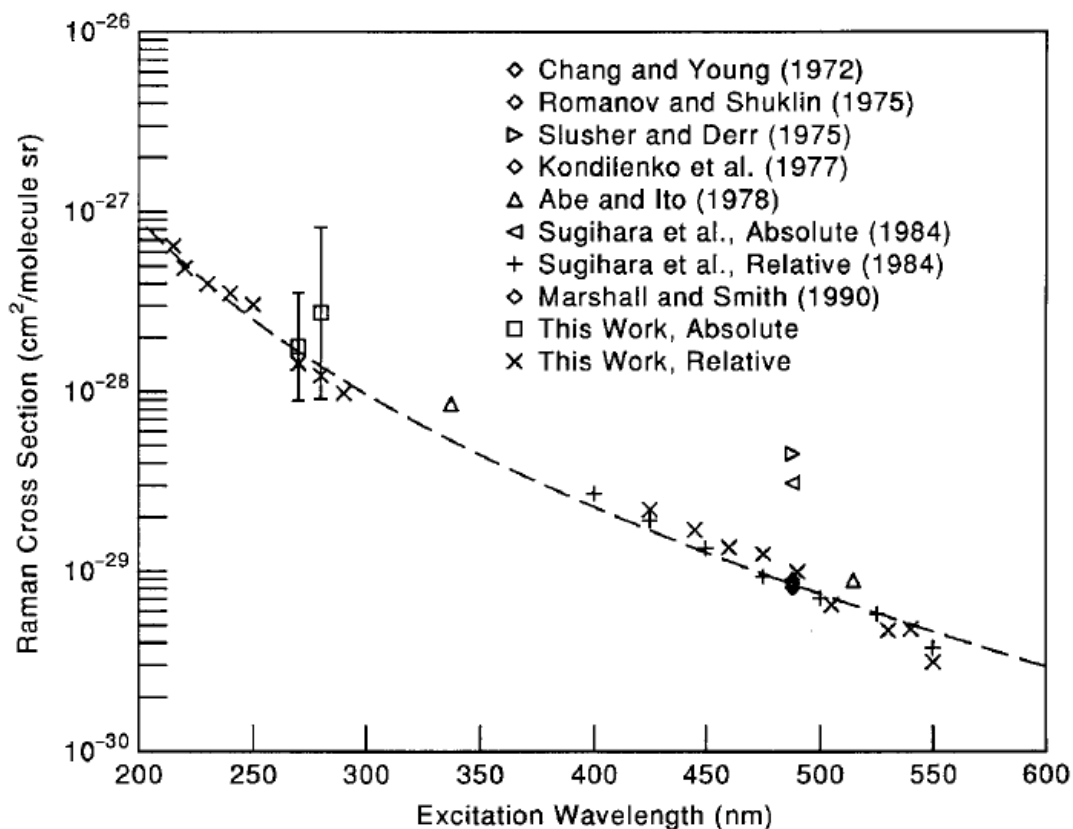


Figure 2.4 Behavior of Raman scattering cross section respects to the excitation wavelength (Faris and Copeland, 1997).

2.3 Stimulated Raman Scattering

Nonlinear material allows photons to interact each other. This material contains the property governed by the efficiency of multiphoton interaction of the molecule called “nonlinear susceptibility”. Stimulated Raman scattering (SRS) is one of the third-order nonlinear processes. This process allows the amplification of the Raman wavelength. The difference of an angular frequency of a pump pulse ω_p and a Stokes pulse ω_s must be equal to an angular frequency of the vibrational mode Ω of the molecule. The SRS can be schematically explained by Figure 2.5, where beams on the right hand of the medium are produced by the interaction in molecules of the sample as shown in Figure 2.6. This results in the amplification of Stoke beam.

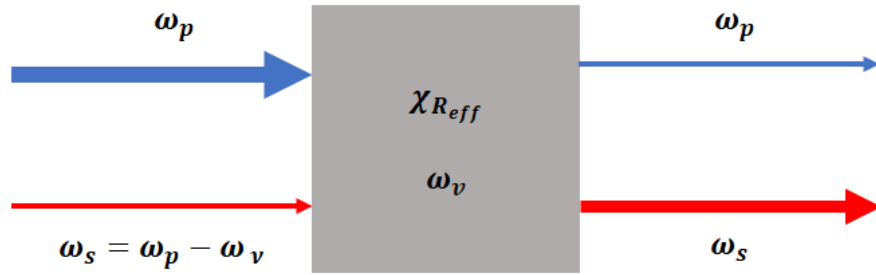


Figure 2.5 The schematic of the SRS process.

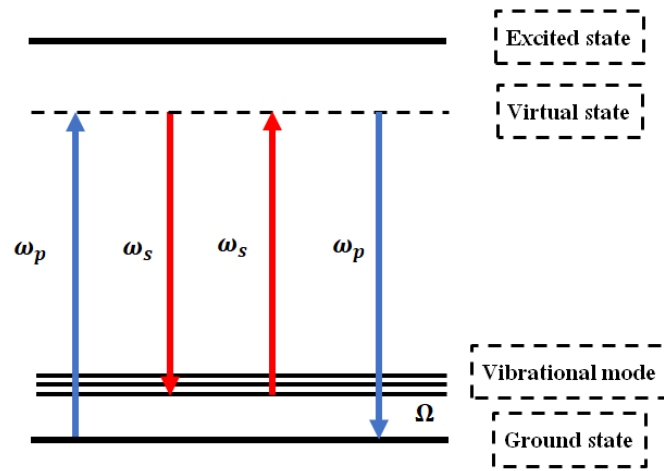


Figure 2.6 The schematic explains a molecular scale interaction of the SRS process.

The source of SRS signal can be described by the form of nonlinear polarization. Nonlinear polarization is generated from the coupling of pump and Stokes fields through nonlinear Raman susceptibility explained by,

$$\mathbf{P}_{\omega_s}^{(3)} = 6\epsilon_0\chi_R^{(3)} : \mathbf{E}_p\mathbf{E}_p^*\mathbf{E}_s, \quad 2.17$$

where ϵ_0 is permittivity of free space, $\chi_R^{(3)}$ is the third-ranked nonlinear susceptibility respect to Raman signal, \mathbf{E}_p is the electric field of pump wavelength and \mathbf{E}_s is the electric field of Stokes wavelength. Nonlinear Maxwell's equation for Stokes signal can be written by,

$$\nabla^2 \mathbf{E}_s - \frac{n_s^2}{c^2} \frac{\partial^2}{\partial t^2} \mathbf{E}_s = \frac{1}{\epsilon_0 c^2} \frac{\partial^2}{\partial t^2} \mathbf{P}^{(3)}_{\omega_s}, \quad 2.18$$

where n_s is the refractive index of the medium at ω_s , and c is the speed of light in free space. As shown in equation 2.18, nonlinear polarization acts as a source term of electromagnetic wave at Stokes wavelength. Substitute $E_s = A_s e^{i(k_s z - \omega_s t)}$ and equation 2.17 into equation 2.18, we obtain the coupled amplitude equation,

$$\frac{\partial A_s}{\partial z} = \frac{3i\omega_s^2}{k_s c^2} \chi_R(\omega_s) |A_p|^2 A_s(\omega_s), \quad 2.19$$

where k_s is the wavevector of Stokes signal, A_p is the amplitude of pump signal and A_s is the amplitude of Stokes signal. Applying relation of $I_i = 2n_i \epsilon_0 c |A_i|^2$, we can determine the Stokes intensity amplification rate,

$$\frac{\partial I_s}{\partial z} = \alpha_s I_s(0), \quad 2.20$$

where the SRS gain coefficient can be defined by,

$$\alpha_s = \frac{3}{2} \frac{i\omega_s^2}{k_s n_p \epsilon_0 c^3} \chi_R(\omega_s) I_p. \quad 2.21$$

The $\chi_R(\omega_s)$ is in form of complex number written by (Boyd, 2008),

$$\chi_R(\omega_s) = \chi'_R + i\chi''_R = \frac{\epsilon_0 \left(\frac{N}{6m}\right) \left(\frac{\partial \alpha}{\partial q}\right)^2}{\omega_v^2 - \Omega^2 + 2i\Omega\gamma}, \quad 2.22$$

where N is the number of molecules, m is the effective mass of molecules, α is the polarizability, q is the internuclear displacement, γ is the damping constant, and $\Omega = \omega_p - \omega_s$. Here, the frequency-dependent behavior of χ'_R and χ''_R are shown in Figure 2.7. When the condition $\omega_s = \omega_p - \omega_v$ matches, $\chi_R(\omega_s)$ becomes an imaginary term,

$$\chi_R(\omega_s) \rightarrow i\chi_R'' = \frac{-i\epsilon_0 \left(\frac{N}{6m}\right) \left(\frac{\partial\alpha}{\partial q}\right)^2}{2\Omega\gamma}. \quad 2.23$$

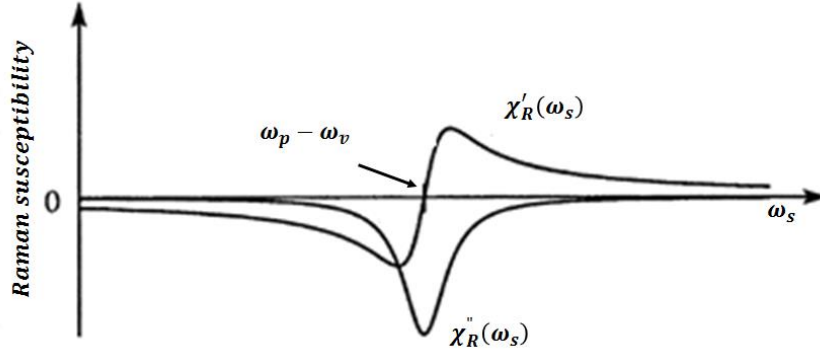


Figure 2.7 The behavior of χ_R' and χ_R'' respect to Stokes frequency.

So α_s becomes a real number which can be expressed by,

$$\alpha_s = \frac{3}{4} \frac{\omega_s \left(\frac{N}{6m}\right)}{\Omega\gamma n_s n_p c^2} I_p. \quad 2.24$$

The Stokes intensity of SRS process at the matched condition is amplified along the propagation direction by,

$$I_s(z) = e^{\alpha_s z} I_s(0), \quad 2.25$$

where $I_s(0)$ is the initial Stokes intensity, and I_p is the pump intensity.

It is noted that, SRS is an automatically phase-matched phenomenon due to terms of vector for the pump and Stoke pulse are self-cancelling while solving the nonlinear Maxwell's equation for SRS process. Therefore, this process is unconcerned for the propagation directions of the beams involved. Basically, SRS process can be categorized into two regimes by the comparison of pump pulse duration (T_p) and optical dephasing time of the process (T_2). The gain coefficient

explained above is considered as steady-state ($T_p \gg T_2$). Another regime is transient gain ($T_p \ll T_2$), in which the intensity of the SRS can be calculated by,

$$I_s(z) = e^{(\alpha_t z - \pi c \Omega T_p)}, \quad 2.26$$

where,

$$\alpha_t = \left(\frac{32\pi^2 c^2 N}{\hbar \omega_s^3 n_s^2} \left(\frac{\partial \alpha}{\partial q} \right)^2 T_p I_p \right)^{\frac{1}{2}}. \quad 2.27$$

The equation shows that SRS process can be produced easier using transient gain mechanism. The SRS, in this gain regime, must be pumped using ultrashort pulse e.g. picosecond pulsed laser (Chunaev and Karasik, 2006). Order of T_2 is in picosecond regime, therefore, the SRS process must be faster than this time window to achieve high efficiency.

2.4 Absorption and effective gain efficiency

As occur in every electromagnetic wave travelling in a medium, the wave experiences loss through absorption process. Furthermore, at intense electric field, stimulated absorption can also occur. Fractional rate of population in ground state related to the absorption process, can be explained by (White, 1981),

$$\alpha_a = \frac{N_1 T_p}{2n_p^2 \epsilon_0} K I_p, \quad 2.28$$

where N_1 is the number of electrons in ground state, n_p is the refractive index of the medium respect to the pump wavelength, T_p is the incident pulsed duration, K is the efficiency of the absorption, and I_p is the intensity of pump radiation. As shown in the equation, absorption of the medium depends on the intensity of the beam. Thus, the intense beam will encounter increasing absorption. This can lead to significant loss of pump energy.

Effective gain efficiency of SRS must be resulted from subtraction of gain term and absorption term as,

$$\alpha_{eff} = \alpha_s - \alpha_a. \quad 2.29$$

Intensity of SRS beam as steady-state gain mechanism reads,

$$I_s(z) = e^{\alpha_{eff}z} I_s(0). \quad 2.30$$

Thus, equation shows that threshold phenomenon of laser signal can be found. Both terms of gain and loss coefficient is nonlinear term, since it depends on pump intensity. The amplified light via SRS process must surpass loss in order to turn on lasing process.

2.5 Behavior of light in a disordered medium

When excite a random Raman gain medium, all of the abovementioned scattering processes, including spontaneous or stimulated Raman scattering can be generated as shown in Figure 2.8. Also, the elastic scattering resulting from multiple scattering upon the particles can predominantly occur for both pump and Raman wavelength. This process plays a key role allowing the pump and Raman power to dwell in the medium for sufficiently long time and create a required optical feedback. The Raman signal can be enhanced by SRS process when the pump and Raman photons are coupled, leading to further conversion of pump power to Raman scattering.

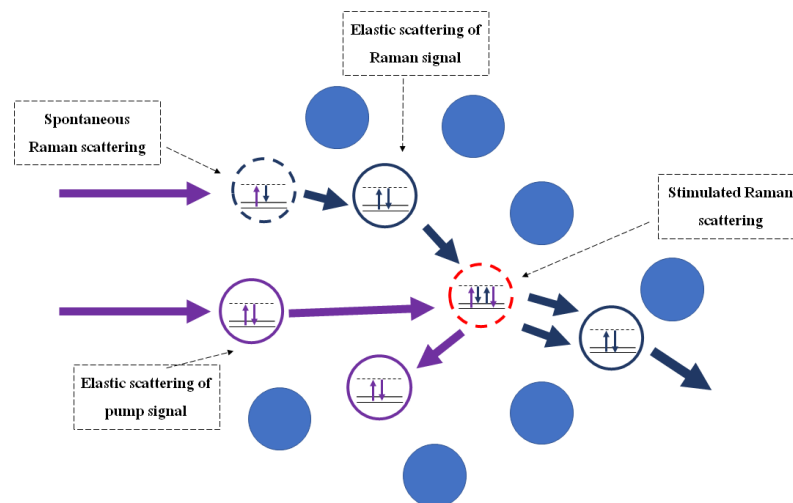


Figure 2.8 Scattering processes in a Raman gain medium.

Photons penetration in a disordered medium is an intriguing topic. The model can be used to explain several behaviors of light in daily-life situation e.g. the scattering property of cloud for weather forecasting, the prediction of colloid concentration in pharmaceutical application. Multiple scattering can be generated when light propagates in a random medium. Basically, multiple scattering allows particles in the medium to behave as light sources. This process allows the medium to confine wave energy in its internal structure, similar to an optical resonator. The incident light diffuses in a sample for sufficiently long time. In Raman random laser, the confined light from multiple scattering process can be used as an optical feedback. Both pump and Raman light are confined in the medium. Behavior of light in the disordered medium is hard to predict via Maxwell's equation. Diffusion nature of light is applied to estimate its behavior in the medium. The energy density of light penetrated in a very large sample i.e. sample dimension is much larger than transport mean free path, can be explained via a diffusion rate equation (Letokhov, 1968),

$$\frac{\partial W(\vec{r}, t)}{\partial t} = D\nabla^2 W(\vec{r}, t) + \sum \frac{v}{l_i} W(\vec{r}, t), \quad 2.31$$

where $W(\vec{r}, t)$ is the photon energy density, $D = cl_t/3n$ is the diffusion coefficient, v is the velocity of light in the medium, and l_i is the coefficient length which correspond to the varying of the energy density. l_t is the transport mean free path which is the average distance of light penetration in the medium. The gain length $l_g = 1/\alpha_s$ is, the shortest distance that light can be amplified by factor of e . The absorption length $l_a = 1/\alpha_a$ is the distance that light intensity is absorbed by factor of e .

In the Raman random lasing process, the pump pulse encounters the loss from the stimulated absorption process and coupling loss to generate Stokes power. Rate equation of energy density for pump wavelength reads,

$$\frac{\partial W_p(\vec{r}, t)}{\partial t} = D\nabla^2 W_p(\vec{r}, t) - \left(\frac{vW(\vec{r}, t)}{l_g} \right)_s - \left(\frac{vW(\vec{r}, t)}{l_a} \right)_p + \frac{I_p}{l_t}, \quad 2.32$$

where I_p is the pump laser intensity. For the Stokes wave, it experiences both gain from stimulated Raman emission and loss from the absorption process. The rate equation of the energy density for Raman wavelength reads,

$$\frac{\partial W_s(\vec{r}, t)}{\partial t} = D\nabla^2 W_s(\vec{r}, t) + \left(\frac{vW(\vec{r}, t)}{l_g}\right)_s - \left(\frac{vW(\vec{r}, t)}{l_a}\right)_s. \quad 2.33$$

Equation 2.32 and 2.33 are coupled equations. The first term on the right-hand side of both equations are energy diffusion term. The second term is in the same notation which explains about gain of the Stokes wavelength. This term has the role of loss for pump wavelength. The third term of both equations are loss term from absorption of the medium which is dramatically enhanced under intense pump radiation. In addition, the fourth term of equation 2.32 is the pump gain from the incident pulse.

Laser threshold of light penetrated in a disordered media can be estimated through the critical volume, calculated by,

$$V_{cr} = \left(\frac{l_t l_g}{3}\right)^{3/2}. \quad 2.34$$

Raman laser can be generated from the disordered medium when $V \geq V_{cr}$ where $V = (l_t l_a / 3)^{3/2}$ is the scattering volume covered by the penetrating pulsed energy (Noginov et al., 2004). The conceptual diagram of both signals is shown in Figure 2.9. Pump signal is lost while Stokes (Raman) signal is gained in the Raman gain medium.

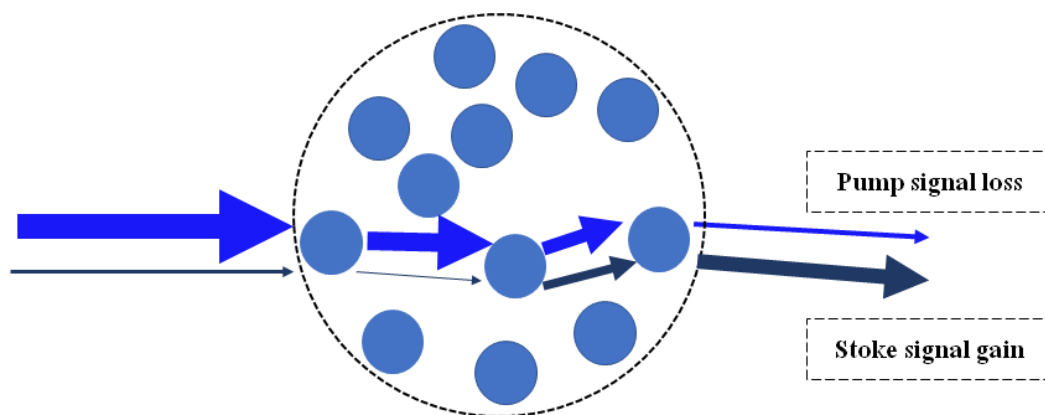


Figure 2.9 Conceptual schematic of pump and Stoke radiation intensity in a Raman gain medium.

CHAPTER 3

METHODOLOGY

In this chapter, the description of the methodology employed in this thesis is presented. The methodology is separated into three sections. Section 3.1 discusses about sample preparation and characterization methods. Experiments used to investigate the evidences of resonant Raman random lasing were explained in section 3.2. Also, the simulation model based on COMSOL Multiphysics was carried out to gain the insight of electromagnetic wave behavior in a disordered medium. This simulation is discussed in section 3.3.

3.1 Sample preparation and standard characterization methods

Barium nitrate (GRM351-500G, HIMEDIA) ($\text{Ba}(\text{NO}_3)_2$), was selected as a Raman-active disordered medium in this study, since it has high stimulated Raman gain coefficient for a quasi-steady-state (nanosecond pulsed laser) pump ($\sim 47 \text{ cm/GW}$) (Lisinetskii et al., 2005). This material has a comparatively long dephasing time ($T_2 \sim 26.5 \text{ ps}$), which relates to high efficiency of SRS process in steady-state condition. (Chunaev and Karasik, 2006). Since the selected $\text{Ba}(\text{NO}_3)_2$ is naturally in powder form, in principle, it can support substantial multiple scattering in its structure. Besides, $\text{Ba}(\text{NO}_3)_2$ contains NO_3^- group in its composition similar to many explosive and hazardous compounds, where the NO_3^- Raman peak is distinctive to detect. $\text{Ba}(\text{NO}_3)_2$ has Raman line at 79.7 cm^{-1} , 139.8 cm^{-1} , 130.2 cm^{-1} , 731.4 cm^{-1} , 1045.9 cm^{-1} , 1352 cm^{-1} , 1384.2 cm^{-1} , and 1401.7 cm^{-1} . The strongest Raman shift of $\text{Ba}(\text{NO}_3)_2$ is at 1045.9 cm^{-1} . The Raman spectrum of the sample for this thesis was confirmed via Raman microscope spectrometer (RAMANforce, Nanophoton, Figure 3.1).



Figure 3.1 Standard Raman spectroscopy characterization system.

For sample preparation method, the $\text{Ba}(\text{NO}_3)_2$ powder was dried in ambient pressure using a baker, heated at 100 °C for overnight. After drying process, the sample was grinded to reduce particle size and improve size homogeneity. At this step, a powder sample was designated as a loosely-packed sample. On the other hand, a closely-packed powder sample was prepared by taking another step further involving sample compression. High pressure (~300 MPa) was applied to the loosely-packed sample using a pellet preparation tool as shown in Figure 3.2.



Figure 3.2 Pellet preparation tool in the process of preparing closely-packed sample.

The fill factor of a sample was calculated via the comparison of sample density and the $\text{Ba}(\text{NO}_3)_2$ crystal density as,

$$\text{Fill factor} = \frac{\rho_{\text{sample}}}{\rho_{\text{crystal}}}, \quad 3.1$$

where ρ_{sample} is the density of powder sample, and ρ_{crystal} is the density of a pure $\text{Ba}(\text{NO}_3)_2$ crystal, which is equal to 3.24 g/cm^3 . The particle size of the sample was determined via scanning electron microscope (SEM, TM3030Plus, Oxford Instrument). The SEM was set at magnification of 100X, 500X, and 4000x with acceleration voltage 15 kV. Particle size was measured from 300 randomly selected particles. The characterization via SEM machine is shown in Figure 3.3.

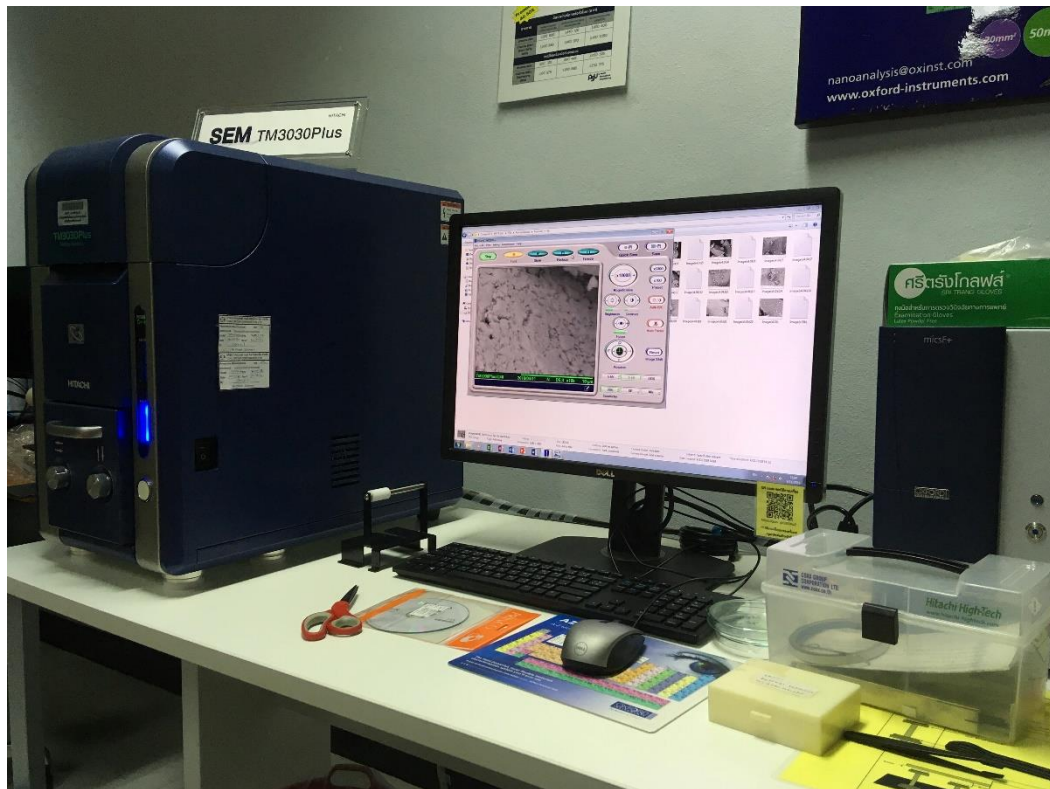


Figure 3.3 Scanning electron microscope machine.

3.2 Study of Raman random lasing

This section discusses about the optical setup to study Raman random lasing near the resonant condition using disordered barium nitrate samples. The detail of optical setup together with information of the studied parameters are explained as followed.

Overall schematic setup is presented in Figure 3.4. The pump of an optical parametric oscillator system (OPO laser) (Opolette 355, OPOTEK), at wavelength of 355 nm, 10 ns pulse width, with 20 Hz repetition rate, was used as a pump pulse to excite stimulated Raman emission at near resonance condition. The pump beam polarization can be controlled via an optical component set (Figure 3.5). The intensity of the pump pulse can be continuously adjusted by changing the relative angle between the pump polarization (in vertical direction) and the axis of a Glan-laser polarizer (LOGLPC-10, Lighten optics). To eliminate any effect of preferred direction of polarization onto sample, the quarter wave plate (LOWPCZ-25.4Q-355, Lighten Optics) was applied to convert the initially linear polarization of the pump pulse to a circular

polarization. The bandpass filter (FLH355-10, Thorlabs) was applied into the optical component line to reject any possible fluorescence and unwanted wavelengths from the OPO with blocking OD > 5. The pump beam was reduced into a smaller size, i.e. from 4 mm to 2 mm, and collimated using a beam-size reducer, composed of a pair of a plano-convex (LOPCXF25.4-150, Lighten Optics) and a plano-concave lens (LOPCCF25.4-75, Lighten Optics) separated by a proper distance. All lenses used here are made of UV-grade fused silica. This modified pump beam was used as incident pulse for the following experiment.

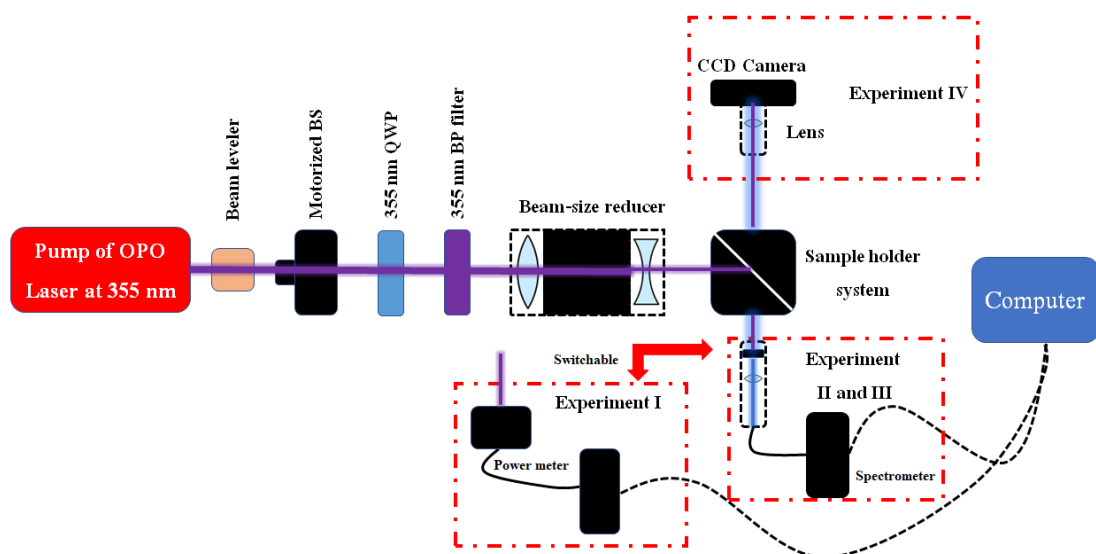


Figure 3.4 A schematic of the setup to observe resonant Raman random lasing signal. The setup used a pump of OPO laser at 355 nm to pump the samples.

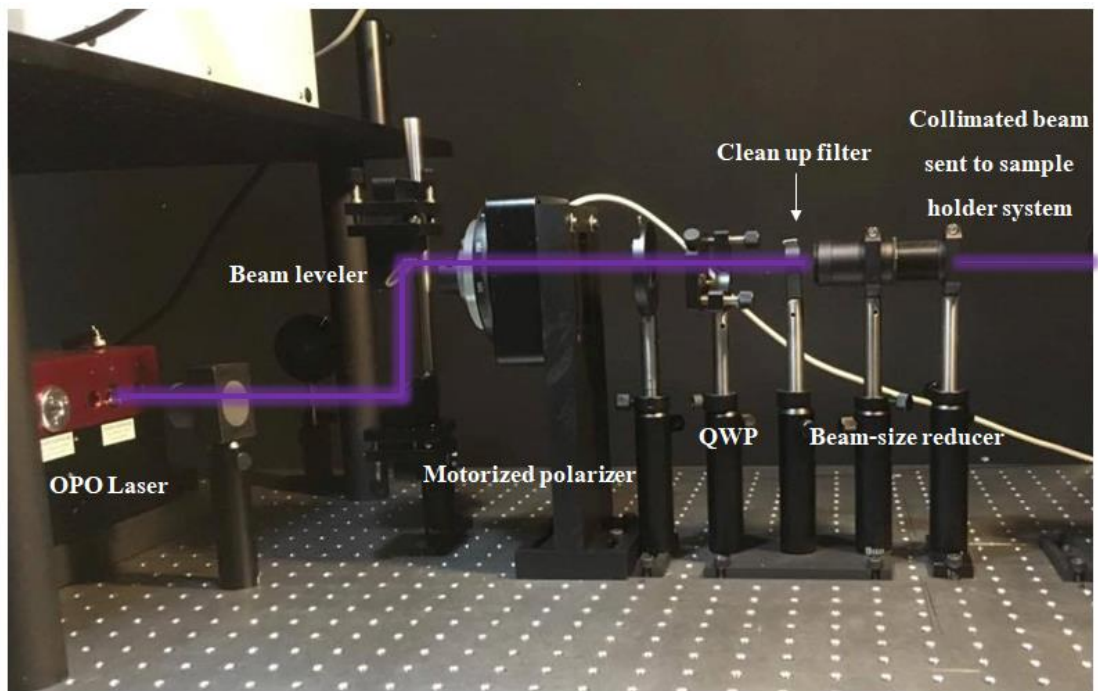


Figure 3.5 Optical component line for preparing the incident pulse.

3.2.1 Experiment I: control of the pump pulse intensity

In this experiment, the pump pulse intensity is measured. This pump intensity was varied by changing the direction of the polarizer axis via a motorized rotary stage. The pump pulse energy was partially reflected (~10%) into the power meter as shown in Figure 3.6. The incident energy can be read through a power meter (PE10-C, Ophir optics). Intensity of the pump pulse can be calculated by

$$I = \frac{P}{A} = \frac{E}{\pi r^2 T_p} = \frac{10 \times E_{mea}}{\pi r^2 T_p}, \quad 3.2$$

where I is pulse intensity, E_{mea} is the measured pulsed energy, r is beam spot radius, and T_p is pulse duration. The measurement angle was set in a range between 10 to 80 degree.

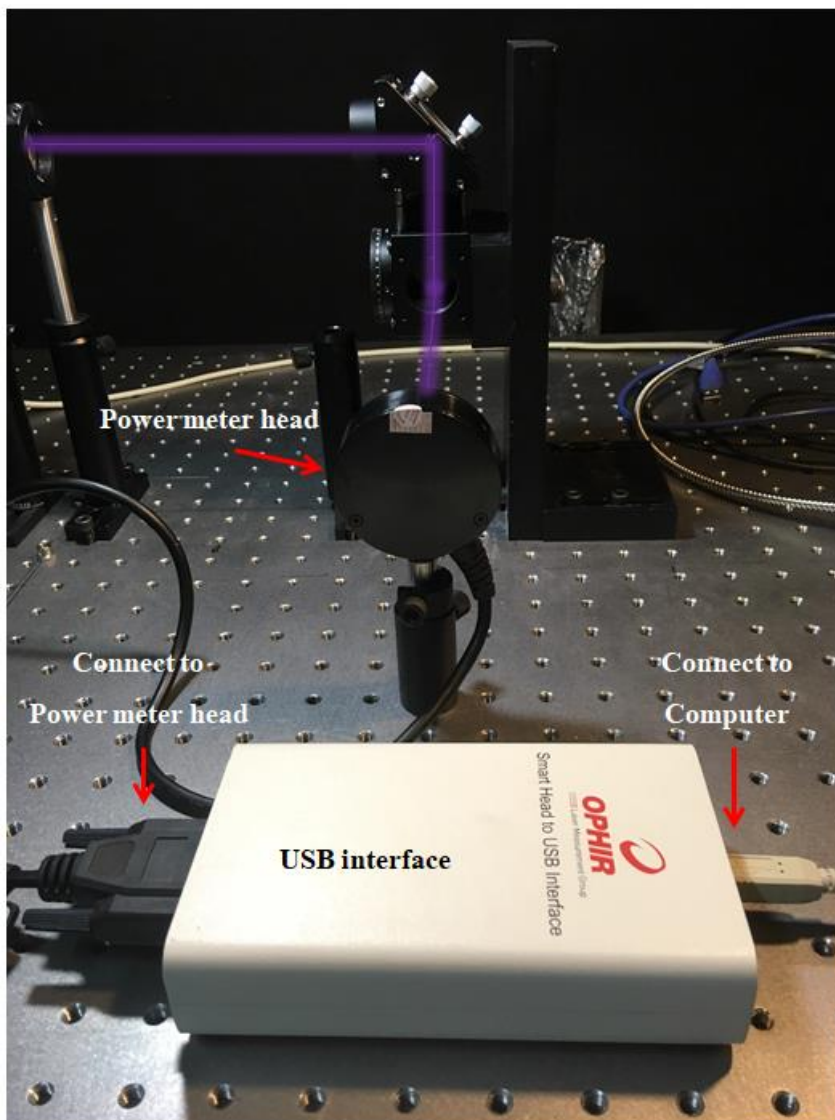


Figure 3.6 Setup for measurement of incident laser pulse.

3.2.2 Experiment II: Investigation of resonant Raman random lasing

In this experiment, resonant Raman scattering signal of the loosely-packed sample was detected under various pump pulse intensity, ranging from 0 to $\sim 21 \text{ MW/cm}^2$. The sample thickness was varied from 1 to 4 mm. The schematic of the setup is shown in Figure 3.7 (a). A sample holder system was constructed from an optical cage cube. The sample was set at the position to be radiated by the incident pulse. A UV fused silica mirror was placed at the center of the optical cage cube to reflect scattered light to optical coupling set. In the coupling set, the scattered light was filtered by a notch filter to reduce Rayleigh scattering signal strength. The signal

was coupled to an optical fiber by a plano-convex lens. Figure 3.7 (b) shows the sample holder system. Through the optical fiber, the scattered signal was delivered to a spectrometer (Exemplar plus, BWTEK) as shown in Figure 3.7 (c). The evidence of resonant Raman random laser can be observed at the principal Raman wavelength at ~ 369 nm or at the Raman shift ~ 1046 cm^{-1} , under varied pump intensity.

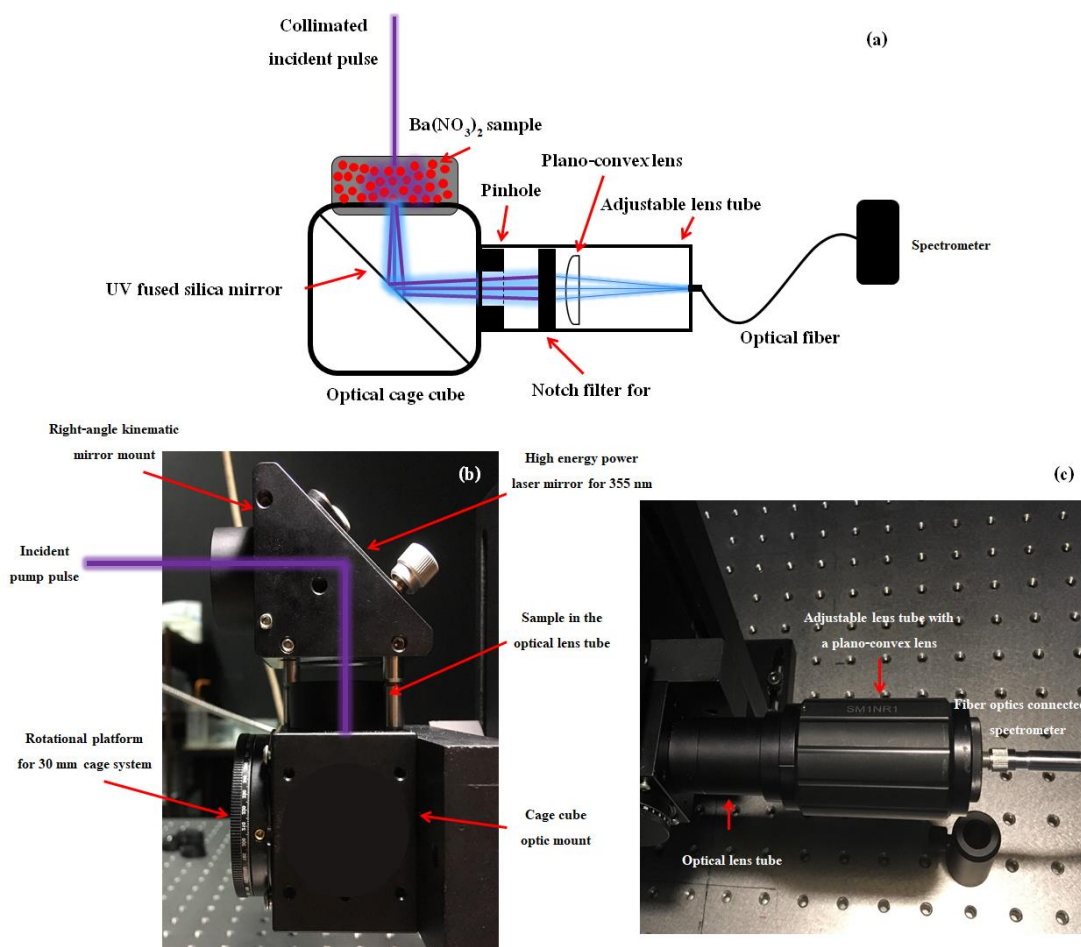


Figure 3.7 The setup for experiment II (a) Schematic of the setup (b) the sample holder system (c) Scattered signal coupling part.

3.2.3 Experiment III: Effect of sample packing structures

In this experiment, forward resonant Raman scattering signal was observed under the change of sample's packing structures. Loosely-packed sample and closely-packed sample at the same thickness were comparatively studied for the

effect of random Raman lasing efficiency. The studying conditions were set as the same to section 3.2.2 for both samples.

3.2.4 Experiment IV: Coherent backscattering

This experiment aims to measure the scattering properties of random media, including I_t and I_a . These values can be used to evaluate the degrees of multiple scattering and absorption inside random medium, which affect the efficiency of stimulated Raman emission process. Schematic for coherent backscattering setup (CBS) is shown in

Figure 3.8 (a). In the setup, the coupled-charged device camera (CCD camera) was used to capture scattered beam profile with respect to scattering angle. Samples of loosely-packed and closely-packed were used in this study. The samples were incident with the pump pulse at three intensities, 0.12, 6.90, and 21.30 MW/cm². The back scattered signal was detected by the CCD camera at fixed distance. The plano-convex lens was carefully adjusted and set at the optimum position for imaging the scattering spot. This setup can cover the maximum backscattered angle in a range of $\pm 4^\circ$. Figure 3.8 (b) shows the setup for CBS measurement. Scattered light intensity at any backscattering angle was detect.

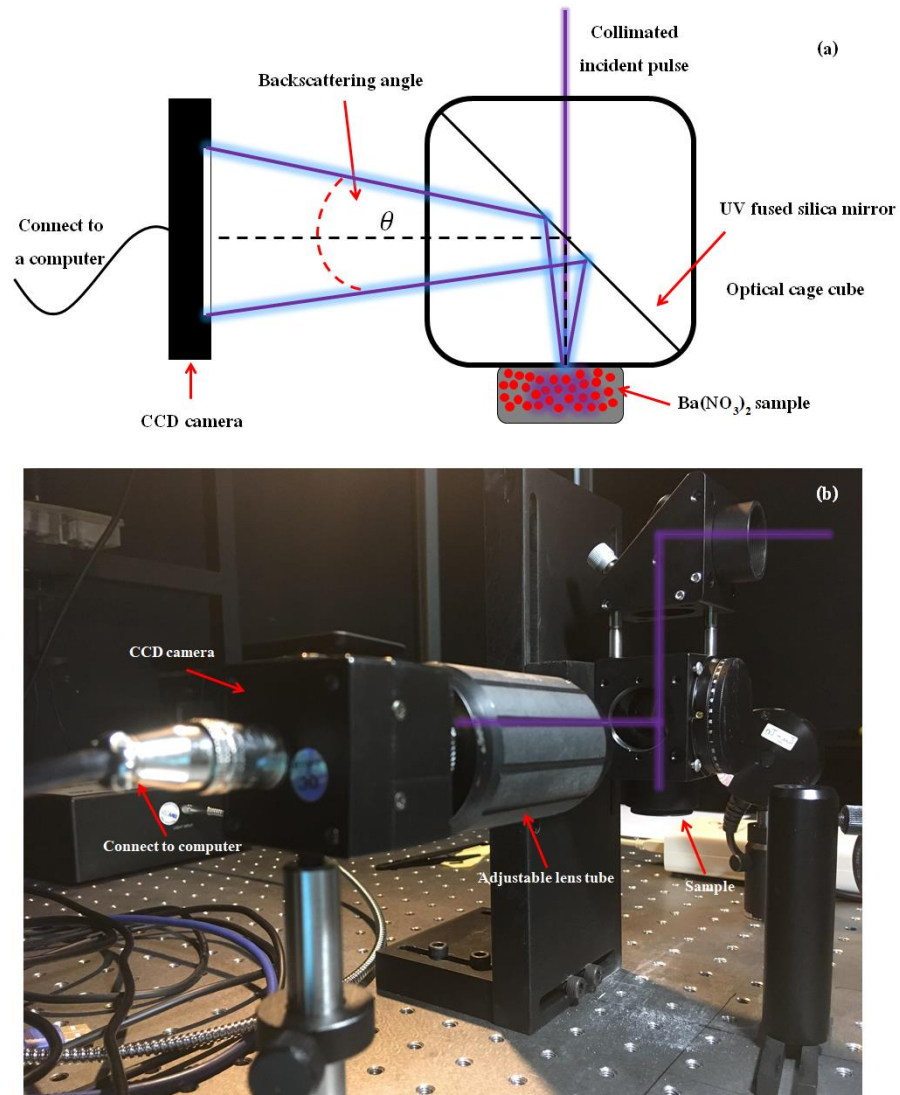


Figure 3.8 The setup for experiment IV (a) schematic of the setup (b) coherent backscattering setup.

This process results as a graph of the scattered light intensity versus backscattered angle as shown in Figure 3.9. By fitting the experimental result with equation 3.4. The transport mean free path (l_t) and absorption length (l_a) related to the internal geometry of a sample can be estimated. The normalized angular shape of backscattered light intensity (γ_c) can be given by (Ramakrishna and Rao, 2000),

$$\begin{aligned}
\gamma_c(\theta, l_t, l_i) = & \frac{3e^{-\eta L}}{2l_t^3 \beta \sinh[\beta(L + 2z_0)]} \frac{1}{(\eta^2 + \delta^2 - \beta^2)^2 + (2\beta\delta)^2} \\
& \left\{ \frac{2\beta}{\eta} (\beta^2 + \delta^2 - \eta^2) \sinh[\beta(L + 2z_0)] \sinh(\eta L) \right. \\
& + 2(\eta^2 + \delta^2 + \beta^2) \cos(\delta L) \\
& + 2(\eta^2 + \delta^2 - \beta^2) \cosh[\beta(L + 2z_0)] \times \cosh(\eta L) \quad 3.3 \\
& + 4\beta\eta \sinh(\beta L) \sinh(\eta L) \\
& - 2(\eta^2 + \delta^2 + \beta^2) \times \cosh(\beta L) \cosh(\eta L) \\
& - 2(\eta^2 + \delta^2 - \beta^2) \cosh(2\eta z_0) \cos(\delta L) \\
& \left. - \beta\eta \sinh(2\beta z_0) \sin(\delta L) \right\},
\end{aligned}$$

where $\beta = \sqrt{(3/l_t l_a + q_{\perp}^2)}$, $q_{\perp} = (2\pi/\lambda)\sin\theta$, $\delta = (2\pi/\lambda)(1 - \cos\theta)$, $\eta = (1 + 1/\cos\theta)/2l_t$, $z_0 = 0.71l_t$, θ is the backscattering angle, and λ is the wavelength.

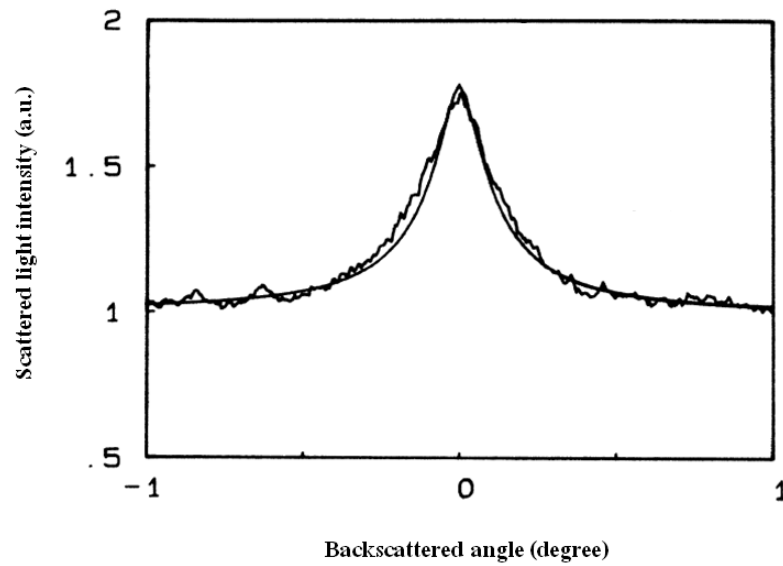


Figure 3.9 Coherent backscattered peak which is the plot of scattered light intensity versus backscattered angle (Akkermans, Wolf and Maynard, 1986).

3.3 Simulation studying via COMSOL Multiphysics

In this section, finite different time domain simulation based on COMSOL Multiphysics is presented. The simulation is used to investigate the behavior

of light penetrating in a multiple scattering sample. The detail of the simulation is explained as follow.

3.3.1 The geometries

A spherical particle with size equivalent to the value obtained from experiment was randomly generated. In particular, particle size in a range 0.9 ± 0.2 μm , with Gaussian distribution similar to the most probable particle size of particles used in the experiment, was randomly created. The fill factor of the geometry was varied as 0.25, 0.5, and 0.8. The particle position was randomly selected inside a square domain with length 25 μm . The refractive index of $\text{Ba}(\text{NO}_3)_2$ particle is set at 1.5756 (Zverev et al., 1999), The created geometry was surrounded by air background, a rectangle domain with size 50 x 75 μm . The maximum mesh size for the simulation was set to be 0.3 μm . Figure 3.10 (a)-(c) show the created geometries with randomized particle packing inside a square domain.

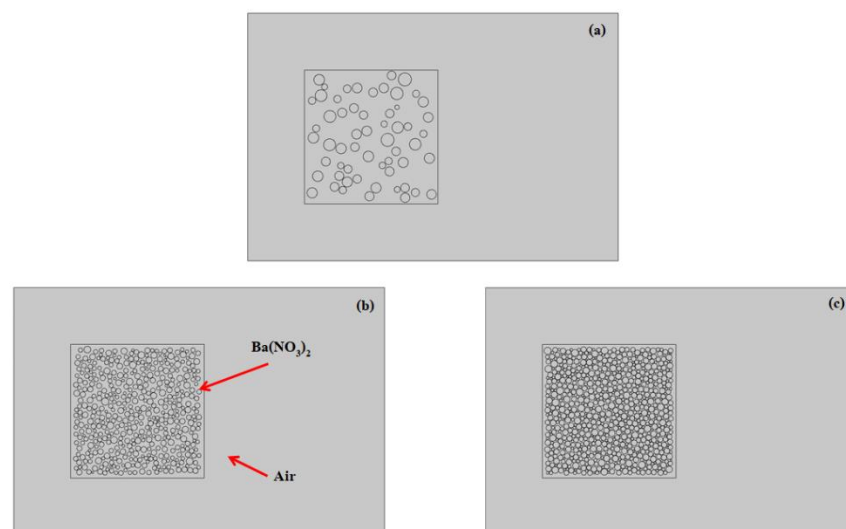


Figure 3.10 The created structure of (a) Fill factor = 0.25 (b) Fill factor = 0.5 (loosely-packed sample), and (c) Fill factor = 0.8 (closely-packed sample).

3.3.2 Transient electromagnetic wave

COMSOL Multiphysics simulation of transient electromagnetic wave was applied to the geometries. The governing equation of the simulation is the wave equation in magnetic potential form expressed by,

$$\nabla \times (\nabla \times \mathbf{A}) + \mu_0 \frac{\partial}{\partial t} \left(\epsilon_0 \epsilon_r \frac{\partial \mathbf{A}}{\partial t} \right) = 0, \quad 3.4$$

Where \mathbf{A} is the vector potential of magnetic field, μ_0 is the electric permeability of the free space, ϵ_0 is the electric permittivity of the free space, and $\epsilon_r = n^2$ is the relative permittivity of the medium, The simulation based on dielectric, non-magnetic material which defines $\sigma = 0$, and $\mu_r = 1$. The above equation can be decoupled to electric (\mathbf{E}) and magnetic (\mathbf{H}) fields from,

$$\mathbf{E} = -\nabla\phi - \frac{\partial \mathbf{A}}{\partial t}, \quad 3.5$$

$$\mathbf{H} = \frac{1}{\mu} (\nabla \times \mathbf{A}), \quad 3.6$$

where ϕ is the electric scalar potential.

3.3.3 Boundary conditions

A Gaussian beam was generated in study of time-dependent EM wave. The electric field of the incident pulse was set as in-plane polarization. The equation of electric field respective to the gaussian beam was written by,

$$\begin{aligned} \mathbf{E} = E_0 \sqrt{\frac{w}{w(x)}} \exp\left(-\frac{(y-y_0)^2}{w(x)}\right) \cos(k_0 ct - k_0 x + \eta(x) \\ - k_0) \frac{(y-y_0)^2}{2R(x)} \exp\left(-\frac{(t-t_0)^2}{T_p^2}\right), \end{aligned} \quad 3.7$$

where E_0 is the amplitude of the applied field, w_0 is the initial beam waist, $w(x) = w_0 \sqrt{1 + (x/x_0)^2}$ is the beam waist at any position, $\eta(x) = \tan^{-1}(x/x_0)/2$, $R(x) = x(1 + (x/x_0)^2)$, and T_p is the pump pulse duration. In this study, the initial condition was set $E_0 = 30 \text{ kV/m}$, $w_0 = 12.5 \text{ }\mu\text{m}$, $x_0 = \pi\omega_0^2/\lambda$, $\lambda = 355 \text{ nm}$, $y_0 = 20.5 \text{ }\mu\text{m}$, $k_0 = 2\pi/\lambda$, $t_0 = 25 \text{ fs}$, and $T_p = 10 \text{ fs}$.

3.3.4 Scattering boundary condition

Boundary conditions of the background rectangle were set to be scattering boundary condition. The Incident field was generated from the left-boundary of the rectangle. The other boundaries were set to be scattering boundary with no incident field as shown in Figure 3.11. The time frame of the simulation was assigned for 1000 fs. The time step for solving the wave equation is set to be 0.1 fs.

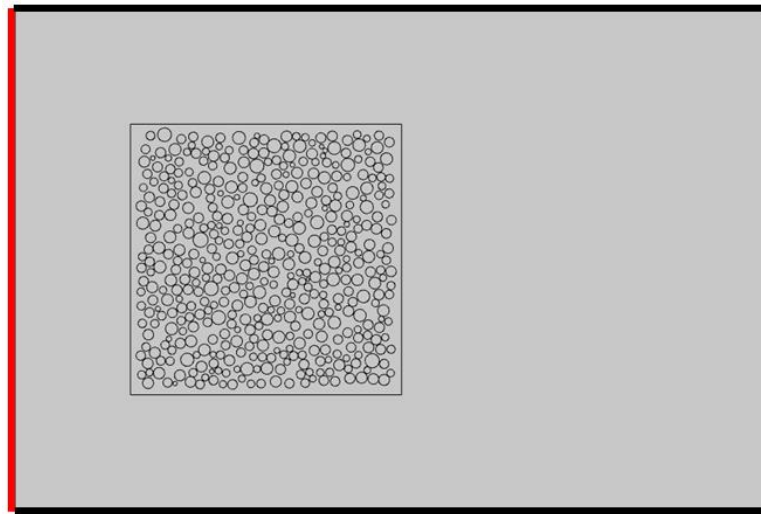


Figure 3.11 Example of boundary condition used for studying. The red line is scattering boundary with Gaussian incident field. The black line is scattering boundary with no field.

3.3.5 Evaluated values

Wave power proportional to $|E|^2$ was investigated to monitor laser pulse propagation in the random medium. Also, the light energy stored inside the powder structure was calculated by surface integration of $|E|^2$ over scattering geometry. The decay of energy stored over time was fitted to determine the time constant as,

$$E(t) = E_0 \exp\left(-\frac{t}{\tau}\right), \quad 3.8$$

where E_0 is the amplitude of energy stored in the structure, τ is the time constant.

3.4 Detection of Raman Random Lasing using a CCD camera

In this section, the test of using a simple CCD camera to detect RRL signal from some distance is explored. The scattering signal from a loosely-packed sample, excited by pump intensity 21.30 MW/cm^2 was captured from standoff distance of ~ 2 meters. A camera of a normal smart phone was equipped with a slit-less SA-100 grating (Star Analyzer) in order to produce a simple spectrogram image. The schematic of the setup is shown in Figure 3.12.

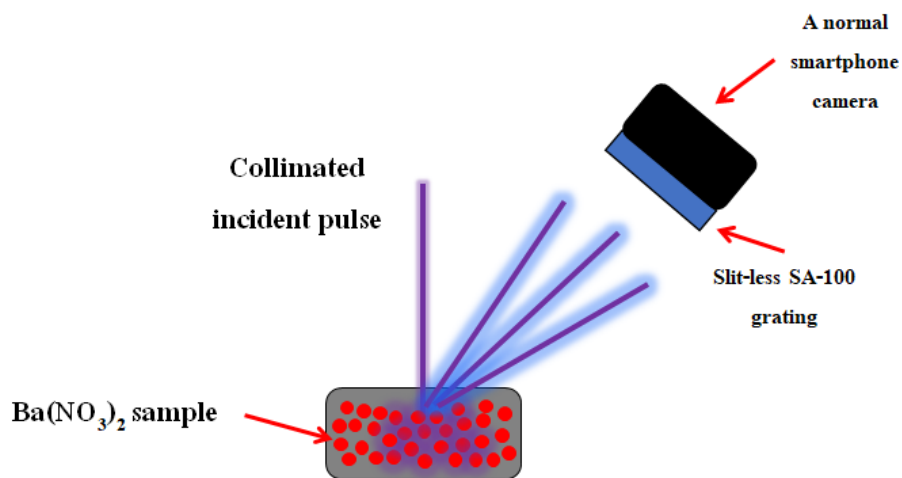


Figure 3.12 Schematic of the setup for capturing color photo of RRL from a loosely-packed sample.

Another monochrome picture was taken by a monochrome CCD camera with a $25 \mu\text{m}$ slit spectrograph. This setup provides higher spectral resolution. Furthermore, this setup allows UV wavelength to be detected, since it is no UV filters at the detection pixels, unlike a normal colored CCD camera. To remove the bright emission of incident wavelength, a long-pass filter was equipped to the setup as shown in Figure 3.13. The detection spectrum was extracted from a spectrogram image using intensity image analysis in Matlab.

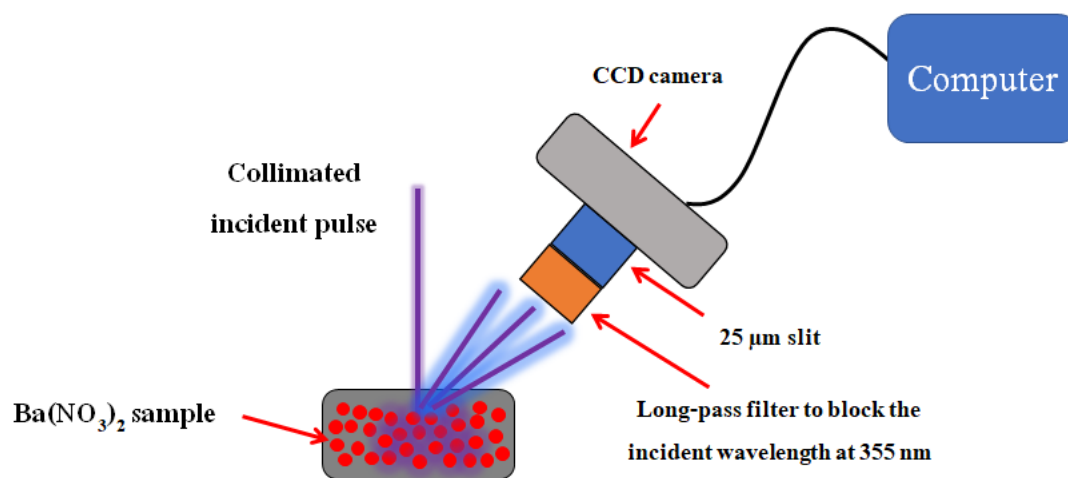


Figure 3.13 Schematic of the setup for capturing monochrome photo of RRL from a loosely-packed sample.

CHAPTER 4

RESULTS AND DISCUSSIONS

The results, with respect to the experiments explained in chapter 3, are presented in this chapter. The behavior of scattering signal, as an evidence of resonant Raman random laser produced by a disordered medium, is discussed. The results from each experimental section are shown as follow.

4.1 Sample characterizations

In this section, the information of sample preparation and characterization results by standard methods explained in section 3.1 are presented as follow.

The result of Raman spectrum measured by a standard Raman microscope shows chemical fingerprint of $\text{Ba}(\text{NO}_3)_2$ powder as displayed in Figure 4.1. The strongest Raman peak of the sample is at 1045.9 cm^{-1} , which is associated with the vibrational frequency of nitrate group (NO_3^-) in the unit cell structure. The other weaker characteristic Raman peaks can also be found at 79.7, 130.2, 139.8, 731.4, 1352.6, and 1384.2 cm^{-1} , respectively. In comparison, the Raman spectrum measured by our optical setup are shown in Figure 4.2. It was an intention to keep the partially filtered pump peak (designated at Raman shift = 0 cm^{-1}) for tracking the scattering information of the pump wavelength, i.e. Rayleigh scattering. The corresponding Raman peaks comparatively agree with the results from standard Raman equipment, especially for the major peak of (NO_3^-) group. However, the distinctive difference is the relatively poorer Raman shift resolution (at 40 cm^{-1} compared to 1.37 cm^{-1} of the standard Raman microscope). This can be attributed to two factors. First, the spectrometer used in the setup is designed with bigger slit size ($25 \text{ }\mu\text{m}$) to allow better light collection at low level, which sacrifices grating spectrum resolving ability. Second, the Raman resolution also depends on pump wavelength. The shorter excitation wavelength, such as 355 nm, give rises to bigger Raman shift step. However, the current Raman shift resolution provided by the setup is still sufficient to perform Raman spectroscopy.

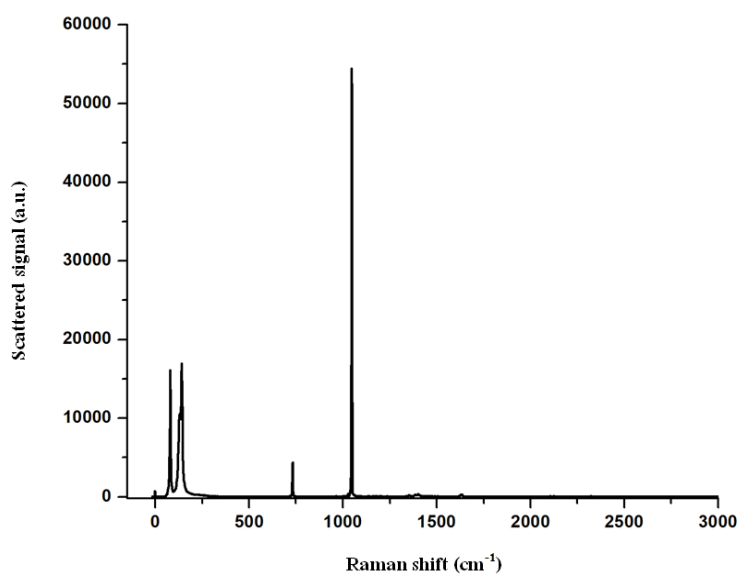


Figure 4.1 Raman spectrum of $Ba(NO_3)_2$ from standard Raman microscope spectrometer.

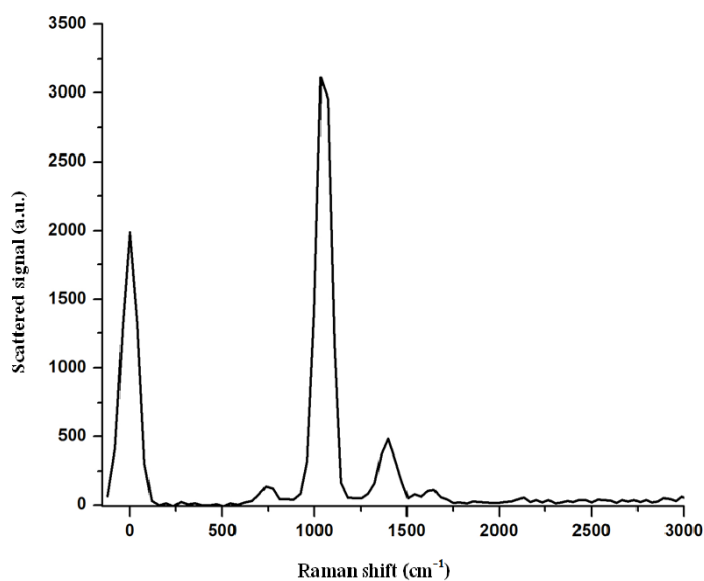


Figure 4.2 Raman spectrum of $Ba(NO_3)_2$ measured by the optical setup at pump intensity ~ 21.3 MW/cm².

The particle size is measured by scaling method of SEM images (Figure 4.3) using ImageJ, performed on 300 particles. From SEM images, it is found that the particles size varies on a wide length scale, ranging from nanoscale to hundreds of micron (distribution shown in Figure 4.4). The number of nanosized particles dominates

the powder structure with fewer existence of micro-scale particles. The particles, especially nanoscale ones, tend to form aggregates rather than separated as primary particles. The averaged particle size is $0.9 \pm 0.2 \mu\text{m}$.

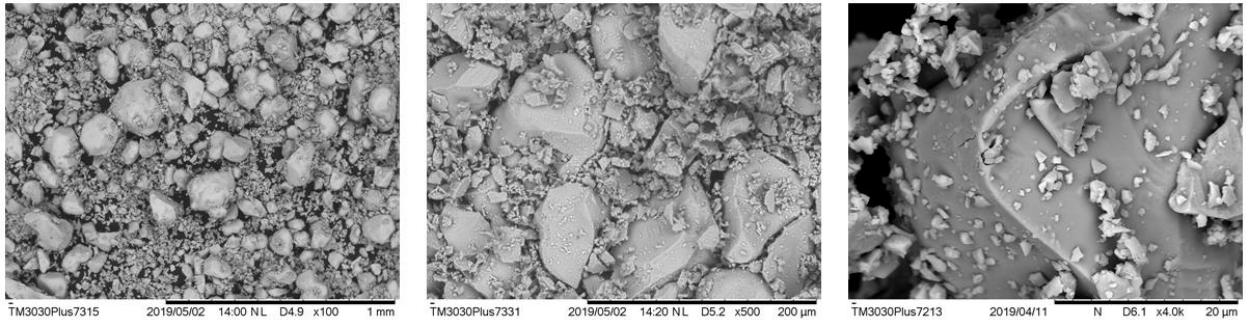


Figure 4.3 SEM image of the sample with magnification 100x (left), 500x (middle), and 4000x (right).

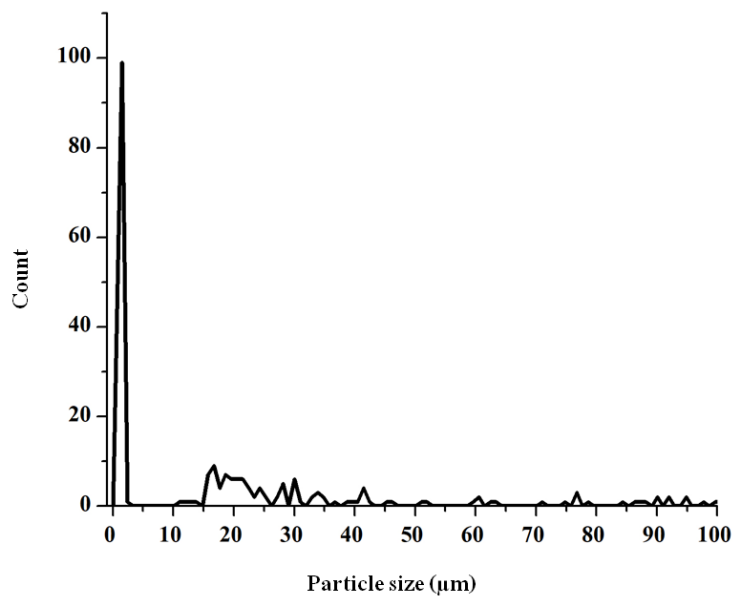


Figure 4.4 Particle size distribution determined from SEM images.

In addition, the fill factor of a sample can be calculated using equation 3.1 for over 5 samples and the average value is determined. The results of fill factor of the loosely-packed sample and the closely-packed sample are 0.50 ± 0.07 and 0.82 ± 0.08 , respectively. The higher in fill factor relates to a greater number of particles in the sample structure.

4.2 Results of Raman random lasing

In this section, experimental results from the optical setups to investigate Raman random lasing are presented. It is separated into 4 sections. The result of each section is presented as followed.

4.2.1 Result I: Control of the pump pulse intensity

Figure 4.5 shows intensity curve at each angle step. Since the polarizer is rotated, the relationship between the pump intensity and relative angle obeys the cosine square law. By mapping the relative angle and the output intensity, it allows a simple approach for continuously changing pump intensity. The intensity of the pump pulse can be adjusted in range of ~ 0 to 21.30 MW/cm^2 which is corresponding to relative angle 10° to 80° respectively.

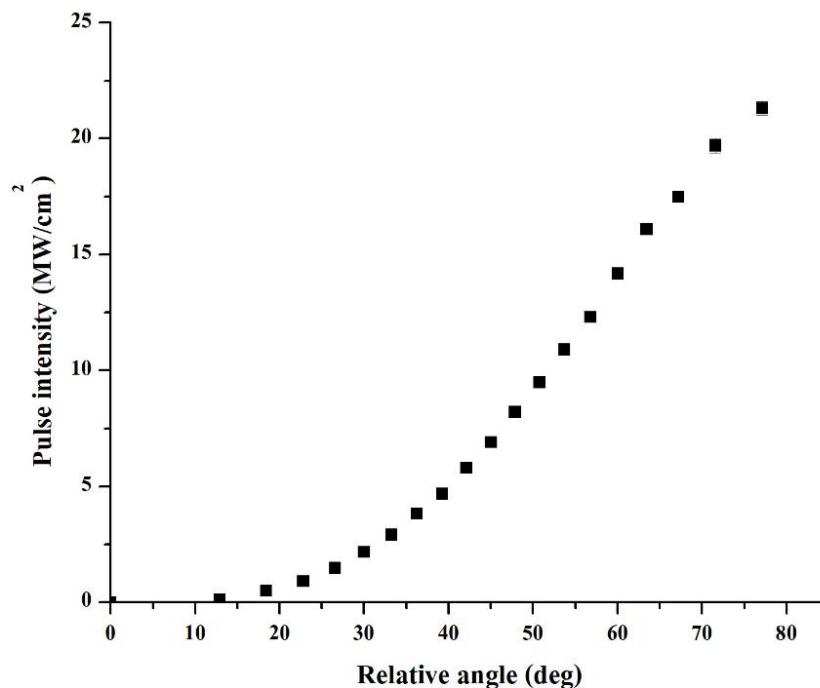


Figure 4.5 Graph shows result of incident pulse intensity versus relative angle.

4.2.2 Result II (1): Threshold of resonant Raman random lasing

Raman spectrum of a loosely-packed sample with thickness of 2 mm is shown in Figure 4.6. The Raman spectrum is founded at 735.2 , 1033.9 , and 1397.8 cm^{-1}

¹. Furthermore, the dominant Raman peak at 1033.9 cm^{-1} was measured for varied pump intensity ranging from 0.12 to 21.3 MW/cm^2 , and the result is shown in Figure 4.7. At the pump intensity below $\sim 2 \text{ MW/cm}^2$, Raman signal is growing linearly to the pump pulse intensity. Then, the increasing rate of Raman intensity gradually drop as the pump intensity increases beyond $\sim 2 \text{ MW/cm}^2$. The slower Raman increasing rate indicates an optical loss mechanism which also depends on the pump intensity. The nonlinear drop of Raman signal be explained by the occurrence of stimulated absorption process for pump power as described by the equation 2.28. In general, the magnitude of stimulated absorption increases with higher pump intensity, which should make Raman growth rate dropped even more along the increasing pump intensity. On the contrary, it was found a steep increase of Raman signal when pump intensity surpasses 18 MW/cm^2 . This indicates that a SRS gain mechanism starts to occur and compete with loss. At sufficiently high gain, Raman random signal rises. The lasing threshold phenomenon from a sample can be observed as Raman scattered signal begins to rise sharply. However, higher pump intensity to study further for the Raman random lasing behavior after 21.30 MW/cm^2 is not possible for the current pump source as it is the ceiling intensity provided by the pump laser system.

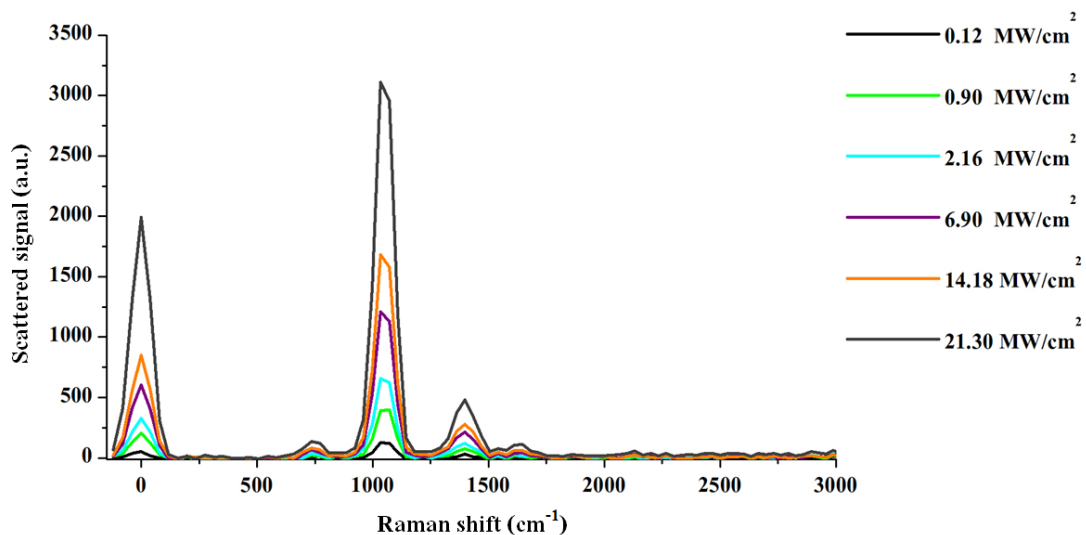


Figure 4.6 Raman spectrum of 2 mm-thickness sample with various pump pulse intensity ranging from 0.12 to 21.30 MW/cm^2 .

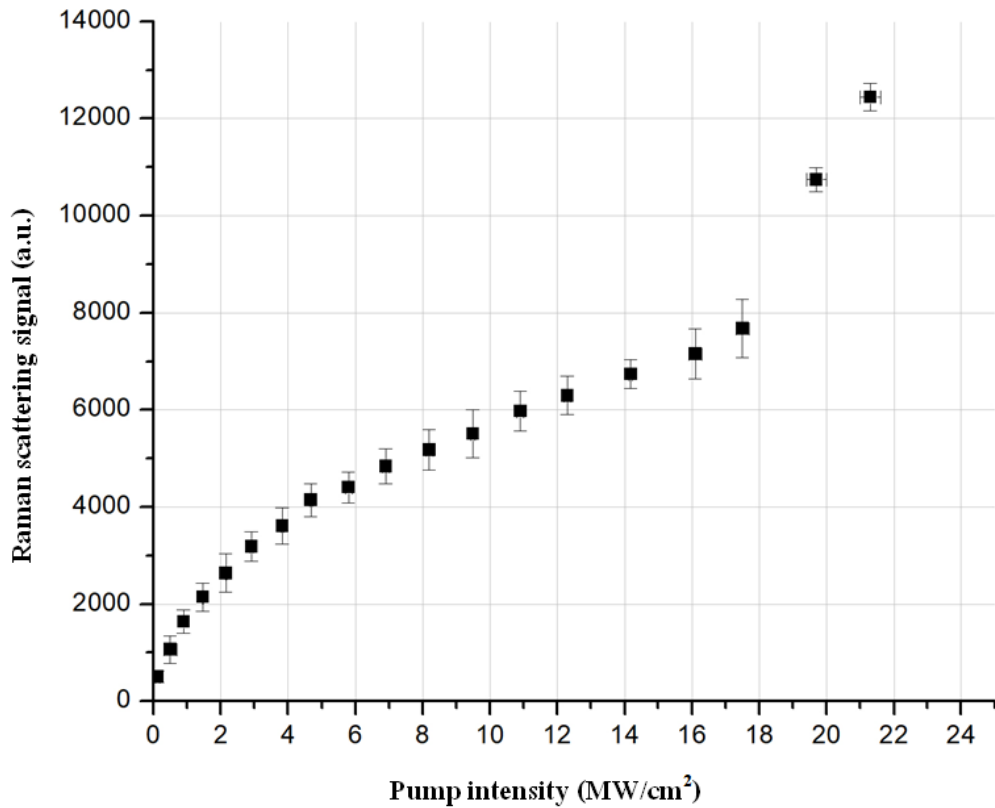


Figure 4.7 Plot of Raman scattering signal versus pump intensity for 2 mm-thickness sample.

The total amount of Raman random lasing power from the above sample can be estimated at pump intensity 21.30 MW/cm². Here, an optical power meter is inserted at the bottom-end of the sample holder system (Figure 4.8). The scattered light is presumed to radiate uniformly around the scattering point. The total value of the Raman lasing power can be determined by the ratio of the spherical surface and the power meter area as,

$$P_{tot} = \frac{4 \times P_{mea} \times D^2}{d^2},$$

where P_{tot} is estimated total Raman random lasing power, $P_{mea} = 1.721 \times 10^2 \text{ W}$ is the measured energy from the power meter, $D = 25.4 \text{ mm}$ is the distance from scattering spot to the power meter, $d = 10 \text{ mm}$ is the clear aperture of the power meter. Total power of the Raman scattered signal is equal to $P_{tot} = 0.449 \text{ W}$. The incident pump

power is $P_{in} = 1.044 \times 10^3 \text{ W}$. Therefore, the Raman conversion efficiency of 4.25×10^{-4} , which is several orders of magnitude higher than typical spontaneous Raman scattering (in order of 10^{-8}).

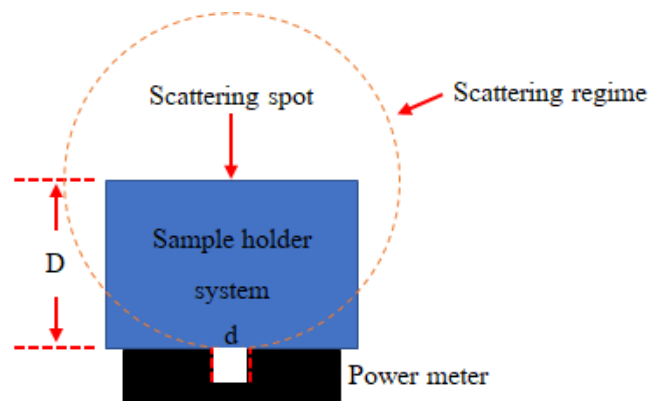


Figure 4.8 Schematic of the experimental setup for determining the RRL power.

4.2.3 Result II (2): Effect of sample layer thickness

The behavior of Raman emission signal strength of samples for various thickness was investigated. The Raman spectrum of loosely-packed sample at every 1mm-increasing thickness is shown in Figure 4.90. The Raman spectrum of every thickness is founded at 735.2, 1033.9, and 1397.8 cm^{-1} . The identical dominant Raman shift of $\text{Ba}(\text{NO}_3)_2$, at $\sim 1034 \text{ cm}^{-1}$, is observed under various pump intensity and the result is presented in Figure 4.10. From the results, the Raman signal versus pump energy of every thickness shows the similar trend as presented in the in section 4.2.2. In general, the level of Raman signal strength dropped for thicker samples, since it causes higher absorption and also the pump beam penetration drop along the travelling distance in a random medium governed by diffused light equation. That is, at thicker medium, light becomes more randomized in direction and less beam power comes out directly to reach the detector area. The random scattering will be eventually absorbed in the medium. There is a case that the 2 mm-thickness sample yields higher signal than 1 mm. This could be assumed that the gain radius is briefly around 2 mm, which is comparable to the size of laser spot. Raman light scattering inside the laser pump spot or within the gain radius is amplified by SRS process. It allows the Raman power to build up along the traveling distance. Beyond the gain radius, however, there is no SRS gain as it is outside the pumping area. The Raman light

will experience only absorption loss upon propagation. Also, it was observed that the lasing threshold phenomenon is not dependent on the sample thickness. All cases the Raman lasing occur at the pumping spot, but they experience different amount of absorption loss while diffusing through the layer thickness.

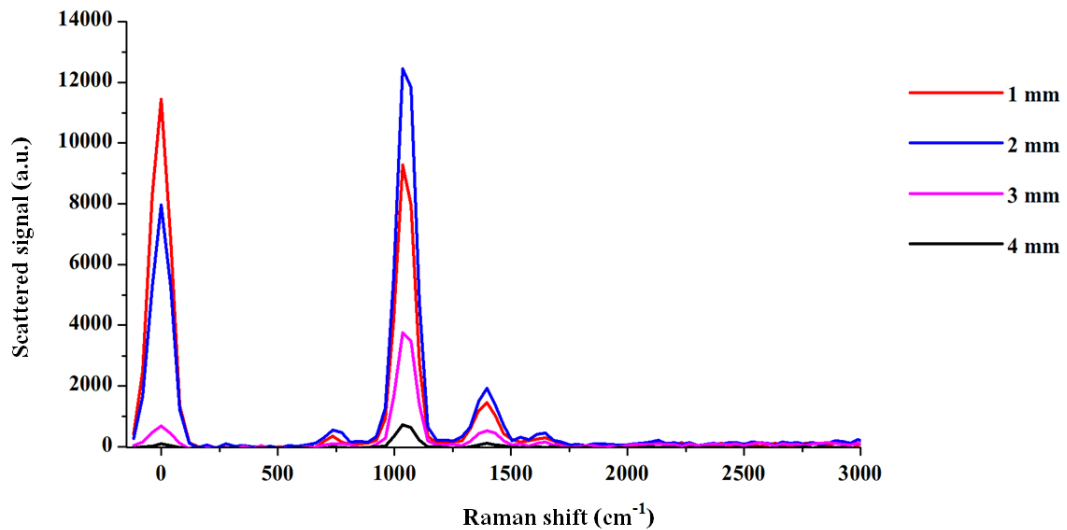


Figure 4.9 Raman spectrum of loosely-packed sample from various thickness, ranging from 1 to 4 mm, using 21.30 MW/cm^2 pump intensity.

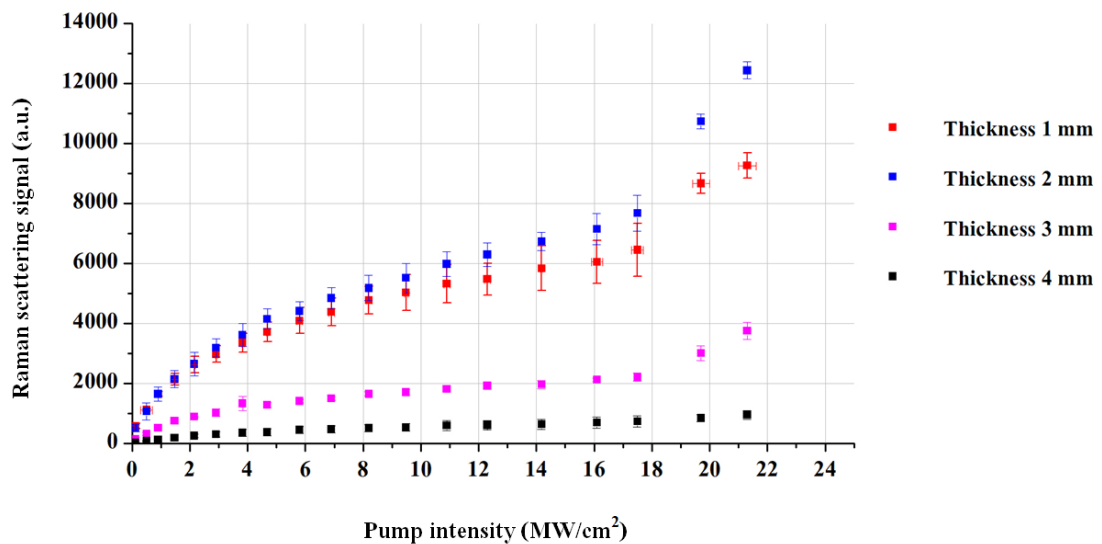


Figure 4.10 Graph of forward Raman scattering signal at 1034 cm^{-1} versus pump intensity at sample thickness 1 to 4 mm.

4.2.4 Result III: Effect of sample packing structures

The stimulated Raman emission of the loosely-pack and closely-packed sample at 2 mm-thickness is studied in comparison. Raman spectra of the loosely-packed sample and closely-packed sample are shown in Figure 4.11. The behavior of the dominant Raman peak of $\text{Ba}(\text{NO}_3)_2$ at $\sim 1034 \text{ cm}^{-1}$ is observed. The result shows the same trend of Raman scattered intensity evolution for pump intensity below 18 MW/cm^2 . For pump intensity higher than 18 MW/cm^2 , i.e. above the threshold, the loosely-packed sample shows greater efficiency of Raman random lasing as shown in Figure 4.12. Considering that the loosely-packed sample has lower density of Raman generating particles, the significantly higher Raman signal should come from stronger lasing efficiency process inside such structure as it could provide high level of multiple scattering. The stronger Rayleigh peak for the loosely-packed sample also confirm the better capability of this structure type to support pump beam penetration into the medium. This high pump beam penetration and high degree of multiple scattering leads to higher Raman random lasing efficiency, when compared to the denser structure. Furthermore, the lasing threshold characteristic of the loosely-packed sample is much clearer than that of the closely-packed one. The threshold of the loosely-packed sample is likely beyond the maximum pump intensity 21.30 MW/cm^2 provided by the laser source.

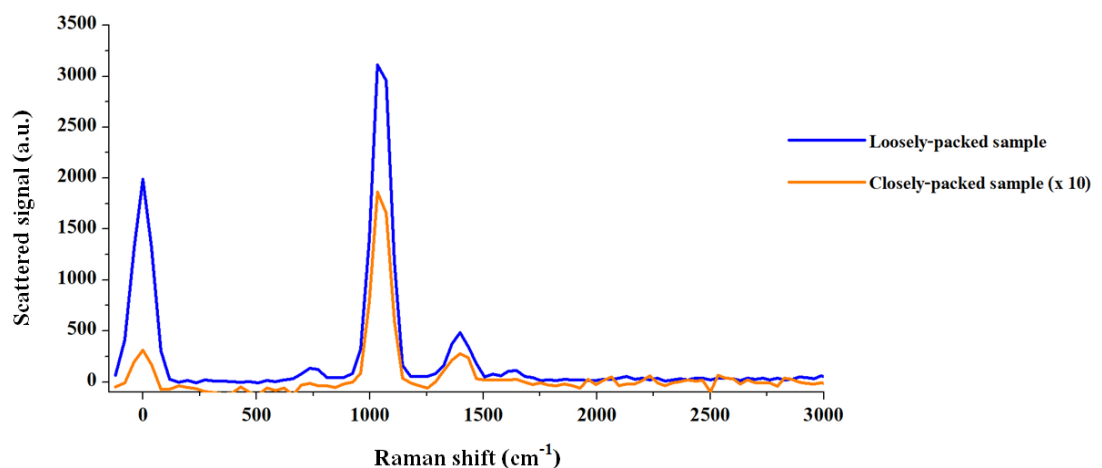


Figure 4.11 Raman spectrum of loosely-packed sample and closely-packed sample using pump intensity 21.30 MW/cm^2 .

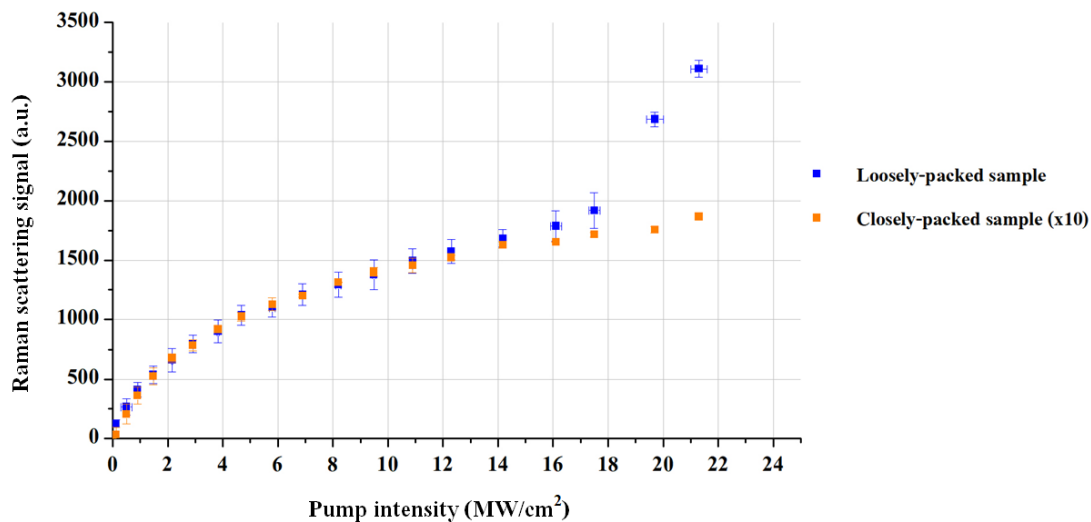


Figure 4.12 Behavior of Raman scattered light at 1034 cm^{-1} evolution of loosely-packed sample and closely-packed sample.

4.2.5 Result IV: Coherent backscattering result

The loosely-packed and closely-packed samples are applied into the coherent backscattering (CBS) characterization, explained in section 3.2.4. The raw data of CBS curve of loosely-packed sample and closely-packed sample is presented in Figure 4.13 and Figure 4.14, respectively. They were measured at different pump intensities, representing low, moderate, and high pump regimes. The result was analyzed to obtain transport mean free path (l_t) and absorption length (l_a) by fitting with the CBS model, shown in Figure 4.15. The results of the fitting for loosely-packed sample and closely-packed sample are shown in Table 4.1 and Table 4.2, respectively.

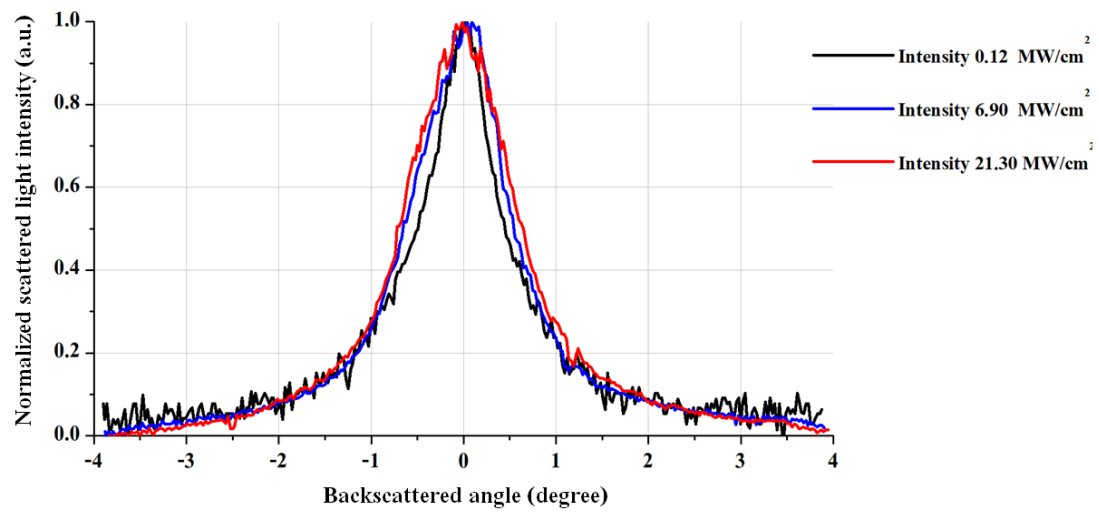


Figure 4.13 Normalized scattered light intensity vs backscattered angle of loosely-packed sample.

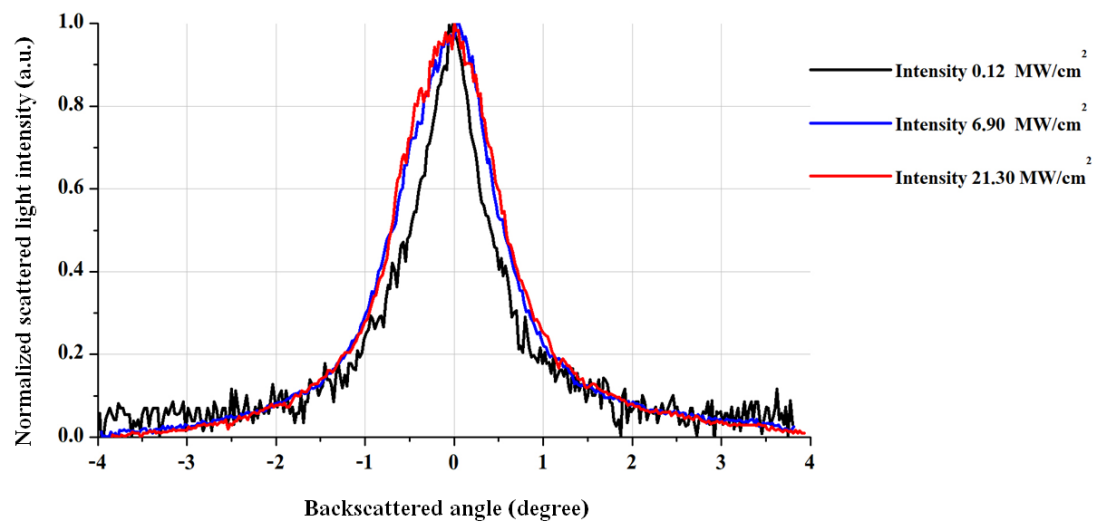


Figure 4.14 Normalized scattered light intensity vs backscattered angle of closely-packed sample.

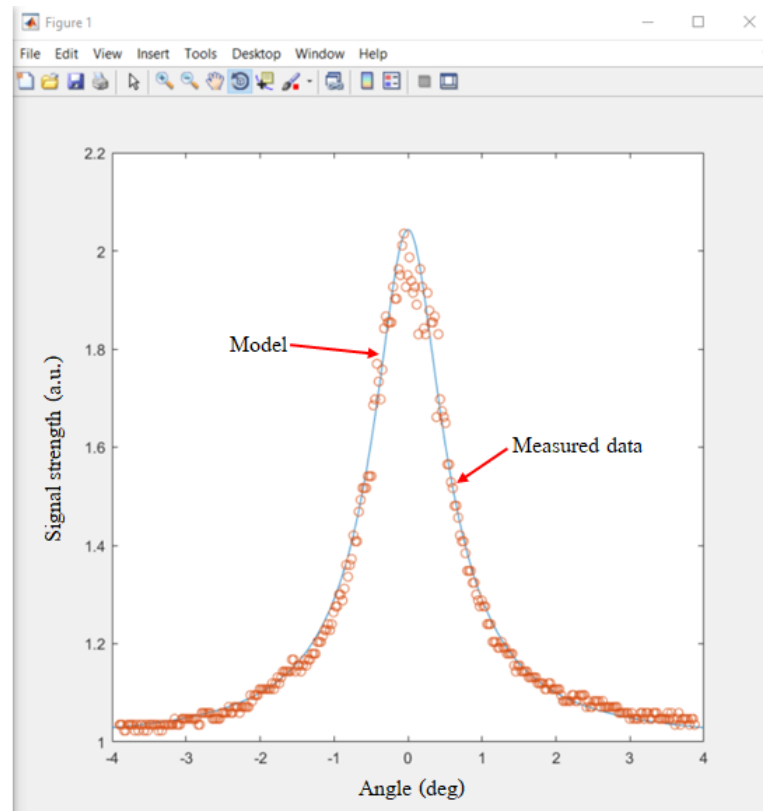


Figure 4.15 Fitting of CBS result with model described in equation 3.3.

Table 4.1 Transport mean free path (l_t) of loosely-packed sample and closely-packed sample.

Pump intensity (MW/cm ²)	Loosely-packed sample (μm)	Closely-packed sample (μm)
0.12 ± 0.06	7.4 ± 0.7	6.8 ± 0.3
6.9 ± 0.1	6.1 ± 0.8	5.7 ± 0.6
21.3 ± 0.3	5.2 ± 0.6	4.8 ± 0.9

Table 4.2 Absorption length (l_a) of loosely-packed sample and closely-packed sample.

Pump intensity (MW/cm ²)	Loosely-packed sample (μm)	Closely-packed sample (μm)
0.12 ± 0.06	51 ± 3	47 ± 4
6.9 ± 0.1	41 ± 5	38 ± 4
21.3 ± 0.3	34 ± 4	32 ± 6

From the results, l_t , and l_a evolution through the pump intensity show the same trend in both samples. They become shorter at high intensity of pump energy compared to those at low intensity. This means the multiple scattering efficiency increases with pump intensity for both samples. The l_t of closely-packed sample is shorter than of loosely-packed sample for every pump intensity values. This leads to the shorter penetration length of the pump power into the Raman medium, resulting in less integration with Stokes light when compared to the loosely-packed sample. The l_a of both samples are roughly one order of magnitude larger than the l_t indicating lower amount of absorption. Also, the l_a of the loosely-packed sample is longer than closely-packed sample indicating comparatively lower absorption loss. The lower absorption in the loosely-packed sample can be explained by the lower density of the absorber. Thus, pump energy experiences more absorption loss in the closely-packed sample, causing lower Raman lasing efficiency.

4.3 COMSOL simulation result

The simulation is set at conditions explained in section 3.3. The behaviors of a short laser pulse penetration in the multiple scattering structure, ranging from a low to high packing density, are shown as follow.

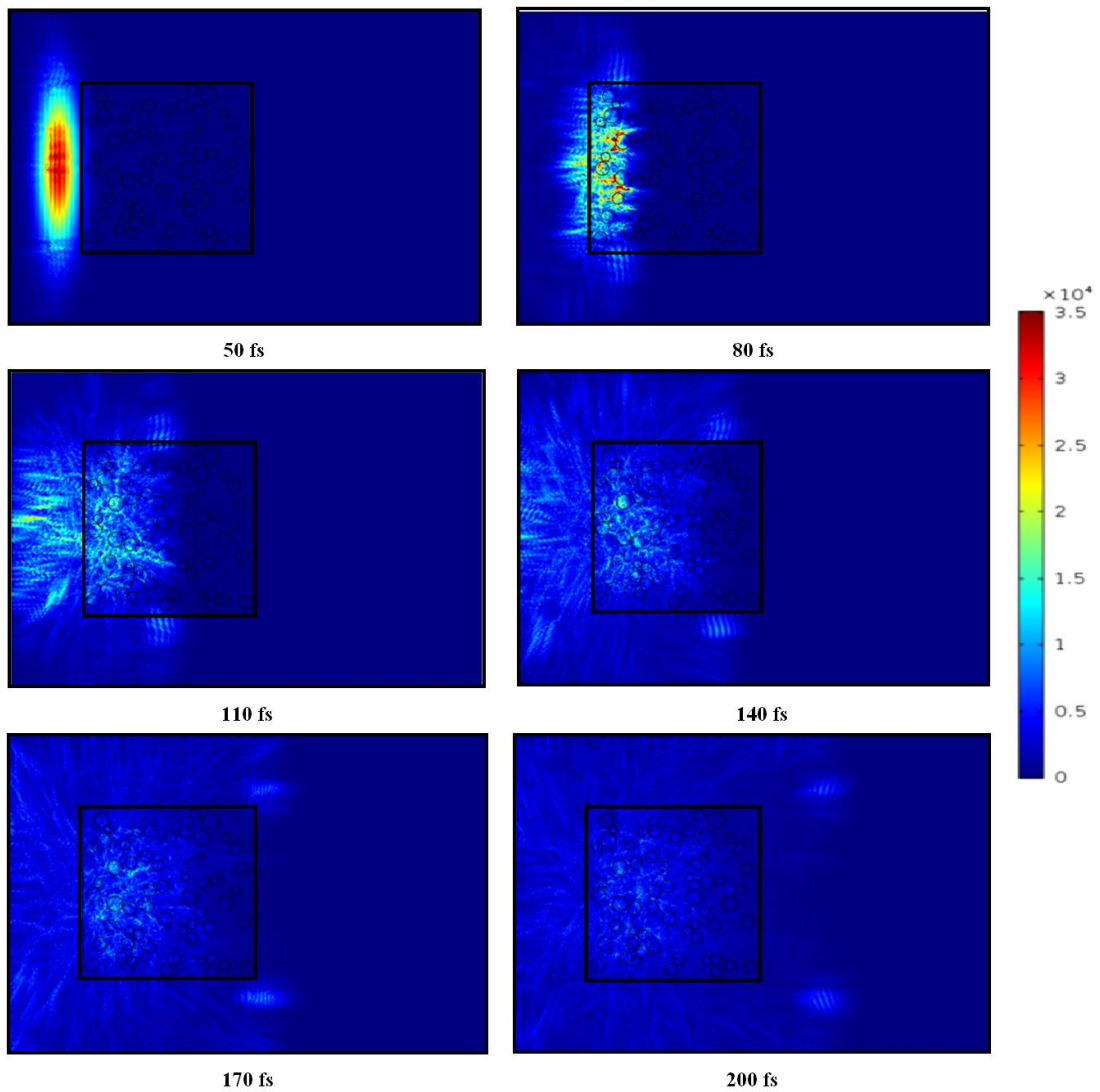


Figure 4.16 Simulated E field of a laser pulse in random medium structure with fill factor = 0.25 at different time step.

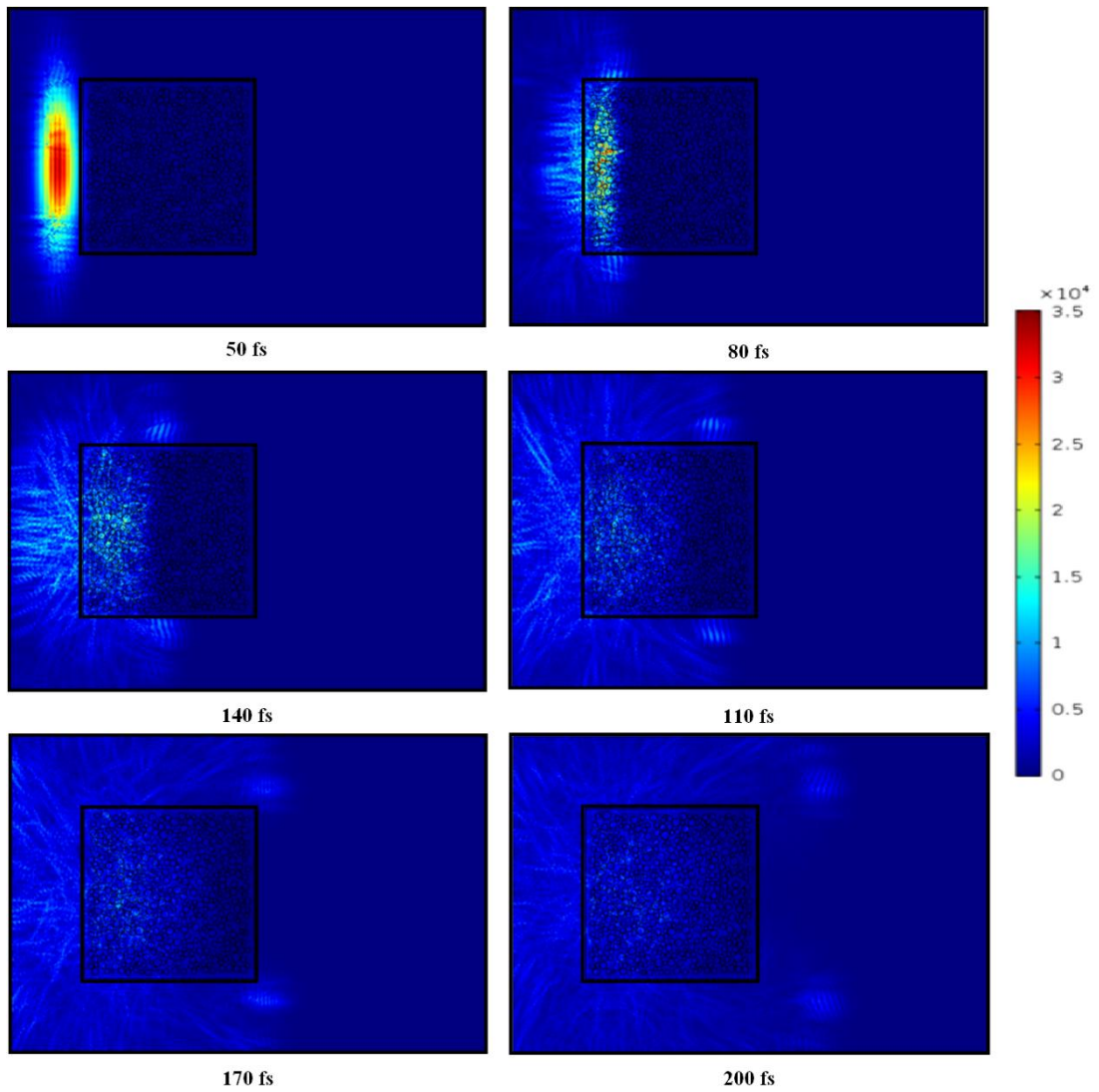


Figure 4.17 Simulated E field of a laser pulse in random medium structure with fill factor = 0.50 (loosely-packed sample) at different time step.

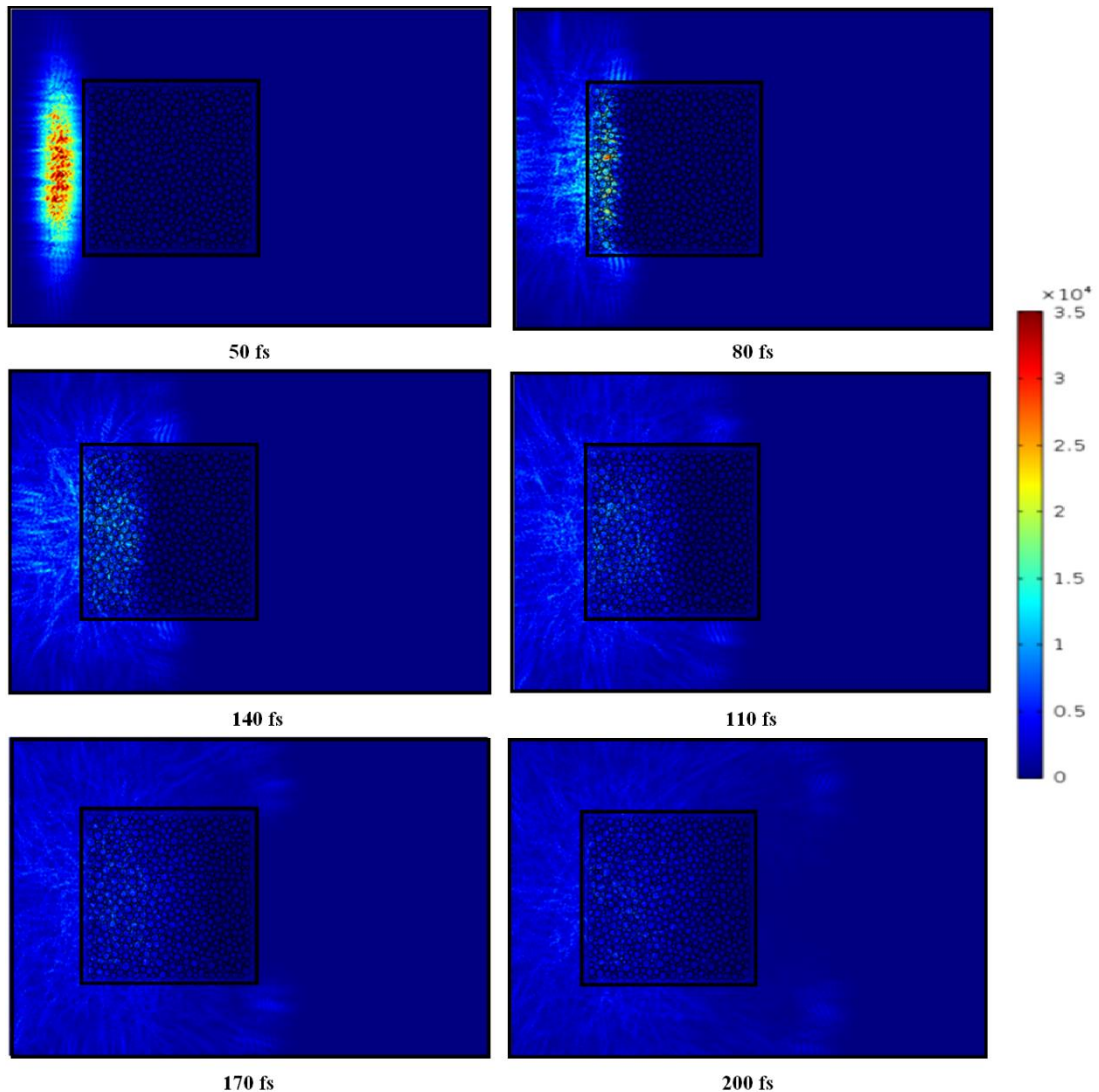


Figure 4.18 Simulated E field of a laser pulse in random medium structure with fill factor = 0.80 (closely-packed sample) at different time step.

The finite difference time domain simulation results show real-time light propagation in multiple scattering media. The incident pulse generated backscattered light, and some of the pulse energy penetrate into the medium. The incident time was set at 50 fs after pulse launching, and the Gaussian pulse is at the input boundary of the multiple scattering medium. After 50 fs, the incident pulse encounters multiple scattering process from the particles in the media. For free space, the short pulse should leave the medium at 170 fs. However, the multiple scattering structure allows the incident energy to inside in the media for longer amount of time, which allow sufficient optical feedback required for lasing process. The time evolution of the wave

energy stored in the structures shows exponential decay behavior as illustrated in Figure 4.19. At the initial time of incident, low-density medium allows more light to penetrate into the medium, corresponding to the longer l_t for loosely-packed case. Also, the simulation suggests that high-density medium losses some energy to backscattering at its interface. However, low-density medium has slightly faster decay rate for energy stored inside the medium. The decay time constant of energy stored τ is 83.54 fs, 117.94 fs, and 151.93 fs for the fill factor of 0.25, 0.50, and 0.80, respectively. The result shows that the medium with higher particle density can slightly prolong the light energy storage time inside the cavity although it may suffer losing more energy at the incident. In summary, there is a tradeoff for low-density and high-density structures. Low-density sample allow more pump power to penetrate inside the medium, while high-density produce more scattering and support longer light energy stored inside the medium. When compared to the real experiment result, in section 4.2, it suggests that the loosely-packed sample may have the better balance of light penetration and stored energy time to generate higher-efficiency RRL, compared to the closely-packed sample. However, this simulation is done for a small domain allowed by the current computing power. This could result in shorter decay time compared to the real situation.

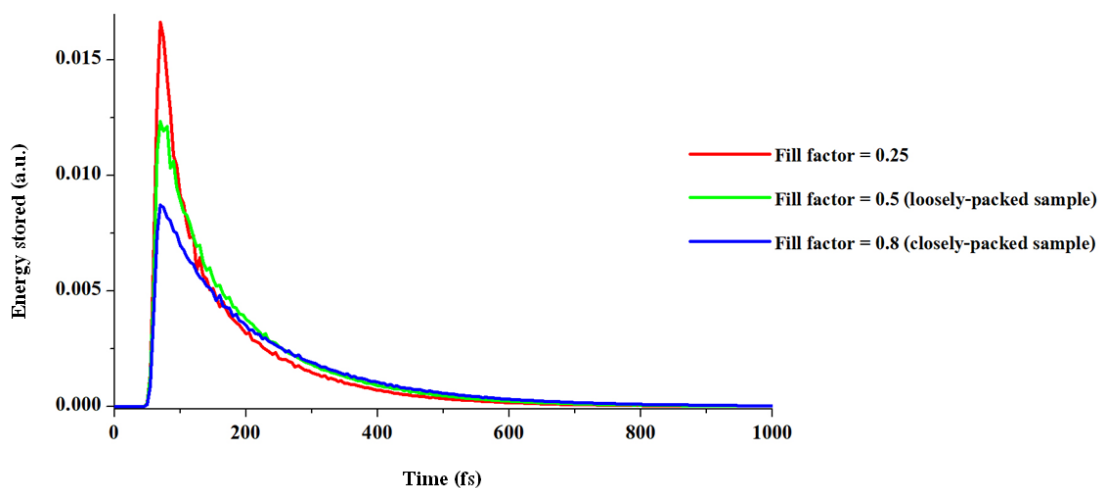


Figure 4.19 Graph of wave energy stored in the random medium when excited by a short laser pulse with pulse duration 10 fs.

4.4 Detection of Raman Random Lasing using a CCD camera

In this section, the very bright scattered photo can be taken by a colored CCD camera in a normal smart phone. The result is shown in Figure 4.20. It shows the incident spot ($m = 0$ diffraction) and the output spectrum ($m = 1$ diffraction) which is the combination of Raman and possible fluorescence.

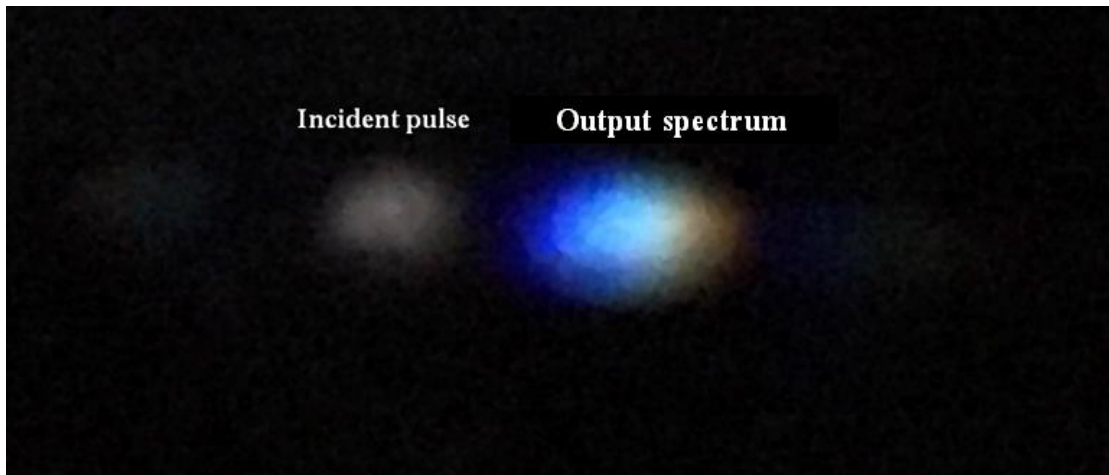


Figure 4.20 Photo of light scattered from a loosely-packed sample. This photo was captured by a cell phone camera (i.e. iPhone SE), bundled with a slit less SA-100 grating.

In monochrome picture, higher wavelength resolution and better spread of the detection spectrum can be captured as show in Figure 4.21. It can be roughly seen the narrow Raman peak near the left of spectrum, well separated with the fluorescence. This is another advantage of using UV laser excitation as Raman wavelength and fluorescence is not overlapped.

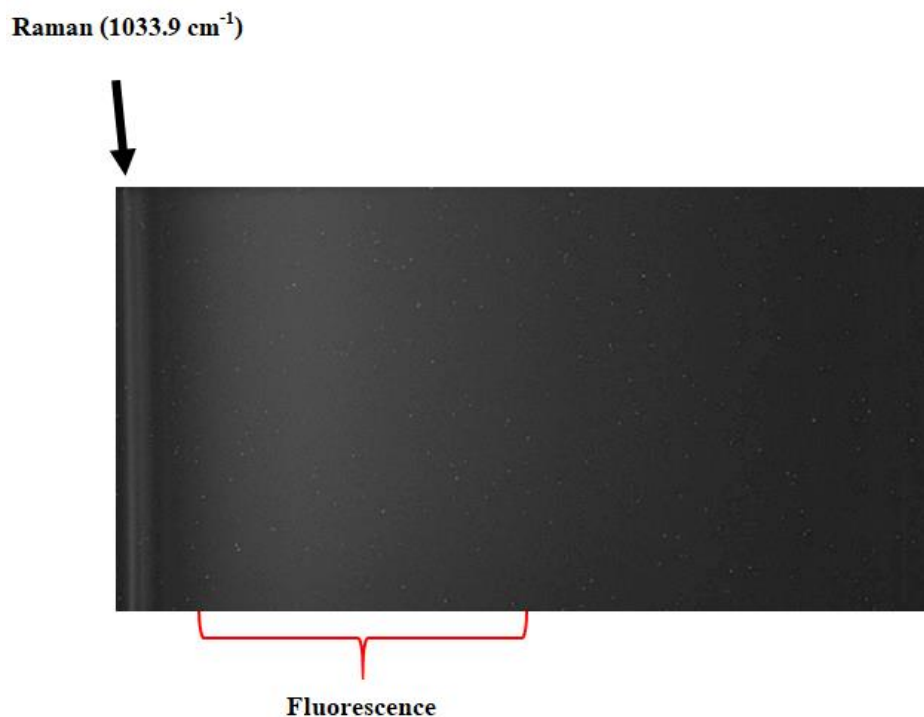


Figure 4.21 Photo of light scattered from a loosely-packed sample taken by a monochrome CCD camera.

The Raman spectrum for the sample was determined from the output spectrum image for the range extended to 8000 cm^{-1} . The spectrum shows broad fluorescence emission from 2500 to 8000 cm^{-1} well separated from the Raman peaks as shown in Figure 4.22. From the spectrum, the fluorescence level is weaker than the dominant Raman peak at 1033.9 cm^{-1} but it still can be seen in the photo since the fluorescence wavelength range is in visible. The Raman peak is in UV wavelength. It cannot be seen by eye nor a colored photo because of the internal filter, but the monochrome camera can capture this Raman spectrum.

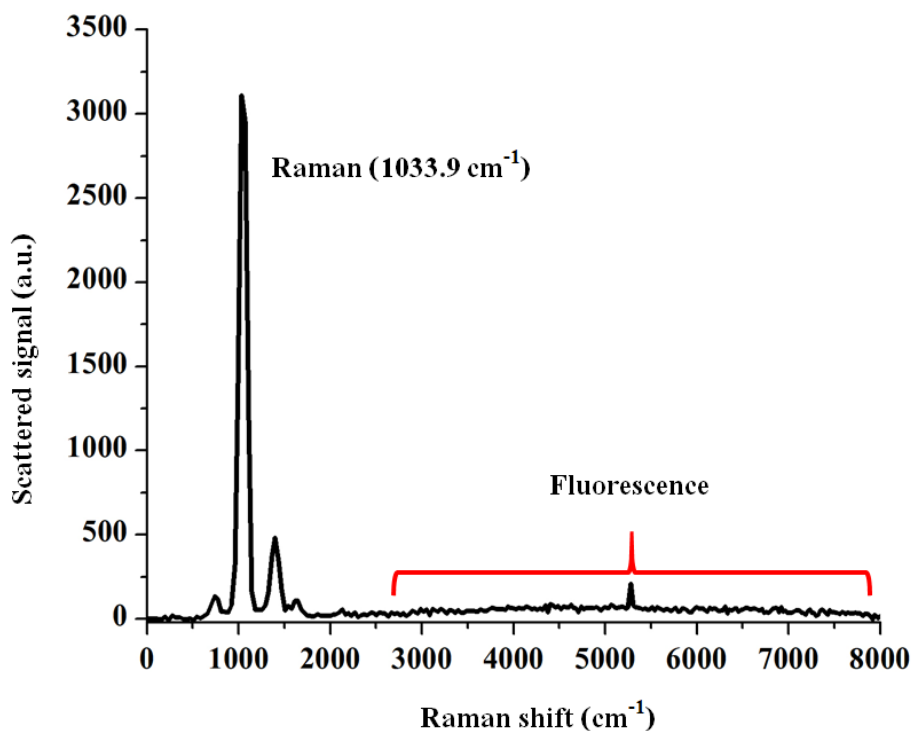


Figure 4.22 Extended Raman spectrum of Barium Nitrate, ranging for 0 to 8000 cm^{-1} , from loosely-packed sample using 21.30 MW/cm^2 pump intensity.

This result is promising that the Raman random lasing is highly efficient and bright process. Even a simple smart phone camera can detect Raman spectrum from a distance which cannot possible for a spontaneous Raman process. With more sophisticated light collection optics and a highly sensitive detection camera, much longer detection range can be envisioned to develop for standoff chemical identification in real use.

CHAPTER 5

CONCLUSION

5.1 Conclusion

This thesis aims to (1) demonstrate the generation of Raman random lasing near resonant condition, pumped by a nanosecond UV pulsed laser, and to (2) investigate the threshold characteristic of resonant Raman random lasing and the effects of medium structures. The conclusions of the results are explained as follow.

The Raman spectrum of barium nitrate can be measured from the optical setup with acceptable quality, i.e. the spectrum peak positions are equivalent to those obtained from a standard Raman system, but the spectral resolution is lower. The strongest Raman peak at $\sim 1034 \text{ cm}^{-1}$ represents the NO_3^- group in the barium nitrate. The nonlinear dependence of Raman signal with pump intensity was observed as the interplay between stimulated absorption loss and SRS gain mechanisms. For loosely-packed sample structure, the lasing threshold appears at pump intensity 18 MW/cm^2 , at which the SRS gain starts to surpass loss processes in the structure. At maximum pump intensity provided by the laser source, 21.3 MW/cm^2 , Raman random lasing efficiency of 4.25×10^{-4} was obtained, which is much higher than conventional Raman case, typically on the order of 10^{-8} .

Also, it was found that the packing structure of the powder sample is one of the crucial parameters to generate Raman lasing. While the loosely-packed sample shows distinct laser threshold, the closely-packed sample appears not to produce Raman lasing emission within the pump intensity range available in the study.

For loosely-packed sample, Raman lasing behavior is independent of the sample thickness. The Raman emission signal shows the same lasing threshold at pump intensity 18 MW/cm^2 for every layer thickness. The RRL efficiency of a sample layer thinner than pump laser spot (2 mm) increases with the increasing thickness, as the Raman energy buildup along the traveling distance within a gain radius. However, samples with thicker layer shows significant drop of RRL efficiency as the generated Raman light experiences only loss when traveling outside the gain radius.

Coherent backscattering results show that the loosely-packed sample has longer transport mean free path and absorption length, compared with the closely-

packed sample. It allows pump power to penetrate into a loosely-packed random medium for longer distance with lower absorption loss. Such that, the loosely-packed sample shows better performance to support lasing phenomenon when compared with the closely-packed sample.

The COMSOL simulation for light penetrated in a multiple scattering structure agrees with the CBS results that a low-density random medium allows more pump energy to penetrate inside the structure. However, the simulation results suggest that a denser medium can uphold light energy inside the medium for slightly longer period of time. This is the result of multiple scattering that stores light energy and provides optical feedback, required for lasing process. Therefore, it should be an optimized particle density that offers a balance of pump energy penetration and multiple scattering level. When compared to the experimental case, the loosely-packed sample with fill factor 0.50 is among the balance condition of pump power penetration and multiple scattering, which gives higher Raman efficiency.

Lastly, it has been demonstrated that the Raman random laser, pumped by nanosecond UV pulsed laser at near resonant condition is relatively bright. That is, the emission light can be detect using a normal CCD camera in a smart phone at distance of ~ 2 m. With better designed light collecting system together with highly sensitive detector, the longer Raman detection distance could be expected.

5.2 Recommendations

1. Higher pulse intensity must be performed on the structure to confirm the exponential growing of resonant Raman random lasing above the threshold.
2. Raman signal should be probed by a small fiber optics attached in the sample to reduce absorption effects from the structure.
3. Full wave simulation including the coupling of pump and Raman wavelengths should be implanted to the simulation geometries.

REFERENCES

- Akkermans, E., P. E. Wolf & R. Maynard. 1986. Coherent Backscattering of Light by Disordered Media: Analysis of the Peak Line Shape. *Physical Review Letters*, 56, 1471-1474.
- Andreasen, J., A. A. Asatryan, L. C. Botten, M. A. Byrne, H. Cao, L. Ge, L. Labonte, P. Sebbah, A. D. Stone, H. E. Tureci & C. Vanneste. 2011. Modes of random lasers. *Advances in Optics and Photonics*, 3, 88-127.
- Åkeson, M., M. Nordberg, A. Ehlerding, L.-E. Nilsson, H. Östmark & P. Strömbeck. 2011. Picosecond laser pulses improves sensitivity in standoff explosive detection. In *SPIE Defense, Security, and Sensing*, 80171C. SPIE.
- Bach, P., J. L. Ma, D. Froment & J. C. Jaureguy. 1993. Chemical weapons detection by fast neutron activation analysis techniques. *Nuclear Instruments and Methods in Physics Research Section B: Beam Interactions with Materials and Atoms*, 79, 605-610.
- Bachelard, N., P. Gaikwad, R. Backov, P. Sebbah & R. A. L. Vallee. 2014. Disorder as a Playground for the Coexistence of Optical Nonlinear Effects: Competition between Random Lasing and Stimulated Raman Scattering in Complex Porous Materials. *Acs Photonics*, 1, 1206-1211.
- Basiev, T. T., A. A. Sobol, P. G. Zverev, V. V. Osiko & R. C. Powell. 1999. Comparative spontaneous Raman spectroscopy of crystals for Raman lasers. *Applied Optics*, 38, 594-598.
- Bingi, J., A. R. Warriar & C. Vijayan. 2013. Raman mode random lasing in ZnS-beta-carotene random gain media. *Applied Physics Letters*, 102.
- Boyd, R. W. 2008. *Nonlinear Optics*. Elsevier Science.
- Brady, J. E., J. L. Smith, C. E. Hart & J. Oxley. 2012. Estimating Ambient Vapor Pressures of Low Volatility Explosives by Rising-Temperature Thermogravimetry. *Propellants Explosives Pyrotechnics*, 37, 215-222.

- Bret, G. & H. Weber. 1968. Transient stimulated Raman scattering in liquids and evaluation of picosecond pulse duration. *IEEE Journal of Quantum Electronics*, 4, 807-810.
- Carter, J. C., S. M. Angel, M. Lawrence-Snyder, J. Scaffidi, R. E. Whipple & J. G. Reynolds. 2005. Standoff detection of high explosive materials at 50 meters in ambient light conditions using a small Raman instrument. *Applied Spectroscopy*, 59, 769-775.
- Chivers, C.J. 2015. Bomb Experts Analyze the ISIS Soda-Can Bomb Photo. *The New York Times*.
- Chunaev, D. S. & A. Y. Karasik. 2006. Temporal characteristics of picosecond stimulated Raman scattering in oxide crystals. *Laser Physics*, 16, 1668-1671.
- Colthup, N. B., L. H. Daly & S. E. Wiberley. 1990. CHAPTER 1 - VIBRATIONAL AND ROTATIONAL SPECTRA. In *Introduction to Infrared and Raman Spectroscopy (Third Edition)*, eds. N. B. Colthup, L. H. Daly & S. E. Wiberley, 1-73. San Diego: Academic Press.
- de Oliveira, P. C., W. Q. Santos, I. N. Oliveira & C. Jacinto. 2019. Random laser and stimulated Raman scattering in liquid solutions of rhodamine dyes. *Laser Physics Letters*, 16.
- Eckhardt, G., R. W. Hellwarth, F. J. McClung, S. E. Schwarz, D. Weiner & E. J. Woodbury. 1962. Stimulated Raman Scattering from Organic Liquids. *Physical Review Letters*, 9, 455-457.
- Ehlerding, A., I. Johansson, S. Wallin & H. Östmark. 2012. Resonance-Enhanced Raman Spectroscopy on Explosives Vapor at Standoff Distances. *International Journal of Spectroscopy*, 2012.
- Eichhorn, M. 2014. *Laser Physics*. Switzerland: Springer International Publishing.
- Ewing, R. G. & C. J. Miller. 2001. Detection of volatile vapors emitted from explosives with a handheld ion mobility spectrometer. *Field Analytical Chemistry and Technology*, 5, 215-221.

- Faris, G. W. & R. A. Copeland. 1997. Wavelength dependence of the Raman cross section for liquid water. *Applied Optics*, 36, 2686-2688.
- Frank, M., S. N. Smetanin, M. Jelinek, D. Vyhlidal, V. E. Shukshin, L. I. Ivleva, E. E. Dunaeva, I. S. Voronina, P. G. Zverev & V. Kubacek. 2019. Stimulated Raman Scattering in Alkali-Earth Tungstate and Molybdate Crystals at Both Stretching and Bending Raman Modes under Synchronous Picosecond Pumping with Multiple Pulse Shortening Down to 1 ps. *Crystals*, 9.
- Freudiger, C. W., W. Min, B. G. Saar, S. Lu, G. R. Holtom, C. W. He, J. C. Tsai, J. X. Kang & X. S. Xie. 2008. Label-Free Biomedical Imaging with High Sensitivity by Stimulated Raman Scattering Microscopy. *Science*, 322, 1857-1861.
- Gazengel, J., N. P. Xuan & G. Rivoire. 1979. Stimulated Raman Scattering Thresholds for Ultra-short Excitation. *Optica Acta: International Journal of Optics*, 26, 1245-1255.
- Germain, M. E. & M. J. Knapp. 2008. Turn-on Fluorescence Detection of H₂O₂ and TATP. *Inorganic Chemistry*, 47, 9748-9750.
- Green, M., D. Andreou, V. I. Little & A. C. Selden. 1975. Stimulated Raman scattering from a multigigawatt liquid laser amplifier. *Journal of Applied Physics*, 46, 4854-4856.
- Gummaluri, V. S., S. R. Krishnan & C. Vijayan. 2018. Stokes mode Raman random lasing in a fully biocompatible medium. *Optics Letters*, 43, 5865-5868.
- Hokr, B. H., J. N. Bixler, M. T. Cone, J. D. Mason, H. T. Beier, G. D. Noojin, G. I. Petrov, L. A. Golovan, R. J. Thomas, B. A. Rockwell & V. V. Yakovlev. 2014. Bright emission from a random Raman laser. *Nature Communications*, 5.
- Hokr, B. H., J. N. Bixler, G. D. Noojin, R. J. Thomas, B. A. Rockwell, V. V. Yakovlev & M. O. Scully. 2014. Single-shot stand-off chemical identification of powders using random Raman lasing. *Proceedings of the National Academy of Sciences of the United States of America*, 111, 12320-12324.
- Hokr, B. H., A. Cerjan, J. V. Thompson, L. Yuan, S. F. Liew, J. N. Bixler, G. D. Noojin, R. J. Thomas, H. Cao, A. D. Stone, B. A. Rockwell, M. O. Scully & V. V. Yakovlev. 2017.

- Evidence of Anderson localization effects in random Raman lasing. 973110. Proc. SPIE.
- Hokr, B. H. & V. V. Yakovlev. 2014. A proposal for a random Raman laser. *Journal of Modern Optics*, 61, 57-60.
- Jitpiromsri, S. 2017. ความขัดแย้งชายแดนใต้ในรอบ 13 ปี. 25. Songkhla, Thailand: Prince of Songkla University.
- Katz, O., A. Natan, Y. Silberberg & S. Rosenwaks. 2008. Standoff detection of trace amounts of solids by nonlinear Raman spectroscopy using shaped femtosecond pulses. *Applied Physics Letters*, 92, 3.
- Letokhov, V. S.. 1968. GENERATION OF LIGHT BY A SCATTERING MEDIUM WITH NEGATIVE RESONANCE ABSORPTION. *SOVIET PHYSICS JETP*, 26, 10.
- Levs, Josh, and Plott Monte. 2013. Boy, 8, one of 3 killed in bombings at Boston Marathon; scores wounded. CNN.
- Li, F., Y. Wang, Z. Li, C. Sun & Z. Men. 2019. H₂O₂-enhanced stimulated Raman scattering of liquid water. *Journal of Raman Spectroscopy*, 0.
- Lisinetskii, V. A., Mishkel, Il, R. V. Chulkov, A. S. Grabtchikov, P. A. Apanasevich, H. J. Eichler & V. A. Orlovich. 2005. Raman gain coefficient of barium nitrate measured for the spectral region of Ti : Sapphire laser. *Journal of Nonlinear Optical Physics & Materials*, 14, 107-114.
- McLaughlin, Elliott, C., and Olarn Kocha. 2015. Tourists among 22 killed in apparent attack on Bangkok shrine. CNN.
- Mogilevsky, G., L. Borland, M. Brickhouse & A. W. Fountain III. 2012. Raman Spectroscopy for Homeland Security Applications. *International Journal of Spectroscopy*, 2012, 12.
- Nagli, L., M. Gaft, Y. Flegler & M. Rosenbluh. 2008. Absolute Raman cross-sections of some explosives: Trend to UV. *Optical Materials*, 30, 1747-1754.
- National Consortium for the Study of Terrorism and Responses to Terrorism (START). (2018). Global Terrorism Database [Annex of Statistical Information Country Reports on Terrorism 2017]. Retrieved from <https://www.start.umd.edu/gtd>

- Noginov, M. A., G. Zhu, A. A. Frantz, J. Novak, S. N. Williams & I. Fowlkes. 2004. Dependence of NdSc₃(BO₃)₄ random laser parameters on particle size. *Journal of the Optical Society of America B*, 21, 191-200.
- Pan, W. W., L. Zhang, H. W. Jiang, X. Z. Yang, S. Z. Cui & Y. Feng. 2018. Ultrafast Raman fiber Laser with Random Distributed Feedback. *Laser & Photonics Reviews*, 12.
- Petterson, A., I. Johansson, S. Wallin, M. Nordberg & H. Ostmark. 2009. Near Real-Time Standoff Detection of Explosives in a Realistic Outdoor Environment at 55 m Distance. *Propellants Explosives Pyrotechnics*, 34, 297-306.
- Petterson, A., S. Wallin, H. Östmark, A. Ehlerding, I. Johansson, M. Nordberg, H. Ellis & A. Al-Khalili. 2010. Explosives standoff detection using Raman spectroscopy: from bulk towards trace detection. In *SPIE Defense, Security, and Sensing*, 76641K. SPIE.
- Powers, P. E. & J. W. Haus. 2017. *Fundamentals of Nonlinear Optics*. Florida, USA: CRC Press Taylor & Francis Group.
- Ramakrishna, S. A. & K. D. Rao. 2000. Estimation of light transport parameters in biological media using coherent backscattering. *Pramana*, 54, 255-267.
- Raman, C. V. & K. S. Krishnan. 1928. A New Type of Secondary Radiation. *Nature*, 121, 501-502.
- Raymer, M. G., J. Mostowski & J. L. Carlsten. 1979. Theory of stimulated Raman scattering with broad-band lasers. *Physical Review A*, 19, 2304-2316.
- Savitski, V. G., S. Reilly & A. J. Kemp. 2013. Steady-State Raman Gain in Diamond as a Function of Pump Wavelength. *Ieee Journal of Quantum Electronics*, 49, 218-223.
- Segev, M., Y. Silberberg & D. N. Christodoulides. 2013. Anderson localization of light. *Nature Photonics*, 7, 197.
- Seifert, G.. 2003. Stimulated Raman gain spectroscopy of low-frequency density of states in liquids by picosecond IR laser pulses. *Chemical Physics Letters*, 370, 309-312.

- Sharma, S. K.. 2007. New trends in telescopic remote Raman spectroscopic instrumentation. *Spectrochimica Acta Part a-Molecular and Biomolecular Spectroscopy*, 68, 1008-1022.
- Sharma, S. K., A. K. Misra & B. Sharma. 2005. Portable remote Raman system for monitoring hydrocarbon, gas hydrates and explosives in the environment. *Spectrochimica Acta Part a-Molecular and Biomolecular Spectroscopy*, 61, 2404-2412.
- White, J. C.. 1981. Stimulated-absorption and spontaneous-emission studies of laser-induced dipole-quadrupole collisions. *Physical Review A*, 23, 1698-1702.
- Wiersma, D. S., P. Bartolini, A. Lagendijk & R. Righini. 1997. Localization of light in a disordered medium. *Nature*, 390, 671-673.
- Wolf, P.-E. & G. Maret. 1985. Weak Localization and Coherent Backscattering of Photons in Disordered Media. *Physical Review Letters*, 55, 2696-2699.
- Wu, M., M. Ray, K. H. Fung, M. W. Ruckman, D. Harder & I. Arthur J. Sedlacek. 2000. Stand-off Detection of Chemicals by UV Raman Spectroscopy. *Applied Spectroscopy*, 54, 800-806.
- Wu, X. H., A. Yamilov, H. Noh, H. Cao, E. W. Seelig & R. P. H. Chang. 2004. Random lasing in closely packed resonant scatterers. *Journal of the Optical Society of America B-Optical Physics*, 21, 159-167.
- Yiou, S., P. Delaye, A. Rouvie, J. Chinaud, R. Frey, G. Roosen, P. Viale, S. Fevrier, P. Roy, J. L. Auguste & J. M. Blondy. 2005. Stimulated Raman scattering in an ethanol core microstructured optical fiber. *Optics Express*, 13, 4786-4791.
- Yui, H., K. Kanoh, H. Fujiwara & T. Sawada. 2002. Stimulated Raman scattering of liquid water under the strong focusing condition: Analysis of local hydration network environments in dilute ethanol solutions. *Journal of Physical Chemistry A*, 106, 12041-12044.
- Zhu, J. X., D. J. Pine & D. A. Weitz. 1991. Internal reflection of diffusive light in random media. *Physical Review A*, 44, 3948-3959.

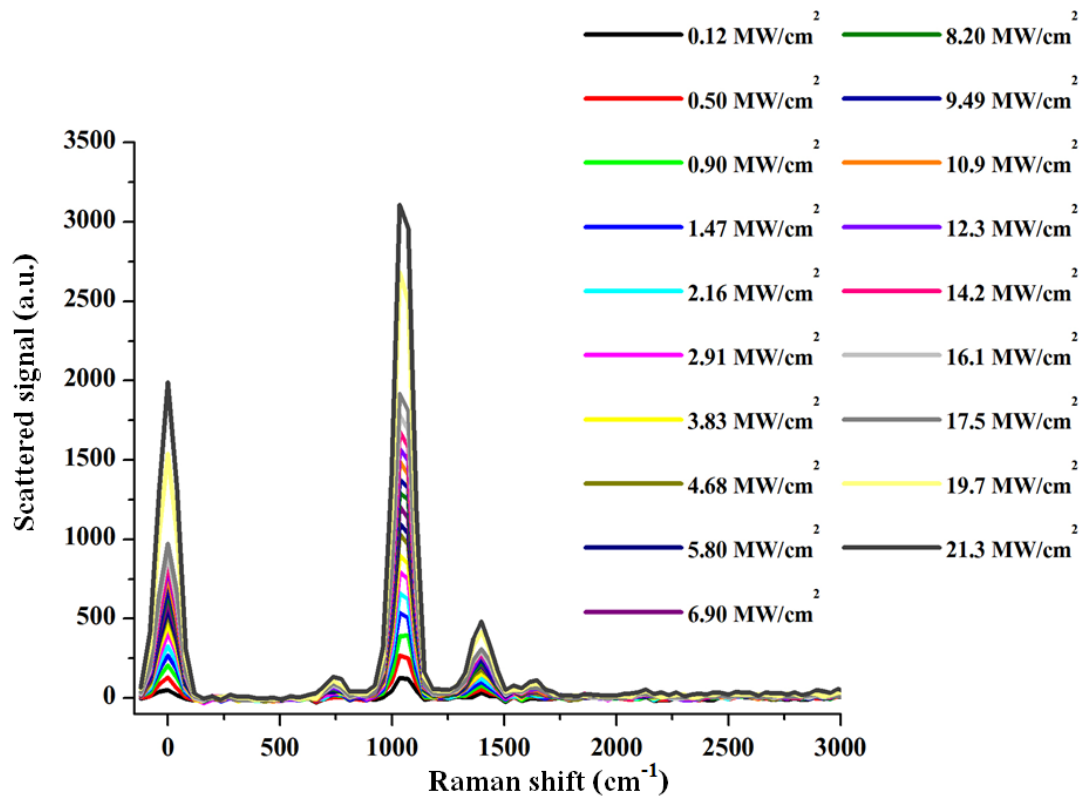
Zverev, P. G., T. T. Basiev, V. V. Osiko, A. M. Kulkov, V. N. Voitsekhovskii & V. E. Yakobson.
1999. Physical, chemical and optical properties of barium nitrate Raman crystal.
Optical Materials, 11, 315-334.

APPENDIX A

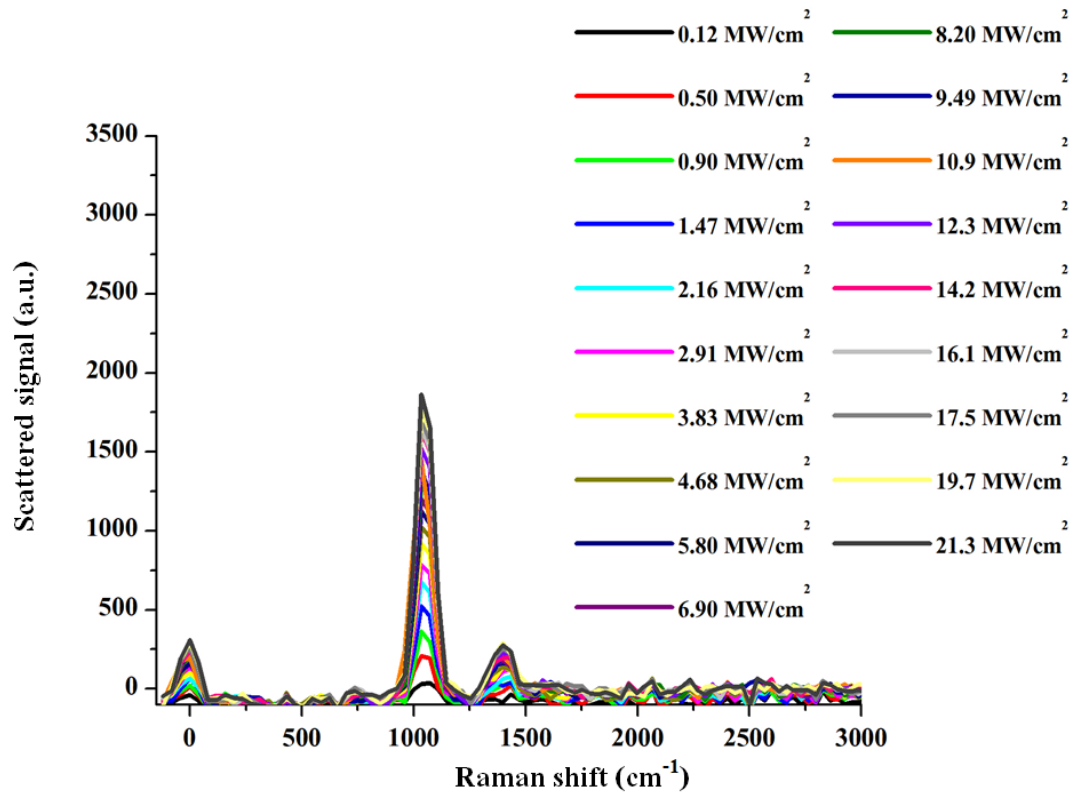
1. Raman spectrum

Raman spectrums of samples, used in the experiment, at every pump pulse intensity are shown as followed. They show the strongest Raman peak at 1033.9 cm^{-1} .

- Loosely-packed sample



- Closely-packed sample



2. Fill factor of samples

- Loosely-packed sample

Sample	Filled density	Fill factor
1	2.01	0.62
2	1.33	0.41
3	1.58	0.49
4	1.65	0.51
5	1.58	0.49
Average		0.50 ± 0.07

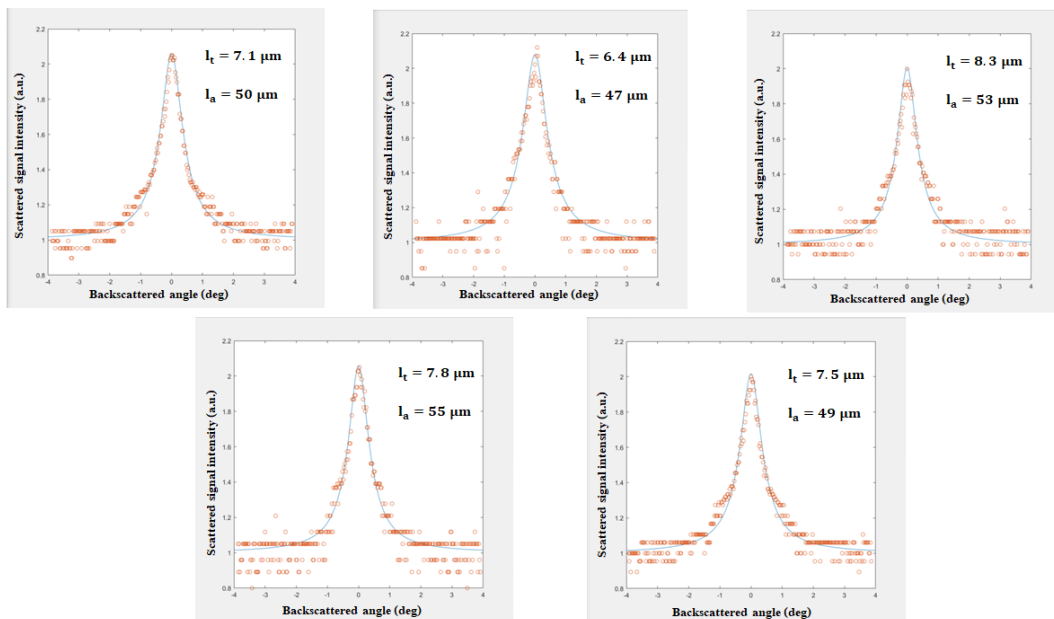
- Closely-packed sample

Sample	Filled density	Fill factor
1	2.82	0.87
2	2.40	0.74
3	3.01	0.93
4	2.47	0.76
5	2.59	0.80
Average		0.82 ± 0.08

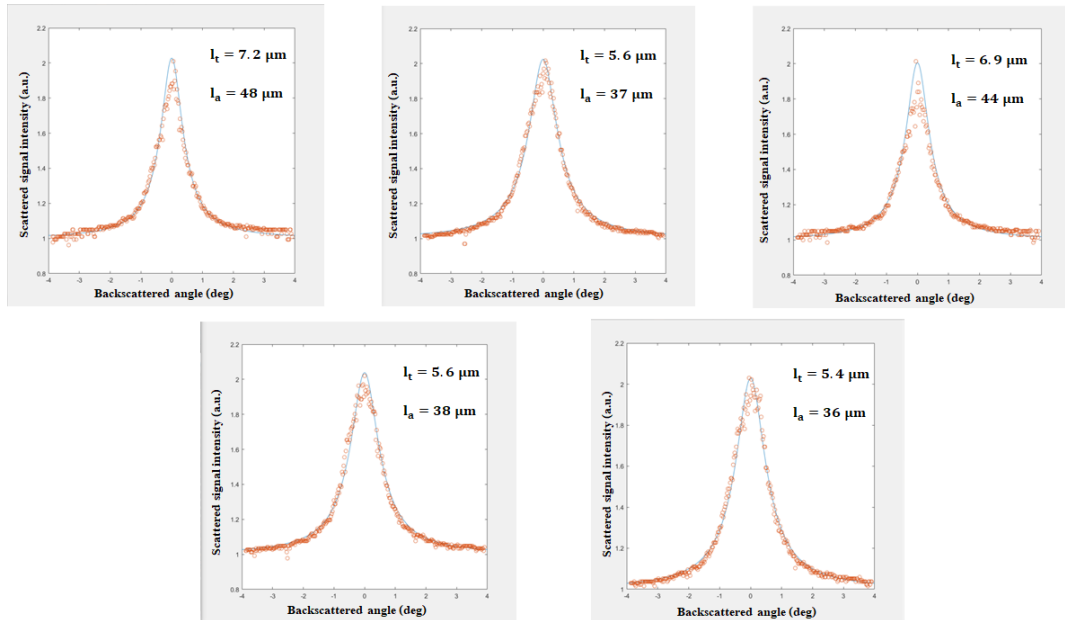
3. Coherence backscattering result

1.1 Loosely-packed sample

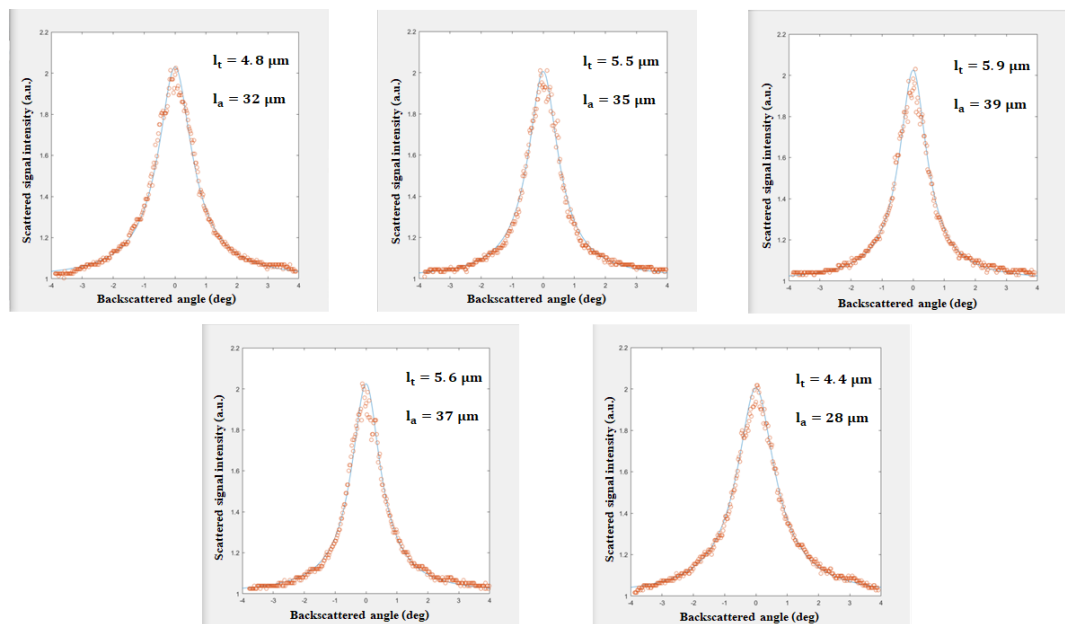
- Incident intensity = 0.12 MW/cm^2



- Incident intensity = 6.90 MW/cm^2

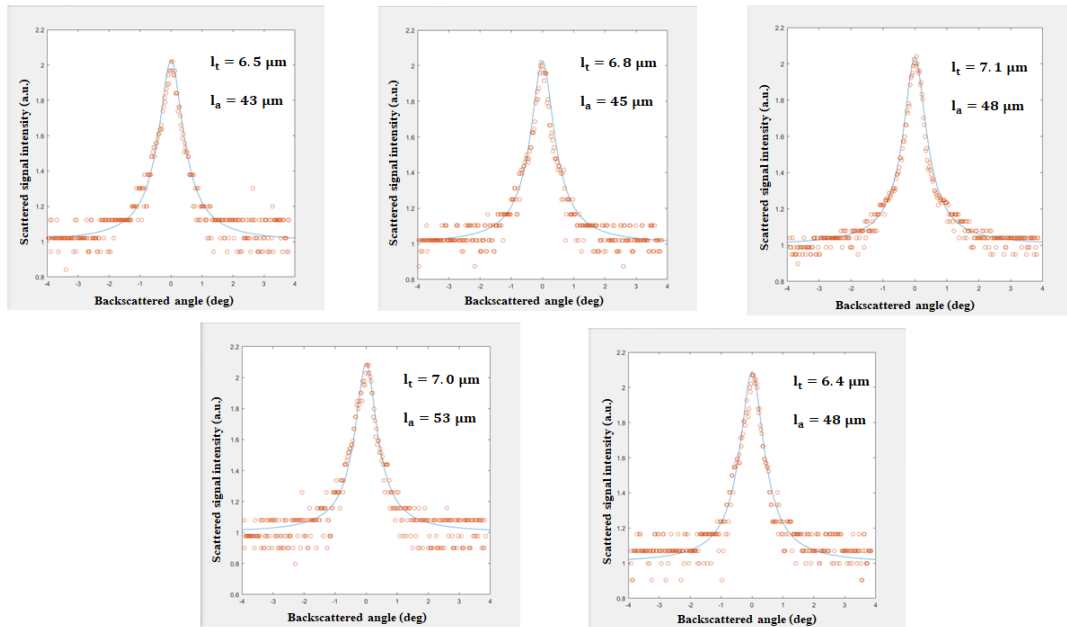


- Incident intensity = 21.30 MW/cm^2

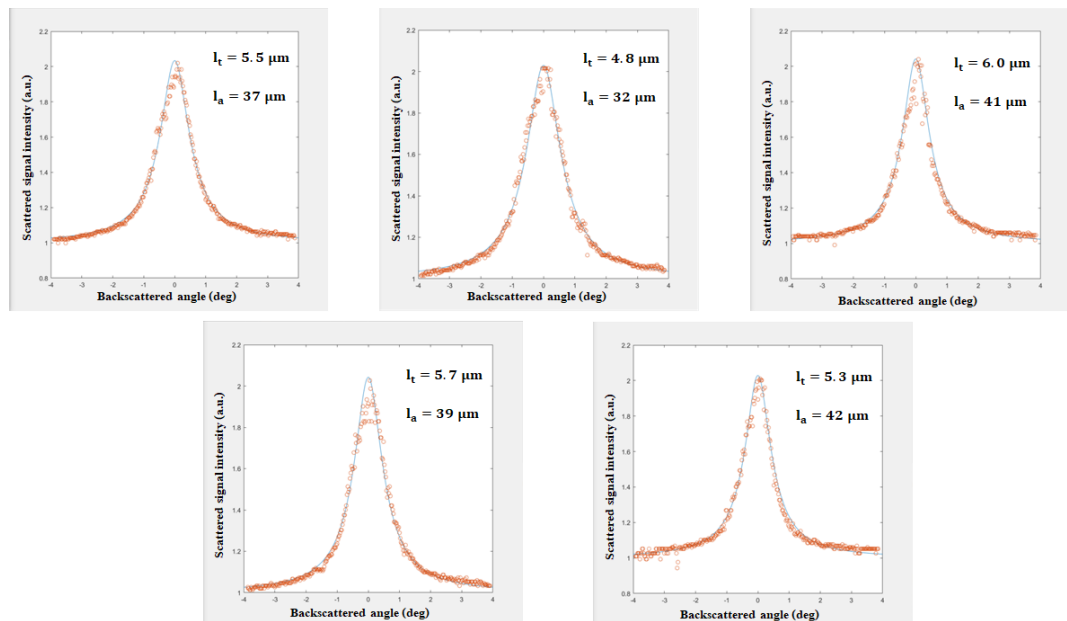


1.2 Closely-packed sample

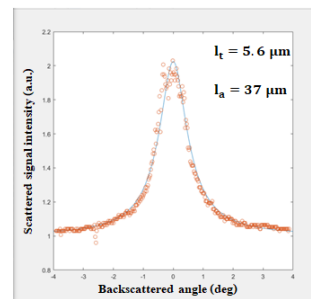
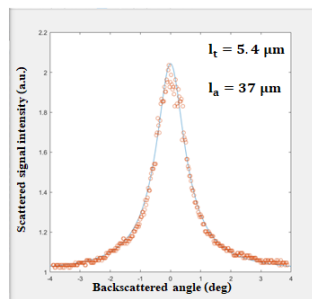
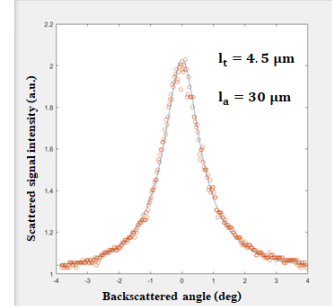
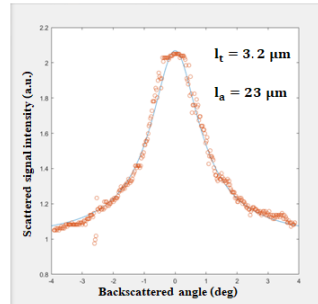
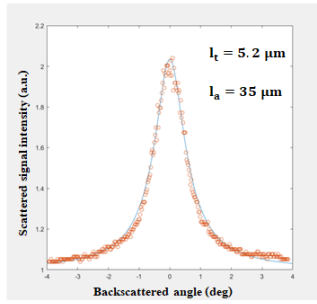
- Incident intensity = 0.12 MW/cm^2



- Incident intensity = 6.90 MW/cm^2



- Incident intensity = 21.30 MW/cm^2



APPENDIX B

Conference proceeding: Nanosecond-Pumped Random Raman Lasing from Bulk Nanogranular Materials (NpTh1H.6), Proceeding of Advanced Photonics Congress 2018. Eidgenössische Technische Hochschule (ETH) Zürich, Switzerland, July 2-7, 2018.

Nanosecond-Pumped Random Raman Lasing from Bulk Nanogranular Materials

Panuwat Srisamran^{1,2}, Paphon Pewkhom^{1,2}, Sirawit Boonsit^{1,2}, Pruet Kalasuwan^{1,2},
Paphavee van Dommelen^{1,2} and Chalongrat Daengngam^{1,2} *

¹Department of Physics, Faculty of Science, Prince of Songkla University, Songkhla, Thailand, 90110

²Thailand Center of Excellence in Physics, Commission on Higher Education, Bangkok, Thailand, 10400

* chalongrat.d@psu.ac.th

Abstract: We demonstrate the evidences of random Raman lasing obtained from highly disordered material, composed of submicron particles and their aggregates, pumped by nanosecond laser pulses and utilized multiple elastic scattering for optical feedback. © 2018 The Author(s)

OCIS codes: (290.5910) Scattering, stimulated Raman; (280.4788) Optical sensing and sensors

1. Introduction

Recently, a new class of random Raman laser emission from three-dimensional stochastically disordered materials has been experimentally confirmed for its bright signal, which enables single-shot chemical identification of powders over distance of 400 m [1]. Essentially, this random Raman lasing process utilizes stimulated Raman scattering (SRS) as gain mechanism, and strictly relies on multiple elastic scattering, or perhaps the controversial 3D Anderson localization of light, to provide feedback into the gain medium in place of an optical resonator. Therefore, most of nanogranular materials with sufficient interaction dimension could potentially act as gain media for generating random Raman lasing without extra sample preparation. Regarded as a third-order nonlinear optical process, the stimulated emission in SRS is different from traditional lasing, where the Raman transition involves virtual states, which is much faster than the real electronic states, to access the vibronic excitation levels of atoms or molecules. Therefore, to realize Raman lasing, a gain medium must be pumped fast and hard normally using high-peak-power picosecond laser pulses to achieve transient SRS. However, such powerful picosecond laser systems are complex, expensive and bulky, unfavorable for the development of portable standoff chemical detection systems.

In this work, alternative to using picosecond laser, we demonstrate that random Raman lasing can also be accomplished within quasi steady-state pumping regime, when pumped by nanosecond laser pulses. We further show that original, loosely-packed form of powders with their natural aggregations somewhat more efficient than the closed-packed structure, in term of Raman lasing efficiency.

2. Experimental setup

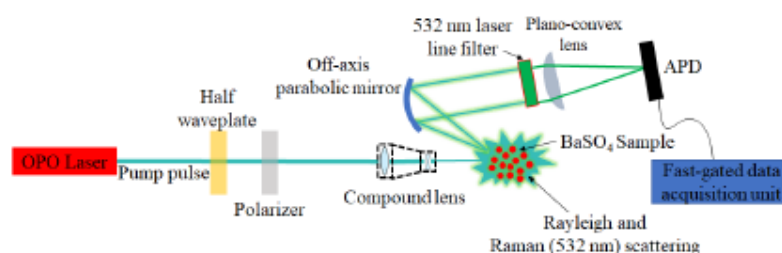


Fig. 1 Experimental Setup

The experimental setup of this work is illustrated in Fig. 1. Pump pulses at wavelength of 505 nm, with pulse duration of ~ 10 ns, were generated from a compact Nd:YAG-pumped optical parametric oscillator (OPO) system. A half waveplate combined with a glan-laser polarizer were employed to adjust the pump pulse energy. To increase the beam intensity while avoiding damage from tight focusing, the pump beam diameter was reduced to less than 1 mm using a compound lens, such that the lens spacing can be controlled to obtain a nearly collimated beam incident onto a sample. Here, commercially available BaSO_4 powder (primary particle size $\sim 160 \pm 30$ nm) was chosen as a Raman-active granular sample, whose constituent particles also act as elastic scattering centers, providing optical feedback into the medium. Particularly, two different packing structures of the granular BaSO_4 media were investigated: original powder with loosely-packed structure, and closely-packed pellets formed by pressing the powder at pressure 300 MPa using pellet preparation equipment. The samples were controlled for their thicknesses to be $L \sim 1$ cm, and placed within a custom-made container. The output scattered lights upon sample excitations were

collected and collimated by an off axis-parabolic mirror before filtered out the pump component using a narrow bandpass filter, 532 ± 1 nm, to select a distinct Raman line at 531.4 nm (corresponding to BaSO_4 Raman shift at 985 cm^{-1}). The Raman signal was then focused by a lens onto an avalanche photodiode (APD). In additional measurement, the Raman wavelength was kept constant at ~ 532 nm while tuning the pump wavelength at 1 nm step to measure Raman output spectrum. The rejection of possible fluorescence and other random noises was ensured using a fast-gated signal acquisition, synchronized with the pump pulse.

3. Experimental results and discussions

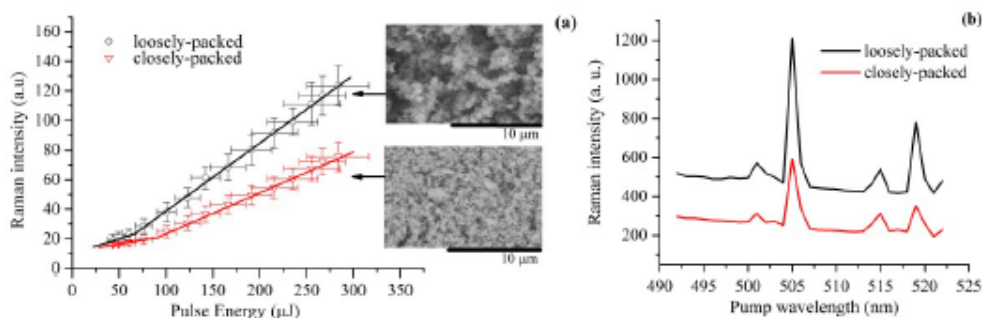


Fig. 2 (a) The Raman lasing intensity measured for varied pump pulse energy. The insets are the corresponding SEM images revealing structures of the granular BaSO_4 media for loosely-packed (top) and closely-packed (bottom) cases. (b) Raman spectra from samples obtained by tuning the pump wavelength while measuring the 532-nm output intensity.

As shown in Fig. 2a, the output Raman intensities versus pump pulse energy indicate lasing threshold characteristics observable for both types of samples. Once the pump energy increases above the threshold, Raman gain exceeds optical loss, allowing stimulated Raman emission with optical feedback from spontaneous Stokes light diffused randomly inside the heterogeneous medium. With structural fill factor of 0.17 and 0.91, the numerical calculation for the scattering mean free path (l_{sc}) of the loosely-packed and closely-packed BaSO_4 samples are approximately $2 \pm 1 \mu\text{m}$ and $0.4 \pm 0.2 \mu\text{m}$ respectively, which are much shorter compared to the sample length, L . Hence, the generated Raman light can be amplified many times before exiting the gain medium. The amplified Raman spectra of both samples are displayed in Fig. 2b where the dominated peak at the pump wavelength of 505 nm is observed, consistent with the BaSO_4 Raman shift at 985 cm^{-1} . All other BaSO_4 Raman shift lines are also noticeable at 460, 627, and 1142 cm^{-1} . Although those nanostructured media show amplification of Raman signal, the initial powder form yields relatively higher Raman conversion efficiency when compared with the closely-packed structure. This result can be explained by considering the effects of two parameters. First, the loosely-packed sample is composed of structural fluctuation in both nanometer and micrometer scale owing to self-aggregation of the nanoparticles. This results in secondary particles with much larger effective sizes, and thus stronger scattering coefficient. Secondly, it can be considered from the equation describing Raman lasing intensity in steady-state SRS [2],

$$I_L = I_0 \exp[(G_R - \alpha)l],$$

where I_0 is the intensity of spontaneous Raman signal, l is the light-medium interaction length, and α is the net optical loss coefficient. The Raman gain coefficient, i.e. $G_R \propto NI_P(d\sigma/d\Omega)$, is proportional to the density of medium, pump intensity, and spontaneous Raman cross section, respectively. Although with lower medium density, the loosely-packed powder sample should allow much longer optical interaction length l due to deeper light penetration through the microscale pores.

4. Conclusion

We demonstrated the evidence of random Raman lasing generated from disordered BaSO_4 samples using nanosecond laser pulse as optical pumping. It was also found that the original powder forms with prevalent micron-sized secondary particles give higher signal than the densely-packed structure. This would be encouraging for the development of practical standoff detection of hazardous or explosive materials in their original powder form.

5. References

- [1] B. H. Hokr, J. N. Bixler, G. D. Noojin, R. J. Thomas, B. A. Rockwell, V. V. Yakovlev, and M. O. Scully, "Single-shot stand-off chemical identification of powders using random Raman lasing," *Proceedings of the National Academy of Sciences of the United States of America* **111**, 12320-12324 (2014).
- [2] Y. R. Shen, *The Principles of Nonlinear Optics* (Wiley, 1984).

VITAE

Name Mr. Panuwat Srisamran

Student ID 5910220049

Educational Attainment

Degree	Name of Institution	Year of Graduation
Bachelor of Science (Physics, Second-class honor)	Prince of Songkla University	2015

Scholarship Awards during Enrolment

2012-Present	Development and Promotion of Science and Technology Talents Project
2016-2019	Teaching Assistant at Department of Physics, Faculty of Science, Prince of Songkla University
2018	Research Grant for Thesis in the Fiscal Year 2018

List of Publication and Proceeding

Srisamran P., Pewkhom P., Boonsit S., Kalasuwan P., van Dommelen P. and Daengngam D. (2018). Nanosecond-Pumped Random Raman Lasing from Bulk Nanogranular Materials. Proceeding of Advanced Photonics Congress 2018. Eidgenössische Technische Hochschule (ETH) Zürich, Switzerland, July 2-7, 2018. NpTh1H.6.